Lawrence Berkeley Laboratory
UNIVERSITY OF CALIFORNIA

Materials & Chemical Sciences Division

Ultrafast Spectroscopic Studies of the Photophysics of Phenyl-Substituted Butadienes in Liquids

R.L. Hoff
(Ph.D. Thesis)

August 1991

Prepared for the U.S. Department of Energy under Contract Number DE-AC03-76SF00098

DISCLAIMER

LBL-31152

Ultrafast Spectroscopic Studies of the Photophysics of Phenyl-Substituted Butadienes in Liquids.

by

Rebecca Lynn Hoff

Ph.D. Thesis

Department of Chemistry
University of California

and

Chemical Sciences Division
Lawrence Berkeley Laboratory
University of California
Berkeley, CA 94720

August 1991

This work was supported by the National Science Foundation, NSF Graduate Fellowship, Office of Naval Research and the U. S. Department of Energy, Office of Basic Energy Sciences, Chemical Sciences Division, Under Contract No. DE-AC03-76SF00098.

Ultrafast Spectroscopic Studies of the Photophysics of Phenyl-Substituted Butadienes in Liquids

by

Rebecca Lynn Hoff

Ultrafast Spectroscopic Studies of the Photophysics of Phenyl-Substituted Butadienes in Liquids

by

Rebecca Lynn Hoff

Abstract

Ultrafast transient absorption techniques are used to investigate the photophysics of phenyl-substituted butadienes. Design considerations for building the laser system used for these experiments, a colliding pulse modelocked dye laser and copper vapor laser based optical amplifier, are discussed. The modifications made to the laser system and the characteristics and routine operation of the finished system are presented.

Transient absorption spectra of diphenylbutadiene (DPB) are measured as a function of probe pulse wavelength, relative beam polarization and pump pulse intensity. No wavelength dependence is observed, and the relative beam polarization measurements show only the rotational diffusion of the DPB molecule as a whole. At high pump pulse energy, the shape of the decay curve is distorted. The transient absorption decay

time is interpreted as a combination of the radiative lifetime and the isomerization time of the DPB. The data is in agreement with the results of previously published fluorescence measurements and calculations which place the $^1B_{1u}$ excited state below the $^1A_{1g}$ state. The results conflict with published reports of a solvent-induced energy level inversion.

The transient absorption decay times of tetraphenylbutadiene (TPB) and tetraphenylmethylbutadiene (TPMB) are measured as a function of solvent viscosity and of probe wavelength. The TPB spectra suggest that after excitation, TPB relaxes to the bottom of the excited state well where it relaxes radiatively to the ground state surface. TPMB transient absorption spectra taken using different probe wavelengths decay on different timescales. This is interpreted as motion along different coordinates on a two-dimensional potential energy surface. At all wavelengths, the signal decays much more rapidly than that of TPB or the diphenyl-polyenes, indicating that relaxation is occurring along the carbon-phenyl coordinate, in addition to the carbon-carbon coordinate. Implications for the applicability of Kramers' theory to liquid-phase isomerization reactions are discussed.

To my parents

Table of Contents

List of Figures

List of Tables

Preface

Although most chemical reactions are performed in the liquid-phase, very little is known about the details of how reactions occur in liquids on a molecular level. The solvent molecules constantly interact with the solute affecting a wide variety of molecular properties. Collisions in a liquid occur on a 100 fsec fimescale, so in order to probe the effect of the dynamics in real-time, light pulses shorter than 100 fsec are necessary. To produce such pulses, we have built an amplified colliding pulse modelocked dye laser system, which is described in chapter 1.

The isomerization of diphenyl-butadiene (DPB) is commonly used as a probe for studies of liquid-phase chemical reaction dynamics. There remains a controversy in the literature, however, as to the proper ordering of the two lowest energy singlet excited states in solution. Chapter 2 addresses the question of the state ordering, and in particular looks at claims in the literature that the order of the energy levels is inverted shortly after excitation by the solvent relaxation.

The isomerization of the diphenyl-polyenes has been used extensively for testing Kramers' theory, a simple theory for liquid-phase reaction rates. Work presented in the literature

suggests that a 2-dimensional potential energy surface may be necessary for a proper description of the reaction dynamics. Chapter 3 begins with a review of Kramers' theory and then describes transient absorption experiments we have performed using the isomerization of tetraphenyl-butadiene and tetraphenyl-methylbutadiene as a probe of Kramers' theory. The results provide further evidence that a 2-dimensional surface is necessary.

Acknowledgements

Many people have helped me in the research presented here, and I would like to take this opportunity to thank some of them.

First I would like to thank Prof. Charles Harris, my research director during this work, for providing the facilities and atmosphere necessary for state of the art research, and the freedom to pursue my own interests. I would also like to thank my undergraduate research advisor, Prof. Jeanne Pemberton, for introducing me to scientific research and encouraging me to pursue a scientific career.

The Harris research group has been a great group of people to work with, always ready to discuss science or come to lab to help with a problem. A few people have been especially important for this work. Ben Schwartz has been my coworker and friend in building the laser system and doing these experiments. Prof. Ashraf El-Bayoumi first brought TPMB to our attention as a possible molecular system for study, and is always willing to discuss new results and help out in the lab in any way. Dor Ben-Amotz and Mark Paige introduced me to ultrafast laser technology and the lab. Finally, Vijaya Narasimhan, Prof. Harris' secretary, is always ready to help

in any way, from cutting through red tape to reassuring frustrated students that things always do work in the end.

I would also like to thank Prof. El-Bayoumi and Prof. M. Nashed for preparing the TPMB and Prof. H. Walborsky for providing the starting material.

I would like to thank the National Science Foundation for supporting this work. I would also like to thank the National Science Foundation for financial support in the form of a predoctoral fellowship. The Office of Naval Research provided the copper vapor laser used in the CPM laser system. The U. S. Department of Energy, Office of Basic Energy Sciences, Chemical Sciences Division, under Contract No. DE-AC03-76SF00098, provided specialized equipment used in this research.

Last but not least, I want to thank my family for their support and encouragement. My sisters Katie and Beth are my good friends and have always been there for me. Blake, my new brother-in-law, is always ready with a joke and a smile. My mother and father provided an atmosphere where learning was highly valued, and always believed in me, pushing me to accomplish as much as I could. I can never repay the sacrifices they have made for me and the support they have given me. And finally, the last year of graduate school has been made by far the happiest by the love of my fiancé, Steve.

Chapter 1

Amplified Colliding Pulse Modelocked Dye Laser System

1.1 Introduction

In a liquid, a molecule collides with other molecules once every 100 fsec on average. These molecular interactions have a large impact on the dynamics of any reaction taking place by affecting energy transfer, shifting the molecular potential energy surfaces, and forcing the reactants to undergo a diffusional motion in order to react. The details of how the properties of the solvent affect a chemical reaction are a very important part of understanding liquid phase chemical reaction dynamics, and until recently have remained a mystery.

By using very short pulses of light, the effects of the solvent on a liquid-phase chemical reaction can be probed spectroscopically in the time domain. Since collisions in a typical liquid occur approximately once every 100 femtoseconds the laser pulsewidth must be on that order. The technology necessary for producing such short laser pulses has been

developed only recently. The first modelocked dye laser, which was built by Ippen, Shank, and Dienes in 1972, produced 1.5 psec pulses[1]. Since that work, pulsewidths have steadily decreased to the point where pulses as short as 6 fsec, which corresponds to three optical cycles, have now been produced.[2]

The standard method for producing short light pulses is modelocking a dye laser. The two most common methods used to modelock dye lasers are synchronous pumping and colliding pulse modelocking. Modelocking, along with the types of ultrafast lasers that are used, are discussed in several review articles.[3,4]

For our liquid-phase studies, we have built a laser system consisting of a colliding pulse modelocked (CPM) dye laser with a copper vapor laser based amplifier. The remainder of this chapter describes the laser system, its construction and its operation.

1.2 CPM Design, Operation, and Performance

The CPM is a continuously pumped, passively modelocked, ring dye laser. A schematic of the laser is shown in figure 1.1. The basic design for the laser has been published in the literature.[5,6] The fact that the CPM is passively modelocked, and therefore does not require a modelocked pump laser, makes it mechanically simple and eliminates the need for precise cavity length control, which is a great advantage over

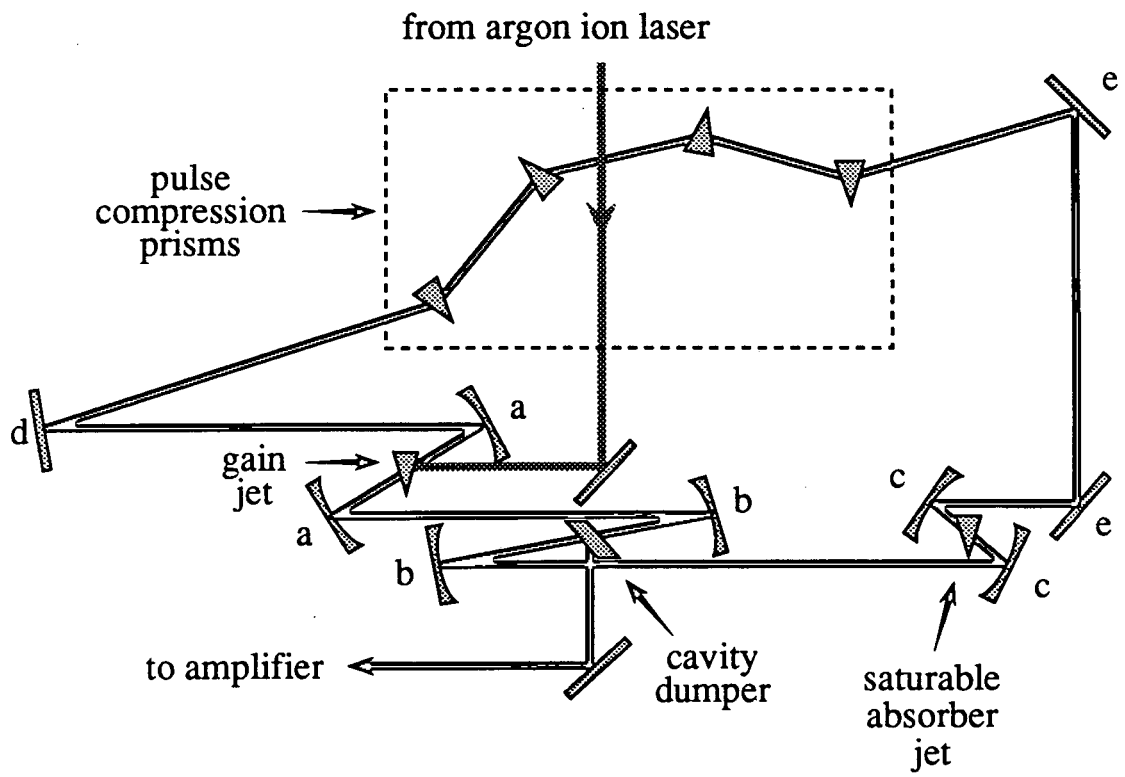

Figure 1.1 Diagram of the CPM laser. The cavity mirrors are labelled as follows: a) 10 cm radius of curvature; b) 20 cm radius of curvature; c) 5 cm radius of curvature; d) output coupler if cavity dumper not in use, otherwise high reflector; e) high reflector

synchronous pumping.

The mechanisms by which the CPM laser produces very short light pulses have been extensively studied both experimentally and theoretically.[7,8,9,10,11,12,13,14] At any given time there are two counter-propagating pulses in the cavity. The independent and combined interaction of these two pulses with the various components of the laser cavity results in the production of the very short light pulses. The distance between the gain and saturable absorber jets is set at one quarter of the total cavity length so that the pulses meet in the saturable absorber and reach the gain jet at a time separation of one-half the round trip time in the cavity, resulting in optimum gain for both pulses.[15] When the pulses meet in the saturable absorber, they overlap and form a transient standing wave. This pattern then forms a transient grating in the dye molecule population which shortens and stabilizes the pulses[15,16]. A second mechanism for pulse shortening is soliton-like shaping in the saturable absorber.[17,18,19] A soliton is a stable solution to the nonlinear Schrödinger equation. In practice this means that a pulse is formed which does not change in time, i.e. the wavepacket does not spread.

The pulseshaping necessary for the formation of solitons is produced by a combination of two phenomena inherent in high peak-power, short pulselength laser pulses: group velocity dispersion (GVD) and self-phase modulation (SPM).[7,8,20] The

minimum number of frequencies contained in a short light pulse can be calculated by taking a fourier transform. For a 75 fsec pulse centered at 620 nm, the bandwidth will cover 10.8 nm, assuming a gaussian pulseshape. Every time the pulse encounters an optical component with normal dispersive properties, the red portion of the pulse travels faster than the blue due to the difference in the index of refraction for the different wavelengths.[21] This results in the pulse spreading out in time and is known as group velocity dispersion.

Self-phase modulation is a process which broadens a laser pulse by adding new frequencies to the leading and trailing edges of the laser pulse.[22,23,24] For high peak power laser pulses, the second-order, intensity-dependent, term in the expansion for the index of refraction, given in eqn. 1.1, must be included.

$$n = n_0 + n_2 \langle E^2 \rangle \tag{1.1}$$

$\langle E^2 \rangle$ is the time averaged value of the instantaneous electric field. The phase modulation due to the intensity-dependence of the refractive index is given by:

$$\delta\phi = (-kL)\,\delta n \tag{1.2}$$

where L is the distance travelled by the light pulse in the liquid. The change in frequency due to the self-phase modulation is given by

$$\delta\omega = \frac{-\partial(\delta\phi)}{\partial t} = \frac{-2\pi L}{\lambda}\frac{\partial(\delta n)}{\partial t}$$

$$\frac{\delta\omega}{\omega} = \frac{-n_2 L}{c}\frac{\partial\langle E^2\rangle}{\partial t} \qquad (1.3)$$

If $n_2 > 0$, the frequencies at the leading edge of the pulse, where $\partial\langle E^2\rangle/\partial t > 0$, are red-shifted, while the frequencies at the trailing edge of the pulse, where $\partial\langle E^2\rangle/\partial t < 0$ are blue-shifted. The net effect is an increase in the bandwidth of the pulse which makes it possible for the light pulse to be shorter in time.

Angular dispersion of a laser pulse contributes a negative component to the group velocity dispersion.[25] This negative group velocity dispersion can be used to temporally recompress laser pulses in which the frequencies have spread.[26,27] In practice, the CPM laser pulses are compressed temporally by using a sequence of four prisms which produces negative group velocity dispersion.[6] The four prism combination is used because it causes no net deviation of the beam from its original path, and is therefore easily installed

in the laser cavity. The group velocity dispersion is given by

$$D=\frac{-L^{-1}dT}{d\lambda}=\frac{\lambda}{cL}\frac{d^2P}{d\lambda^2} \qquad (1.4)$$

Where L is the physical length of the light path, P is the optical path length, λ is the optical wavelength in air, and T is the time required for the light pulse to travel the distance L. By trigonometric arguments, it can be shown that

$$\frac{d^2P}{d\lambda^2}=4l\left\{\left[\left(\frac{d^2n}{d\lambda^2}\right)+\left(\frac{2n-1}{n^3}\right)\left(\frac{dn}{d\lambda}\right)^2\right]\sin\beta-2\left(\frac{dn}{d\lambda}\right)^2\cos\beta\right\} \qquad (1.5)$$

where l is the separation between the two prisms in the long leg of the set-up and β is the angle between two different wavelength components of the beam. Equation 1.5 shows that as long as the second derivative of the index of refraction with respect to wavelength is relatively small compared to the

first derivative, the four prism combination has negative dispersion.

Building a CPM laser requires careful attention to a number of design details due to the delicate balance of optical properties necessary for short pulse generation.[20] The size of the CPM laser cavity determines the repetition rate of the laser, which in our case is 85 MHz. Although the jets need to be spaced approximately one-quarter of the cavity length apart for proper modelocking, the separation does not need to be exact. The CPM laser cavity was rebuilt several times, and the jet spacing was varied between about one-third and one-fifth of the cavity length and no effect was observed on the modelocking quality.

The type of mirrors used in the cavity is a critical design consideration. Two criteria must be met. First, all mirrors must be single-stack dielectrics. Every time the beam hits a mirror, the pulse is broadened by group velocity dispersion (GVD). If multi-stack dielectrics are used, the GVD is too large for the CPM to modelock. When single-stack dielectric mirrors are used, group velocity dispersion is reduced to a level such that it can be compensated for with a set of four prisms, as discussed above. Second, the coatings must be broadband. For a gaussian spectral amplitude, a fourier transform limited 75 fsec pulse centered at 620 nm has a 10.8 nm bandwidth, therefore the coating bandwidth must exceed 10.8 nm. The CPM cavity mirrors are all broadband,

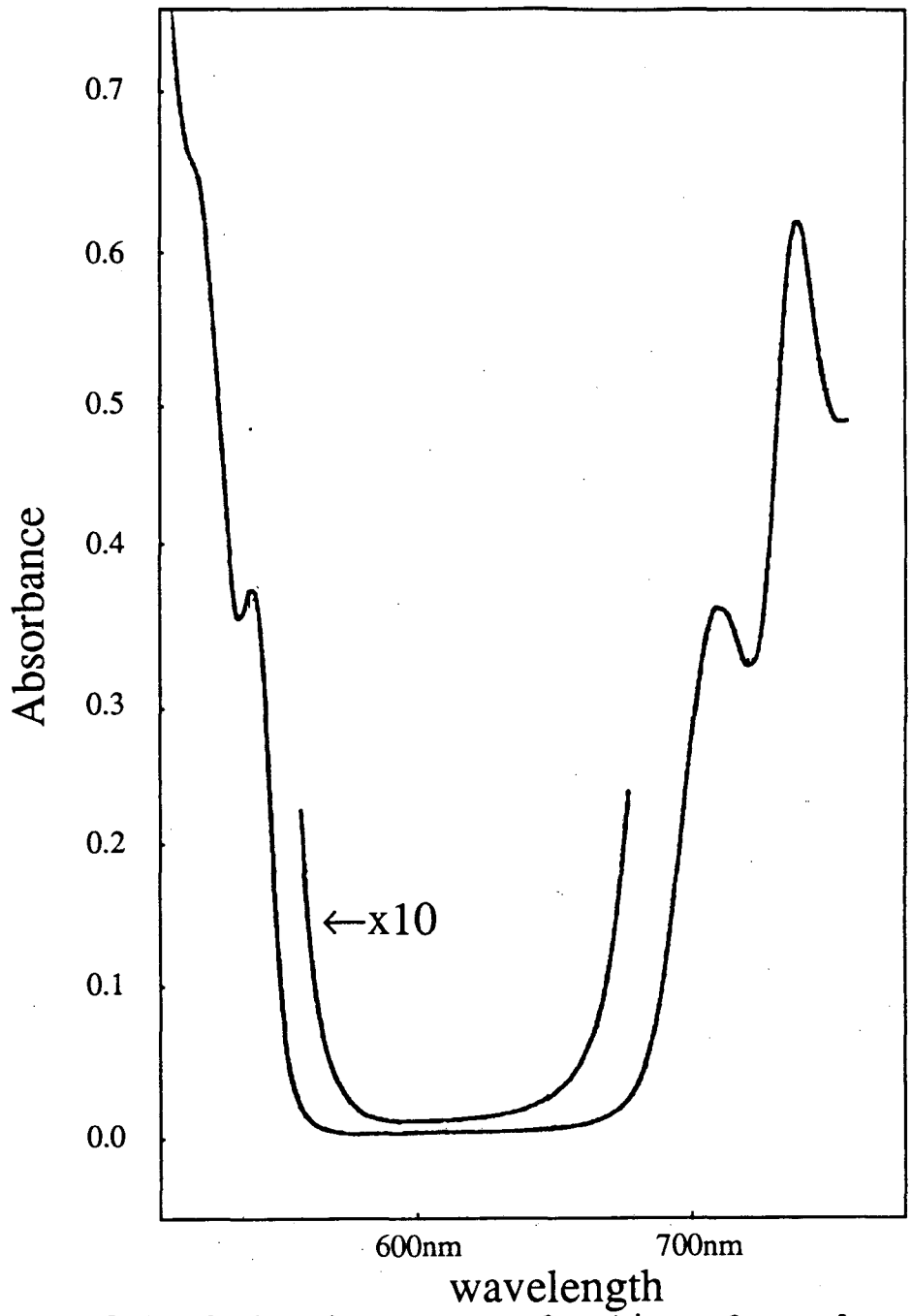

Figure 1.2 Plot of absorbance as a function of wavelength for a CPM cavity mirror. The mirror coating is a broadband, single-stack dielectric coating centered at 620 nm.

single-stack dielectric mirrors coated for a center wavelength of 6190 Å. The bandwidth of a typical cavity mirror is about 120 nm. A reflection spectrum of one of the mirrors is shown in figure 1.2.

The mirror mounts are all made out of stainless steel. Aluminum mounts were used initially, but the lack of thermal stability resulted in unacceptable laser drift. The 1.3% output coupler which was originally installed in the CPM was incorrectly coated with a narrowband coating, and the CPM could not be modelocked. The problem was detected by noticing that the CPM lazed red even when the saturable absorber was shut off, rather than at the fluorescence maximum of the R6G dye, which is yellow.

The only exception to the broadband, single-stack dielectric coating requirement is the mirror that focusses the argon ion laser beam into the gain jet, which has a standard argon ion laser coating. That mirror, along with the mirror next to it which recollimates the R6G fluorescence, are each coated on one-half of a circular mirror substrate. The two semi-circular, focussing mirrors are mounted on separate translation stages, enabling the focal parameters of each to be adjusted independently of the other. This translational independence was found to be very important for optimizing the CPM cavity. It allows the foci of the two mirrors to be adjusted independently, so the argon ion laser can be focussed to the smallest diameter possible before the onset of thermal

blooming in the jet, while the CPM cavity mirror can be simultaneously adjusted to mode-match all of the sub-resonators. It also allows the beam position on the CPM cavity mirror to be conveniently adjusted to minimize astigmatism in the beam.

There are three pairs of curved mirrors in the CPM cavity. One pair focusses the beam into the gain jet with a 10 cm radius of curvature. Another pair focusses the beam into the saturable absorber jet with a 5 cm radius of curvature. The third pair focusses the beam into the cavity dumper crystal with a 20 cm radius of curvature. The gain jet mirror radius of curvature is set at 10 cm to ensure that the argon ion laser and the CPM laser beam diameters are matched when the argon ion laser is focussed as tightly as possible in the gain jet without causing thermal blooming. The saturable absorber radius of curvature is set at 5 cm to focus the beam tightly enough to efficiently saturate the DODCI. This then allows most of the beam intensity to interact with the ethylene glycol resulting in the self phase modulation necessary for producing sub-100 fsec pulses. The cavity dumper radius of curvature is set at 20 cm to avoid focussing the CPM beam tightly enough to burn the crystal, while still focussing tightly enough for efficient diffraction.

Whenever the beam hits a mirror, passes through a jet or the Bragg cell, the light pulse is broadened by group velocity dispersion. This dispersion is compensated by the four prism

combination, which produces negative group velocity dispersion, as discussed above. The prisms are made of quartz and are cut at Brewster's angle to minimize reflection losses. For quartz at 620 nm, typical values are n=1.457, $dn/d\lambda$=-0.03059 μm^{-1}, and $d^2n/d\lambda^2$=0.1267 μm^{-2}.[28] The important parameter for effective GVD compensation is the separation of the prisms in the two long legs of the prism sequence. Currently the separation in our laser cavity is 30 cm from the tip of one prism to the tip of the other, which provides enough negative dispersion to compensate for about 7 mm of quartz. The effective prism separation can be easily adjusted by a small amount by translating the prisms such that the laser beam travels through different lengths of quartz.

The output wavelengths which can be produced by a CPM laser are limited in number due to the fact that the overlap of the emission and absorption curves of the dyes must provide the bandwidth necessary to support pulses less than 100 fsec long. CPM lasers have been developed which produce light at 800 nm[29], 685 nm[30], and 581 nm[31]. However, our CPM is limited to a wavelength of 620 nm by the mirror coatings, which are single-stack dielectrics and therefore reflect in only a fairly limited region. Rhodamine 6G is used as the gain medium in our oscillator and 3,3'-diethyloxadicarbocyanine (DODCI) is used as the saturable absorber medium. The solvent used for both jets is ethylene glycol. The R6G concentration is set to absorb 85% of the

incident argon ion laser power when the argon ion laser is running at 4 W on the 5145 Å line. Modelocking quality is very sensitive to the DODCI concentration, so no predetermined absorbance value can be used. The DODCI concentration is adjusted by adding small amounts of dye until the CPM modelocks well and the laser wavelength is centered at 620 nm.

When aligning the CPM from scratch, it is easiest to start with only a few components in the laser cavity, and add more components a few at a time. First, the argon ion laser is focussed as tightly in the gain jet as possible without causing thermal blooming. Then the output coupler and one of the corner mirrors are used to optimize the gain sub-resonator without the saturable absorber or cavity dumper sub-resonators in the cavity. It is essential that the laser always be in the TEM_{00} mode. When setting up any of the three sub-resonators, it is important to make the "Z" around the dye jet (or Bragg cell) as small as possible to minimize astigmatism. Next, the saturable absorber and cavity dumper sub-resonators are added to the cavity and the corner mirrors are added to form a ring laser. There should be no DODCI in the jet, just ethylene glycol, and the Bragg cell should not be inserted yet. It is very important that the three sub-resonators be mode-matched. This is done by decreasing the size of the sub-resonators to increase the size of the mode until it is constant around the entire cavity. A crescent shaped fluorescence spot on the corner mirror next to the saturable absorber indicates that

the sub-resonators are too small. Again, it is very important the CPM run in TEM_{00}, otherwise it will never modelock properly.

At this point the prisms can be inserted into the cavity. They must be level and not shift the beam path horizontally. Initially the beam should travel through the tips of the prisms, then once the CPM is modelocked more prism can be translated into the beam to achieve the shortest pulse. If too much of the prism is in the beam, the CPM will not modelock at all. Now the saturable absorber jet should be set to slightly off the focus and DODCI should be added until the CPM modelocks. An EG&G Electro-Optics FOD100 photodiode can give an initial indication of when the laser is near modelocking, by showing that pulses have formed. Once pulses can be seen with the photodiode, the CPM beam should be autocorrelated to determine if the CPM is modelocked, and to optimize the pulsewidth and modelocking stability. In general, both the prisms and the saturable absorber position must be adjusted to optimize dispersion compensation for the shortest pulses.

For both dye jets, the beam should pass through the jet at a point about 2/3 of the distance down from the nozzle to the point where the jet width is at its minimum. This ensures that the beam hits an optically flat part of the jet. The jet should hit the catcher tube at the point where the jet width is at its minimum to minimize acoustic waves which can travel

back up the jet and adversely affect the jet stability. The pump pressure is set at 44 psi for the gain jet and at 18 psi for the saturable absorber.

Once the laser is running, the Bragg cell can be placed in its sub-resonator. It is very important that the Bragg cell be positioned at Brewster's angle, which is empirically determined to be 42°. For the Bragg cell currently in the cavity, this means that the white line on the black mount should be perpendicular to the beam. Adding the Bragg cell to the CPM cavity translates the fluorescence horizontally, and the fluorescence must be walked back to its original path with the sub-resonator mirrors, at which point the CPM will laze again. To optimize the Bragg cell diffraction efficiency, center the beam in the cell side to side and position it towards the bottom of the cell. Turn the cavity dumper driver to the "cw" position to maximize the amount of light being diffracted from the cavity during the initial optimization. Optimize the diffraction efficiency by adjusting the angle of the crystal relative to the beam, and the x, y, and z positions. This diffraction optimization is particularly sensitive to the angle of the crystal and to the vertical translation. The addition of the Bragg cell introduces another source of GVD, which can be compensated by translating the prisms further into the beam.

When this CPM was originally constructed, a 1.3% output coupler was used, and there was no cavity dumper. The 1.3%

output coupler was replaced with a 3% output coupler to increase the pulse energy. Pulse energy increased as expected when the transmittance of the output coupler was increased, without any decreased stability in the CPM due to the lower intracavity power. When the cavity dumper was added to further increase the pulse energies, the output coupler was replaced by a 1% output coupler. If at some point the higher peak powers and lower average energies obtained by cavity dumping are no longer needed, the 3% output coupler should be used.

The modelocking quality of the CPM depends on the characteristics of the saturable absorber jet, so several types of nozzles were tried. Sapphire nozzles produce a very high optical quality jet, so two thicknesses of sapphire nozzles were tried. Literature reports indicated that a very thin jet was necessary, so the first nozzle tried was 50 μm thick.[5] The 50 μm nozzle never produced a usable jet. Another sapphire nozzle, this one 300 μm thick was tried, and also proved to be unsatisfactory. Although a flat, optical quality flow was produced, the tranverse width of the jet was significantly larger than that produced by a Coherent nozzle. As mentioned above it is very important to minimize the angles in the sub-resonators to avoid astigmatism, and the relatively large angle necessary to get the beam around the jet produced by the sapphire nozzle resulted in unacceptable amounts of astigmatism. A standard, unsqueezed Coherent nozzle, 375 μm

thick, was used, and was found to work adequately. In an effort to increase the cavity stability and shorten the pulse length, the standard Coherent nozzle was replaced with a Coherent nozzle which had been squeezed to 100 μm thick. The changes observed were not dramatic, but the squeezed nozzle did improve the CPM performance slightly. It is very difficult to squeeze a nozzle narrower than 100 μm and it is unnecessary to do so.

The cavity dumper is a standard Spectra-Physics model 454 Cavity Dumper Driver with a model 451 power supply and electronic chassis. The Bragg cell is a CTI model 2389 AO cavity dumper. The cavity dumper is run at an 8 kHz repetition rate to maximize the pulse energy. It was installed for three reasons. First it helps stabilize the CPM. Second, before installing the cavity dumper, each copper vapor laser pulse amplified multiple femtosecond pulses. Adding the cavity dumper decreased the CPM repetition rate, which helped minimize this problem. Third, it increases the amplifier stability by increasing the CPM pulse energy such that the first few passes through the amplifier are effectively saturated.

The operating characteristics of the CPM are very similar to those published in the literature[5,6]. The average output power is about 6 mW using a 3% output coupler and about 0.09 mW running the cavity dumper on CW. When the cavity dumper is run at 8 kHz, the average power is about 0.007 mW, however

Figure 1.3 Autocorrelation trace of CPM laser pulse with a FWHM of 90 fsec.

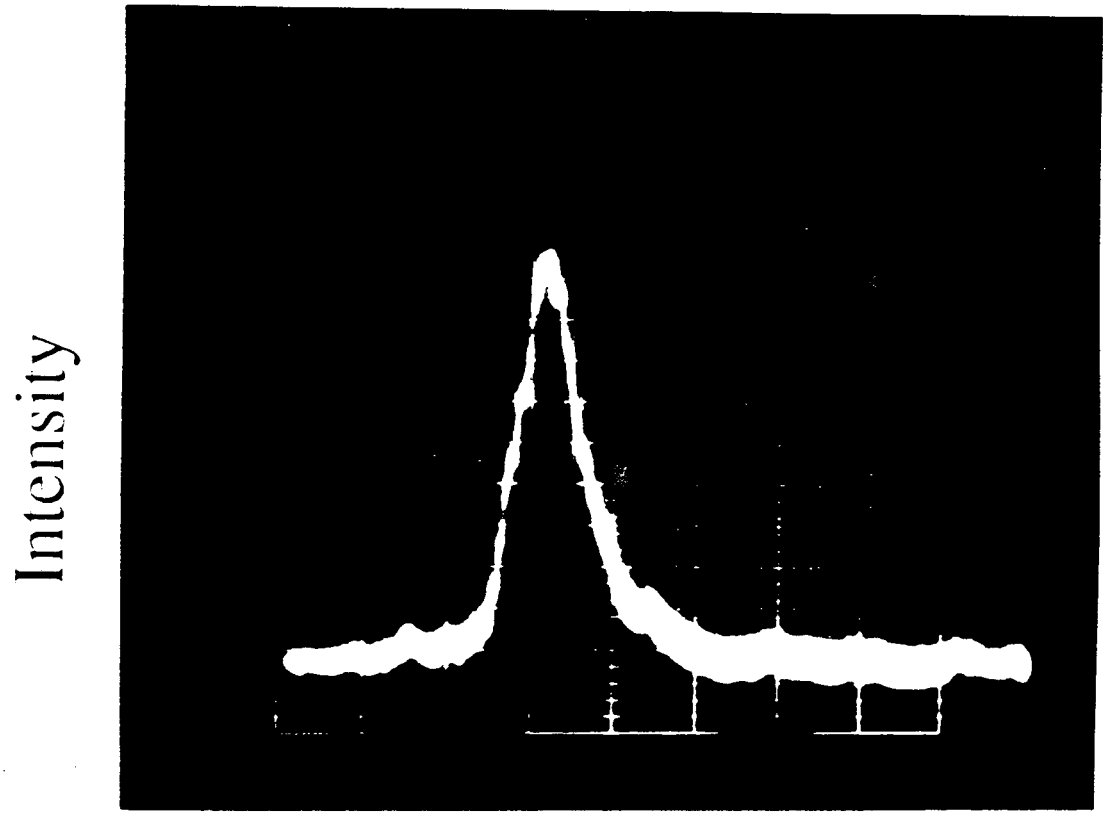
Intensity
1 msec/div

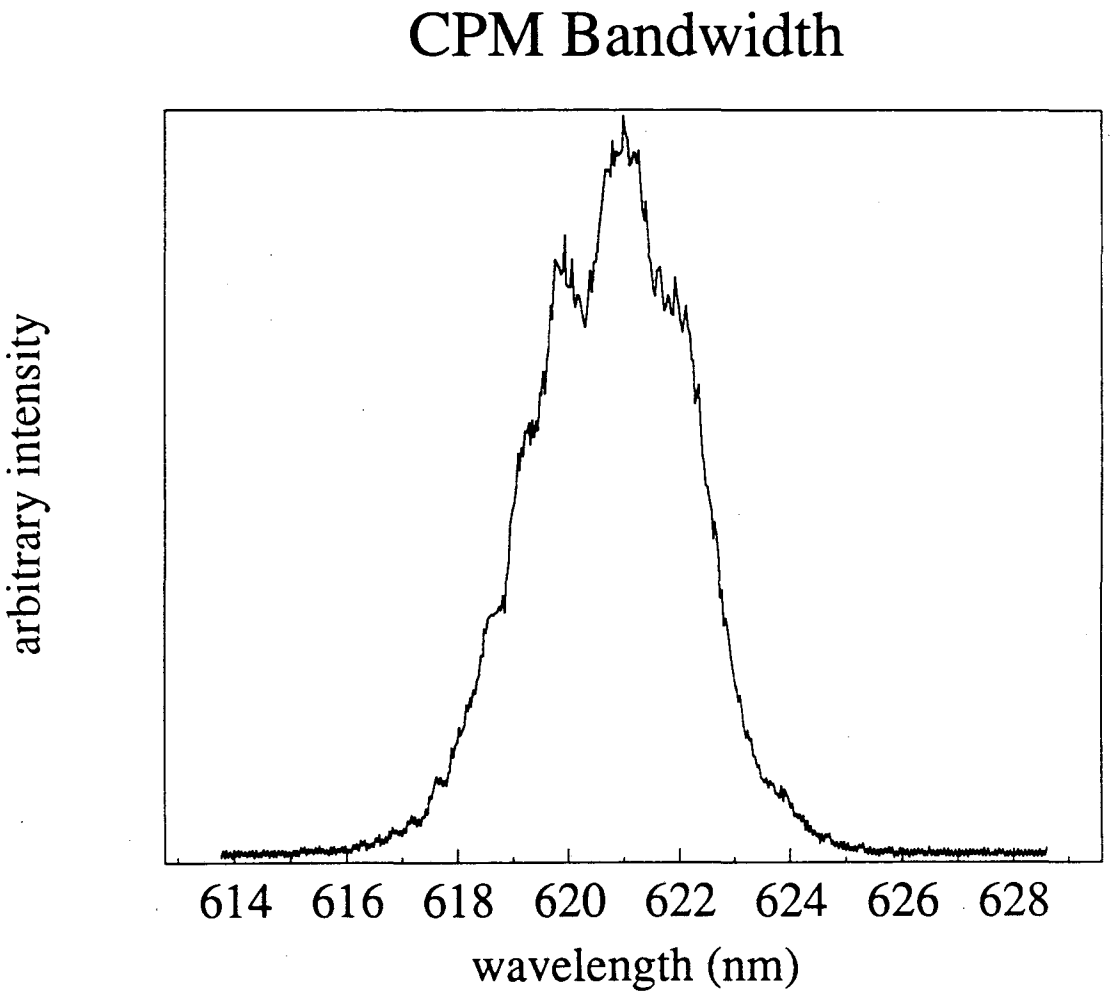

Figure 1.4 Spectrum of the CPM pulse showing a bandwidth of 3.7 nm FWHM centered at a wavelength of 620.5 nm.

this measurement is at the lower limit of the detectable power on our power meter. These values correspond to pulse energies of 60 pJ/pulse, 0.9 pJ/pulse, and 875 pJ/pulse respectively. The pulsewidth is typically between 80 and 100 fsec assuming a hyperbolic sech autocorrelation pulseshape. This was measured with an Inrad model 5-14a/7.5 autocorrelator using a $LiIO_3$ "B" cut crystal. A sample trace is shown in figure 1.3. The bandwidth of the pulse was determined to have a FWHM of 3.7 nm centered around 620.5 nm for an 80 fsec pulse. The pulse spectrum was measured using an OMA, and the wavelengths were calibrated using a neon lamp. These results correspond to a time-bandwidth product $\Delta\nu\Delta t=0.25$. This is smaller than the 0.31 value expected for a hyperbolic sech pulse, but is consistent with that pulseshape if the laser pulsewidth is actually 100 fsec. A plot of the CPM spectrum is shown in figure 1.4.

1.3 Amplifier Design, Operation, and Performance

The pulse energy produced by the CPM is on the order of nanojoules, which is about a factor of 1000 too small for the experiments planned for this laser system. The pulse energy needs to be amplified to the microjoule range or higher. This provides high enough pulse energy to utilize non-linear optical techniques, such as frequency doubling and continuum generation, and opens up whole classes of experiments such as

pump-probe transient absorption spectroscopy. A wide range of amplifier designs exists, the details of which are discussed in a recent review article[32].

In choosing an amplifier design, there is a trade off between peak power and repetition rate. Amplifiers using a Nd:YAG laser running at 10 Hz produce peak powers on the order of millijoules, however signal averaging is slow using one of these systems. To circumvent the slow signal averaging problem, we built an amplifier using a copper vapor laser (CVL) as the amplifying laser, following a design from the literature[33]. A schematic of the amplifier is shown in figure 1.5. The amplifier design is a basic "bow-tie" configuration. The gain jet is pumped by a copper vapor laser. The CPM pulse makes six passes through the gain jet and one pass through the saturable absorber jet. The copper vapor laser can be run at an 8 kHz repetition rate, resulting in an amplified femtosecond pulse train at 8 kHz. This greatly increases the signal averaging efficiency. Dye jets are used for the gain and saturable absorber media. The short laser pathlength in the jets results in far less group velocity dispersion than would be encountered if amplifier cells were used. The primary disadvantage of this laser system is that the pulse energies are relatively low, particularly if the beam is frequency doubled to 310 nm, and therefore if it is to be used for transient absorption experiments, the absorbing species must have a very large

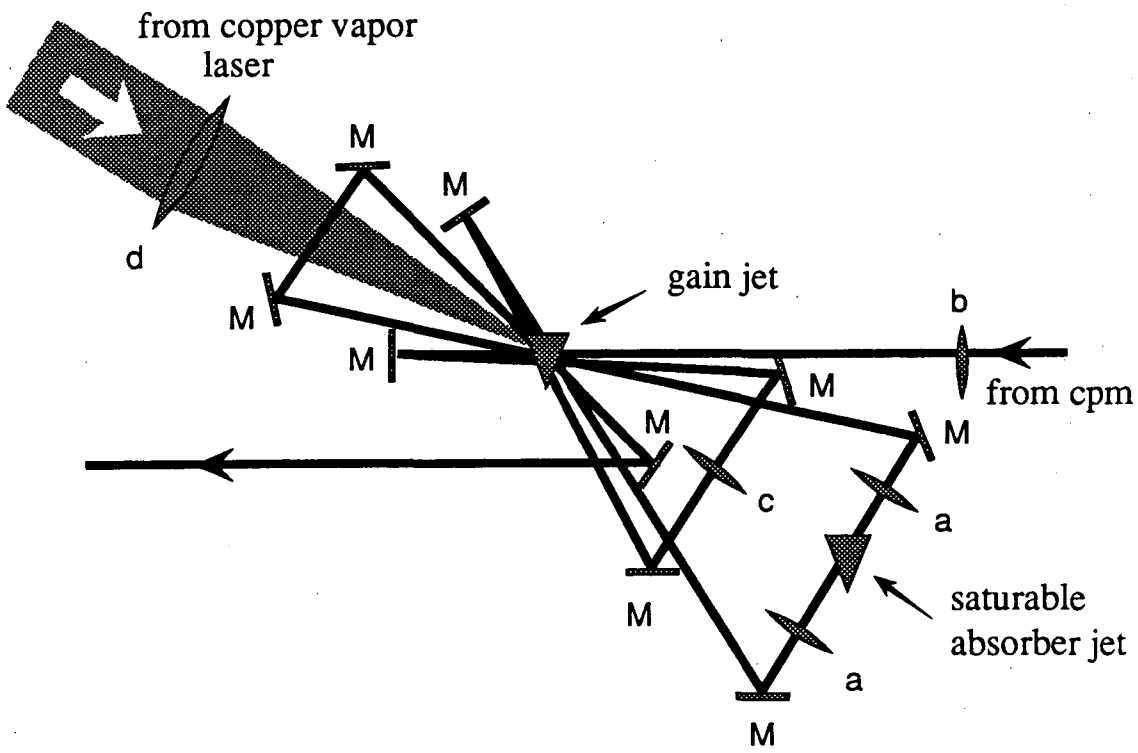

Figure 1.5 Schematic of the copper vapor laser based optical amplifier. M indicates a high reflectivity mirror. Lenses are labelled by a - d, with focal lengths a = 25 mm, b = 500 mm, c = 250 mm, and d = 250 mm.

extinction coefficient.

Although the amplifier design is fairly simple, there are a few important considerations in setting it up. The nozzles used in the amplifier are made from sapphire, which produces optically flat jets. The amplifier saturable absorber nozzle is 300 μm thick and the gain nozzle is 1.25 mm thick. Amplification of the CPM beam requires a long pathlength in the gain jet, and thus a thick nozzle. The 1.25 mm thick sapphire nozzle produces an interferometrically flat jet over a 1 mm^2 area located in the center of the jet, just below the nozzle. It is very important that all the beams pass through this spot. This constrains the angles the CPM beam makes with the jet and the size of the CPM beam in the jet. The angles should be made as small as possible. The first two lenses should be positioned such that the beam focusses on the mirrors after the first and third passes through the gain jet. This minimizes the spot size for the first four passes, ensuring that the beam passes through the optically flat part of the jet. It also helps saturate the gain, resulting in a more stable amplified beam. The two lenses immediately before and after the saturable absorber jet should be positioned such that the beam is diverging slightly coming out of the amplifier. This allows the fifth and sixth passes to be optimized in the same manner as the first four.

The dyes used in the amplifier are Rhodamine 640 for the gain medium and malachite green for the saturable absorber

medium. The R640 concentration is set such that 85% of the CVL power is absorbed. Dye is then slowly added to the reservoir while looking at the pulse height on an FOD100 photodiode until the pulse energy stops increasing. The amplified pulse energy is very sensitive to the R640 concentration. The malachite green concentration is set to between O.D. 3 and O.D. 4 at 620 nm. For the current pump configuration, that translates to about 0.2 g of malachite green in a full dye reservoir. For both dyes, ethylene glycol is used as the solvent. The gain jet has about 10% glycerine added to the ethylene glycol to stabilize the jet. The dye solution is cooled to 21°C by a circulating water bath on the line leading to the nozzle. If the dye is not temperature controlled, frictional heating results in jet instabilities. The pump pressures are set at 23 psi for the gain jet and 52 psi for the saturable absorber jet.

The CVL beam should be focussed as tightly as possible without causing thermal instabilities in the gain jet. Any thermal instability can be seen as spatial fluctuations on the amplified beam. It is also important to have the CVL pass through the gain jet before it focusses to avoid hot spots in the beam which can occur after the beam has passed through a focus. When focussed, the CVL can burn through many materials, including black paint, therefore a slab of graphite is used as a beam block for the portion of the CVL beam not absorbed by the gain jet.

The mirrors are all aluminum with a protective coating. Four lenses are used in the amplifier. The first lens which the CPM beam encounters before entering the amplifier has a focal length of 500 mm. The second lens, which refocusses the beam after two passes through the gain jet has a 250 mm focal length. Two 25 mm lenses focus the laser beam into the saturable absorber jet and recollimate the beam afterwards (the amplified beam is actually diverging slightly coming out of the amplifier). The lenses used are as thin as possible and do not have any anti-reflection coatings to avoid pulse broadening. The CVL is focused into the gain jet using a 250 mm focal length lens.

A schematic of the timing circuit for controlling the timing between the CPM and CVL pulses is shown in figure 1.6. The CVL requires a trigger pulse approximately 600 nsec long, dropping to ground from 4 V at an 8 kHz repetition rate, terminating in 50 Ω. It is very important that the pulse be very clean, since any spikes on the pulse will destroy the MOSFETs in the thyratron driver. The piece of equipment in the timing circuit that is labeled "black box" is a device designed at Bell Labs and modified by the chemistry department electronics shop to minimize the jitter between CVL and CPM pulses due to drift in the time between when the CVL is triggered and when it produces a light pulse. The way in which it works and how to use it are explained in Appendix I.

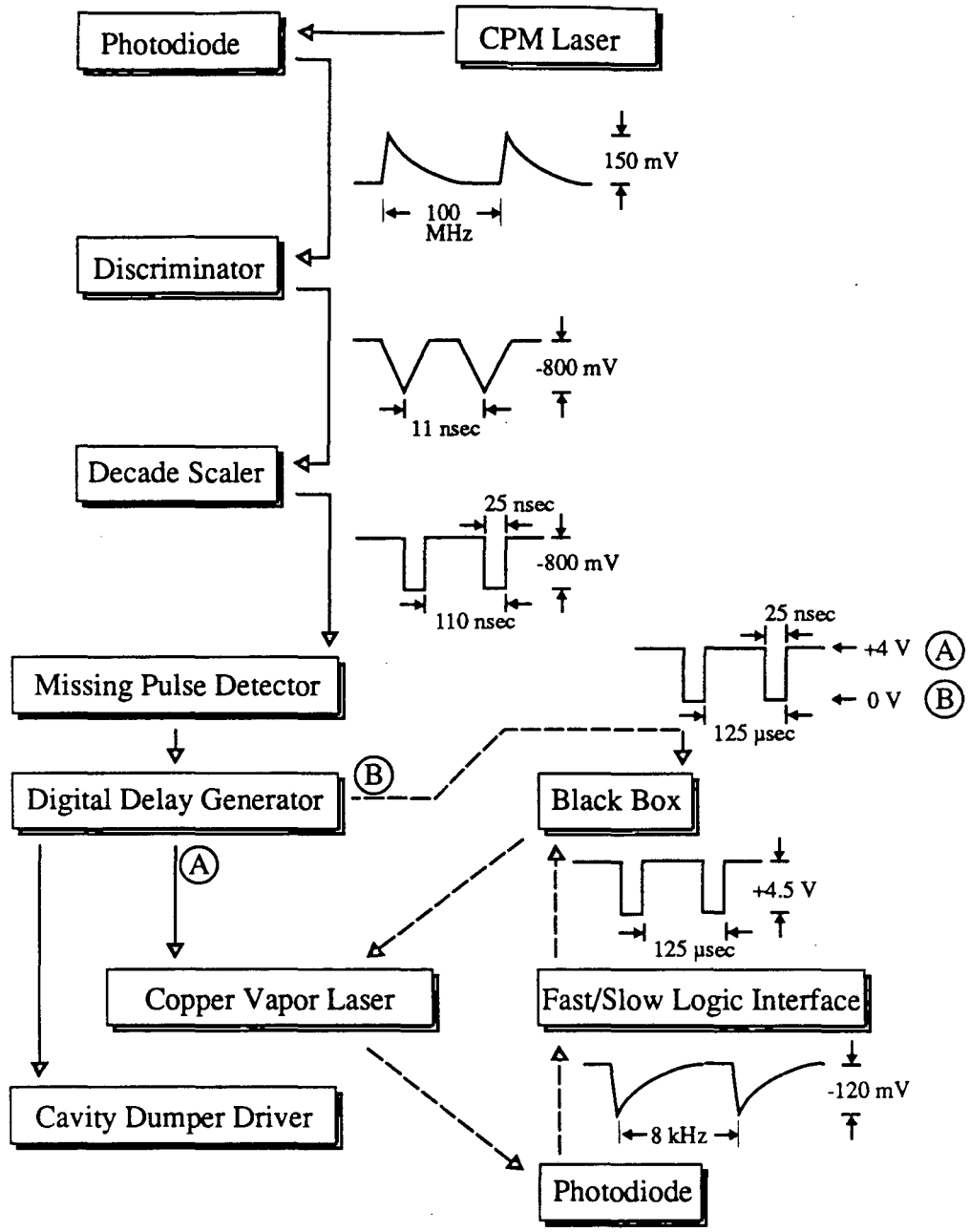

Figure 1.6 Schematic of the timing electronics between the CPM laser and the CVL.

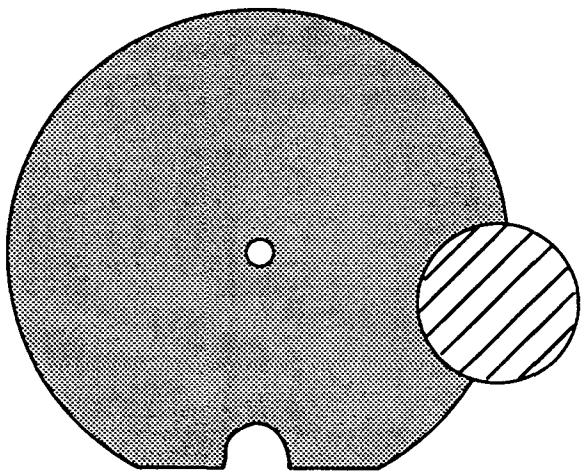

Figure 1.7 Diagram of proper back-reflection alignment as determined by the pulse outline on the first turning mirror outside the CVL output coupler. The laser profile is the large solid circle, the back-reflection is the smaller circle with diagonal lines.

The CVL needs to produce pulses with a pulsewidth no longer than 10 nsec and with a minimum of 27 Watts average power to efficiently amplify the CPM. These specifications can be achieved by running the laser hot, that is at high neon pressure (about 60 Torr), low neon flow rate (about 1/4 turn), and high input voltages (about 8 kV). The exact operating parameters vary from tube to tube. When the CVL is running properly, the beam looks more yellow than green, but a purely yellow beam indicates an overheated tube. Typical operating parameters are an 8 kHz repetition rate, an average output power of about 27 W and a FWHM pulsewidth of about 25 nsec. In order for amplification to take place, the pulsewidth in nanoseconds must be shorter than the power in watts.[34] The CVL pulsewidth can be shortened further by placing an uncoated glass flat in the laser beam perpendicular to the laser beam about five feet from the CVL output coupler. The back reflection needs to be slightly off axis, and the image on the turning mirror immediately outside of the laser tube should look like figure 1.7. The 8% reflection back down the CVL tube suppresses the stimulated emission after the laser pulse, thereby eliminating the last of the three peaks on the CVL pulse, providing CVL pulses <20 nsec FWHM. When these CVL pulses are used to amplify the CPM, only one CPM pulse is amplified, with no evidence of a second pulse. By using the back-reflection technique, the CVL can be run slightly cooler, that is at lower neon pressure and lower input voltage, than

without the glass flat, prolonging the life of the CVL tube. Using the glass flat produces shorter laser pulses with negligible loss of usable power.

The amplified CPM laser has the following characteristics: a wavelength of 620 nm; 150 fsec pulsewidth, assuming a gaussian pulseshape; a pulse energy of about 3 μJ; and an 8 kHz repetition rate. No attempt is made to compensate for GVD after the amplifier, so if the pulses were recompressed, shorter pulsewidths may be obtained. The pulses can be focussed to <100 μm, a focal size larger than the diffraction limit, determined by beam quality.

The amplified CPM pulse peak powers are high enough for efficient frequency doubling to take place. A 300 μm thick KDP crystal cut for 0° angle of incidence, an incident wavelength of 620 nm, and purchased from Cleveland Crystals, is used for frequency doubling. Conversion efficiencies of between 10% and 15% of the incident power are routinely obtained. A 100 mm focal length lens is used to focus into the KDP crystal, which must be placed slightly in front of the focal point to avoid damaging the crystal. A thin crystal must be used with the 150 fsec pulses to minimize pulsewidth broadening due to group velocity dispersion. A 500 μm thick BBO crystal has also been used for frequency doubling. The BBO crystal produces about 50% more UV light than the KDP crystal and is much more difficult to damage. The BBO crystal

has the disadvantage that the acceptance angle is much smaller than for KDP, so alignment is much more difficult.

The amplified beam peak power is also high enough to generate continuum in a wide variety of solvents[33]. Carbon disulfide and acetone have been found to be very useful continuum generation solvents in the vicinity of their stimulated Raman lines. CS_2 has a 656 cm^{-1} Raman shift, for an intense line at 646 nm, and acetone has a 2925 cm^{-1} shift, for an intense line at 757 cm^{-1}. However, benzene has been found to be the most generally useful liquid for continuum generation, producing enough continuum for pump/probe experiments over the wavelength range between 584 nm and 690 nm. Benzene has a Raman line at 992 cm^{-1}, allowing particularly efficient continuum generation at wavelengths of 552 nm, 584 nm, 661 nm, 680 nm, and 690 nm.

Before conducting any experiments, we needed to ensure that the femtosecond laser system and our data collection apparatus were working properly. We measured the transient absorption decay time for DPB in hexane with the pump and probe polarizations parallel. We found the results to be very reproducable. The data fit very well to a pulsewidth limited risetime with a single exponential decay with a time-constant of 460 psec. This time-constant agrees very well with the results of fluorescence measurements made by Velsko and Fleming, in which they obtained a 460 psec fluorescence decay-time for DPB in alkane solvents.[35] Since we originally made

these measurements, the transient absorption spectrum of DPB in a variety of solvents at a range of temperatures has been measured.[36,37] The observation of a single exponential decay time of 460 psec for DPB in pentane is in good agreement with our results. These results strongly indicate that the femtosecond laser system is working properly.

1.4 Noise Characterization and Solutions

The data obtained with the amplified CPM laser system was initially very noisy. Because the laser system produces only 3 μJ pulse energies, producing only small signals for transition absorption experiments, it is important to be able to normalize down to the bit noise of the A/D converter, which is effectively the limiting factor in noise reduction. In our case we use an eleven bit A/D, so a noise level of 0.15% of the signal should be attainable.

The noise was characterized by using a DT110 photodiode to monitor the amplified beam and then saving a string of data where the intensity of every pulse in the 8 kHz pulse-train is recorded by the personal computer. The data was then autocorrelated and fourier transformed to determine the frequency components. A sample plot is shown in figure 1.8. It was determined that most of the noise was low frequency. In particular, as expected, large components existed at

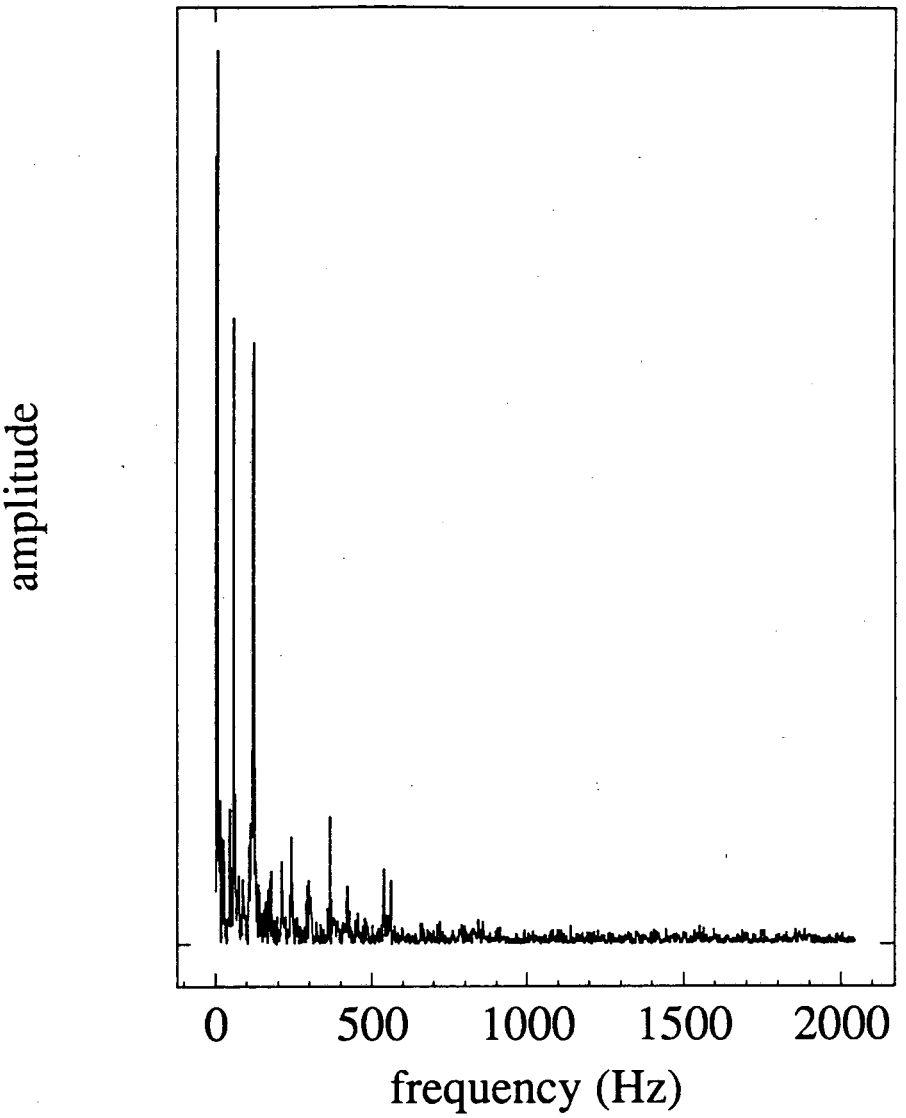

Figure 1.8 Fourier transform of the autocorrelation of the amplitude of the amplified CPM laser pulses.

frequencies of 60 Hz and 120 Hz, the frequency of the line voltage. However, there are also some high frequency components in the kilohertz frequency range. The low frequency noise at 60 Hz and 120 Hz can be seen on the unamplified CPM beam by looking at the signal from a photodiode on an oscilloscope. This noise is probably due to fluctuations of the argon ion beam at that frequency. The high frequency components are due to pickup at the detector of noise radiated by the copper vapor laser, which radiates large amounts of radio-frequency noise due to the firing of the thryatron.

Several different steps were necessary to eliminate the noise problem. A very important step was stabilizing the CPM as much as possible by the methods described above, including stainless steel mounts, cavity dumping, and squeezing the saturable absorber nozzle. The CVL arrived from the factory with absolutely no RF shielding, so the next step was constructing an electrically isolated mu-metal box to shield the copper vapor laser. The CVL umbilical cord, which carries a 6 kV signal to trigger the thyratron was also originally unshielded. The umbilical cord was, therefore, shielded using 4 inch diameter type U. A. Anaconda metal hose coated on the outside with plastic. This shielding virtually eliminated the RF noise problem. Amplifier gain jet stability, achieved by cooling the jet and adding 10% glycerol to the ethylene glycol, was also found to be important. The contacts on the

A/D convertor must be well shielded and it is essential that good contact be made. If these steps are taken, the noise on the signal is routinely observed to be the bit noise of the A/D.

Although the noise on the amplified laser beam has been minimized, there remains the problem that when the noise on the beam appears in the data it is correlated. This means that the noise cannot be averaged away as rapidly as uncorrelated noise can, and the effective repetition rate of the laser system is reduced to about 200 Hz.

1.5 References

1. E. P. Ippen, C. V. Shank, and A. Dienes, Appl. Phys. Lett., **21**, 438 (1972)

2. R. L. Fork, C. H. Brito Cruz, P. C. Becker, and C. V. Shank, Opt. Lett., **12**, 483 (1987)

3. E. P. Ippen, Hyperfine Interactions, **37**, 165 (1987)

4. R. L. Fork, H. Avramopoulos, and J. A. Valdmanis, American Scientist, **78**, 216 (1990)

5. R.L. Fork, B.I. Greene and C.V. Shank, Appl. Phys. Lett., **38**, 671 (1981)

6. J. A. Valdmanis, R. L. Fork, and J. P. Gordon, Opt. Lett., **10**, 131 (1985)

7. O. E. Martinez, R. L. Fork, and J. P. Gordon, J. Opt. Soc. Am. B, **2**, 753 (1985)

8. O. E. Martinez, R. L. Fork, and J. P. Gordon, Opt. Lett., **9**, 156 (1984)

9. J. A. R. Williams, P. M. W. French, and J. R. Taylor, IEEE J. Quantum Electron., **26**, 1434 (1990)

10. H. Avramopoulos, P. M. W. French, G. H. C. New, Magda M. Opalinska, J. R. Taylor, and J. A. R. Williams, IEEE J. Quantum Electron., **25**, 2469 (1989)

11. M. S. Stix, and E. P. Ippen, IEEE J. Quantum Electron., **QE-19**, 520 (1983)

12. G. H. C. New, IEEE J. Quantum Electron., **QE-10**, 115 (1974)

13. H. A. Haus, IEEE J. Quantum Electron., **QE-11**, 736 (1975)

14. D. K. Kuhlke, W. Rudolph, and B. Wilhelmi, IEEE J. Quantum Electron., **QE-19**, 526 (1983)

15. R. L. Fork, C. V. Shank, R. Yen, and C. A. Hirlimann, IEEE J. Quantum Electron., **QE-19**, 500 (1983)

16. W. Dietel, Opt. Comm., **43**, 69 (1982)

17. L. F. Mollenauer, R. H. Stolen, and J. P. Gordon, Phys. Rev. Lett., **45**, 1095 (1980)

18. F. W. Wise, I. A. Walmsley, and C. L. Tang, Opt. Lett., **13**, 129 (1988)

19. F. Salin, P. Grangier, G. Roger, and A. Brun, Phys. Rev. Lett., **56**, 1132 (1986)

20. J. A. Valdmanis, and R. L. Fork, IEEE J. Quantum Electron., **QE-22**, 112 (1986)

21. E. Hecht, Optics, (Addison-Wesley Publishing Co., 1987)

22. D. H. Auston in Ultrashort Light Pulses, S. L. Shapiro, ed. NY, Springer Verlag 1977.

23. F. Shimizu, Phys. Rev. Lett., **19**, 1097 (1967)

24. R. H. Stolen and C. Lin, Phys. Rev. A, **17**, 1448 (1978)

25. O. E. Martinez, J. P. Gordon, and R. L. Fork, J. Opt. Soc. Am. A, **1**, 1003 (1984)

26. R.L. Fork, O.E. Martinez, and J.P. Gordon, Optics Lett., **9**, 150 (1984)

27. J. P. Gordon and R. L. Fork, Optics Lett. **9**, 153 (1984)

28. D.Marcuse, Appl.Opt. **19**, 1653 (1980)

29. W. H. Knox, J. Opt. Soc. Am. B, **4**, 1771 (1987)

30. P. Georges, F. Salin, G. Le Saux, G. Roger, and A. Brun, Opt. Comm., **69**, 281 (1989)

31. P. M. W. French, and J. R. Taylor, Opt. Comm., **61**, 224 (1987)

32. W. H. Knox, IEEE J. Quantum Elect., **24**, 388 (1988)

33. W.H. Knox, M.C. Downer, R.L. Fork and C.V. Shank, Optics Lett, **9**, 552 (1984)

34. Private communication from Wayne Knox

35. S. P. Velsko and G. R. Fleming, J. Chem. Phys., **76**, 3553 (1982)

36. Ch. Gehrke, J. Schroeder, D. Schwarzer, J. Troe, and F. Voss, J. Chem. Phys., **92**, 4805 (1990)

37. G. Maneke, J. Schroeder, J. Troe, and F. Voss, Springer Proc. Phys., **4**, 156 (1985)

Chapter 2

Diphenylbutadiene electronic structure

2.1 Introduction

The spectroscopy and dynamical behavior of the diphenylpolyenes have been extensively studied over the last twenty years[1,2]. Interest in this class of molecules has been high because they serve as a good model for isomerization reactions of the type important in the vision process and are readily accessable spectroscopically. Until the discovery in 1972 by Hudson and Kohler of a low-lying $^1A_{1g}$ excited state in 1,8-diphenyloctatetraene,[3] it was believed that for all diphenylpolyenes the lowest lying singlet state had $^1B_{1u}$ symmetry. Since then, it has been established that the lowest excited singlet state in stilbene has $^1B_{1u}$ symmetry, while diphenylhexatriene and longer chain diphenylpolyenes have a lowest excited singlet state with $^1A_{1g}$ symmetry[4,5,6,7]. In diphenylbutadiene (DPB) these two lowest excited singlet states are nearly degenerate, and the ordering has not yet been determined for DPB (see figure 2.1) in solution. This uncertainty in the ordering of the excited state potential

surfaces complicates the interpretation of any spectroscopic studies of DPB.

The order of the two low-lying electronic states of DPB has been determined for the molecule under isolated conditions. The ground state of DPB is known to have $^1A_{1g}$ symmetry. Molecular beam experiments performed by Zewail and coworkers using one and two-photon fluorescence spectroscopy showed that under isolated conditions the lowest excited singlet state has $^1A_{1g}$ symmetry, and the $^1B_{1u}$ state is the second excited singlet state.[8] Several pieces of evidence support this assignment. First, the two-photon fluorescence spectrum is shifted 34 cm^{-1} from the lowest energy bands in the one-photon spectrum. Also, the one-photon excitation experiments, in which excitation is below the activation energy for isomerization, exhibit lifetimes an order of magnitude longer than expected for allowed electronic dipole transitions.

When the molecule is in solution, however, interactions with the solvent can shift the energy of the excited states and may in fact invert the ordering of the two levels. The transient absorption spectrum of DPB in solution has a single maximum at 650 nm[9,10], much like stilbene. In contrast, the transient absorption spectra of diphenylhexatriene and diphenyloctatetraene have two distinct maxima. This suggests that the electronic structure of DPB is more like that of stilbene than it is like that of the longer-chain

Diphenylbutadiene (DPB)

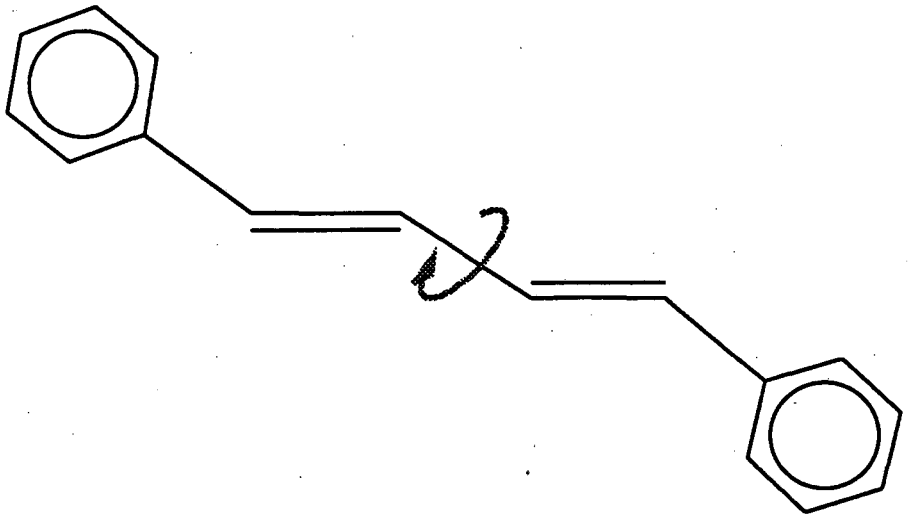

Figure 2.1 Structure of trans,trans-1,4-diphenyl-1,3-butadiene

diphenylpolyenes.

Fluorescence measurements indicate that the absorbing and emitting state are the same, which requires that the lowest excited singlet state has $^1B_{1u}$ symmetry.[11] This was determined by changing the solvent polarity, which should shift the states and change the reaction rate if absorption to the $^1A_{1g}$ state is taking place. No appreciable change in the radiative rate was observed.[11, 20]

However, condensed-phase, two-photon absorption measurements indicate that the $^1A_{1g}$ state is lower. In the dipole aproximation, the $^1B_{1u}$*←$^1A_{1g}$ transition is one-photon allowed, while the $^1A_{1g}$*←$^1A_{1g}$ transition is two-photon allowed. Swofford and McClain observed a shoulder on the two-photon absorption spectrum about 200 cm^{-1} lower in energy than the origin of the one-photon spectrum. They interpret this to mean that the two-photon allowed, $1A_{1g}$ state is 200-600 cm^{-1} lower than the $^1B_{1u}$ state.[5] This interpretation is supported by two-photon absorption and emission measurements by Bennett and Birge for DPB in EPA glass at 77 K.[4] For the EPA glass measurements, the expected fluorescence rate from the $^1A_{1g}$ state, assuming the $^1A_{1g}$ state is lower, was calculated using the strong vibronic coupling to the $^1B_{1u}$ state. The energy splitting between the two states was calculated to be 300 cm^{-1}, in agreement with Swofford and McClain's measured value. Bennett and Birge also point out that the low-energy shoulder on which the state assignment is based has a two-photon

absorptivity about 100 times weaker than the maximum two-photon absorptivity, and suggest that this indicates that the shoulder could be due to a two-photon hot band rather than the system origin, leaving open the possibility that the $^1B_{1u}$ state could be the lower state.

Another test of whether the absorbing and emitting states are the same is whether the measured radiative lifetime and the radiative lifetime calculated from the Strickler-Berg relation are the same. The ratio of the calculated radiative lifetime to the measured lifetime should be about one if the absorbing and emitting states are the same. For DPH, the ratio is 0.18 and for DPO the ratio is 0.05; for both of those molecules, the lowest state is $^1A_{1g}$. For DPB in solution, the ratio is 0.83, which is consistent with either a lowest excited state of $^1B_{1u}$ symmetry or very closely lying lying $^1A_{1g}$ and $^1B_{1u}$ states.[12]

The transient Raman spectrum of DPB has been published,[13,14] but does not provide any consistent or conclusive evidence about the order of the states. One study suggests $^1B_{1u}$ as the more likely lower state,[14] while an assignment of the lowest excited singlet state to a $^1A_{1g}$ symmetry is more consistent with the other set of data.[13]

Measurements of the isomerization rate as a function of pressure show that, like stilbene, the rate decreases with increasing pressure. This argues for the lower state having $^1B_{1u}$ symmetry.[11, 20]

Several calculations have also been done to try to determine the state ordering.[9,15,16,17] All of these calculations agree that the $^1B_{1u}$ state is lower when the excited state molecule is still in its ground state equilibrium geometry. In addition, a paper by Rulliere, et. al.[17] predicts that a phenyl ring rotation will invert the order of the two levels, such that at the excited state equilibrium geometry, the $^1A_{1g}$ state will be lower.

In an attempt to reconcile the conflicting data, Rulliere and coworkers have done a transient absorption study of DPB in solution.[18] Their experiments included time and wavelength dependent dynamics and the effect of temperature and of the intensity of the excitation pulse on the shape of the absorption spectrum. They claim that their results indicate that they are seeing a solvent induced reordering of the two lowest lying excited singlet states. The initial one photon absorption is to the $^1B_{1u}$ state, which is higher in energy than the $^1A_{1g}$ state. After a photon is absorbed, the molecule rotates around a carbon-phenyl bond, which inverts the order of the two levels. The DPB molecule then fluoresces from the lowest excited singlet state, which is now $^1B_{1u}$.

Part of the motivation for studying the isomerization of DPB was to resolve the controversy surrounding the correct ordering of the two low-lying singlet states. The paper by Rulliere, et. al.[18, 62] attempts to provide a picture consistent with their data and the previous fluorescence and two-photon

absorption data. In many instances, however, the Rulliere paper makes claims which seem to exceed the quality of the data presented. The changes in relative spectral amplitude, on which their arguments are based, are not significantly larger than the noise on the spectra. This leads to some questions regarding the reproducibility of their results, which will be discussed in detail later. Other studies of the transient absorption of DPB in solution with better time resolution have observed single exponential decays with no other dynamics.[10, 23] The experiments presented here were designed, then, to reproduce their data with a better signal to noise ratio and time resolution. The Rulliere study was limited by the fact that they used a 25 psec laser pulse. The CPM laser system used to obtain these results produces light pulses are $\leq$ 100 fsec in duration. Our femtosecond laser system has sufficient time resolution that if the risetimes reported by Rulliere, et. al. are accurate, we should be able to easily resolve the risetimes they report and see if there are any additional fast components.

Another advantage to using the CPM laser system to measure the transient absorption spectrum of DPB is that it produces an excite pulse with a wavelength better suited to DPB absorption than the 353 nm or 265 nm wavelength pulse Rulliere uses. These wavelengths are in the very wings of the DPB absorption spectrum, shown in figure 2.2. At these wavelengths, very high excite intensities must be used to

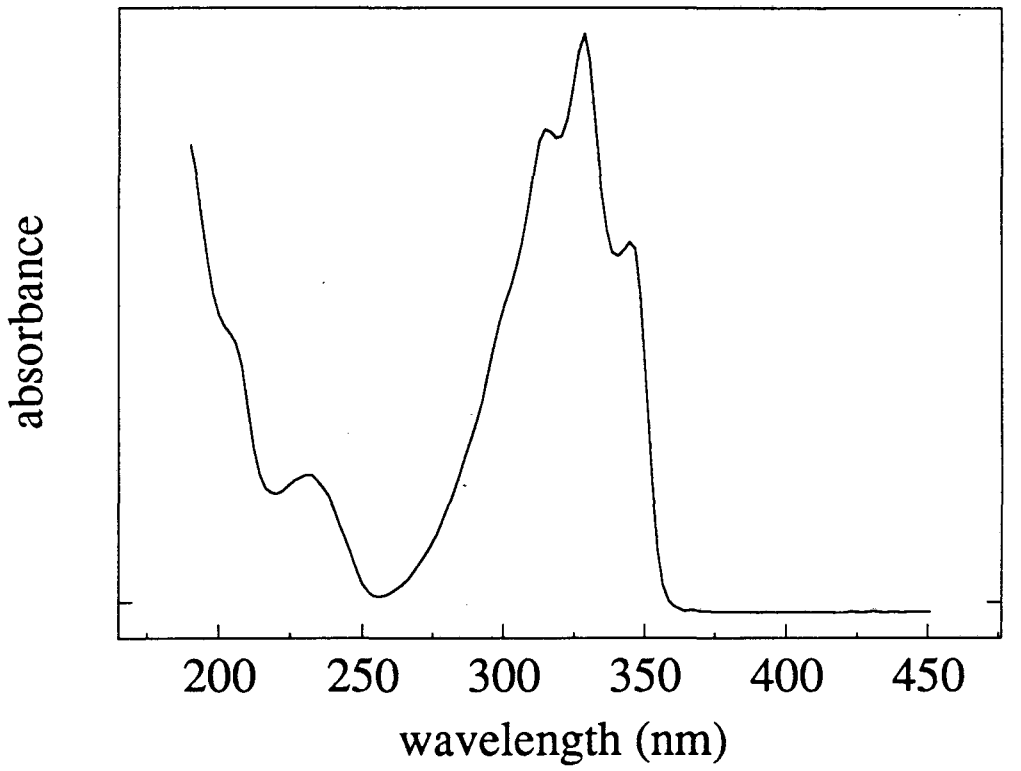

Figure 2.2 Electronic absorption spectrum of diphenylbutadiene in hexane

obtain transient absorption spectra, and it is possible that two-photon processes are occurring. The amplified CPM laser system used in our experiments excites the DPB at 310 nm, which is close to its absorption maximum, so we should be able to obtain spectra with good signal-to-noise without any interfering two-photon processes.

2.2 Experimental procedure

A colliding pulse modelocked dye laser (CPM) was used for most of these experiments.[19] The CPM laser was cavity dumped at an 8 kHz repetition rate, amplified by a copper vapor laser using the standard bow-tie amplifier,[20] and produced light pulses with a wavelength of 620 nm, duration of 150 fsec, and energy of 3 μJ. This laser system has been described in detail elsewhere in this thesis.

A different amplified dye laser system, which produces picosecond light pulses, was used for the experiments to determine the effect of very large excite intensities on the shape of the transient absorption decay curve. This laser system has been described in detail elsewhere.[21,22] A modelocked argon-ion laser synchronously pumps a dye laser, producing 1 psec light pulses at a wavelength of 590 nm. These pulses are amplified by a Q-switched Nd:YAG laser using three longitudinally pumped dye cells. The amplified laser

system typically produces 1 psec light pulses, at a wavelength of 590 nm, and a repetition rate of 10 Hz.

A diagram of the experimental apparatus used with the femtosecond laser system is shown in figure 2.3. The experimental set-up associated with the picosecond laser system is virtually identical.[21,22] In order to obtain the UV light necessary for excitation of the DBP, a portion of the laser beam is frequency doubled using a 300 μm thick KDP crystal cut for 0° angle of incidence. The resulting UV pulses have a wavelength of 310 nm and a pulse energy of 0.3 μJ. The UV pulses are separated from the visible pulses by using a 1/4 inch thick dichroic mirror from CVI optics which transmits >85% of the 620 nm beam and reflects >99.5% of the 310 nm beam. All of the optics used in this experiment are either uncoated or have a single stack dielectric coating. Multi-stack dielectric coatings cannot be used because they broaden the 100 fsec pulse considerably in time due to group velocity dispersion. Any residual 620 nm light in the UV beam is removed with a 1 mm thick UG-11 filter from Schott Glass. The amount of UV light in the visible beam, at less than 0.1nJ/pulse, is undetectable. In addition, the mirrors used in the visible leg of the experimental set-up are not coated to reflect UV light, so no UV reaches the sample from the visible leg.

The 310 nm pulses are used as the excite pulse for transient absorption spectroscopy. The probe pulse for all of

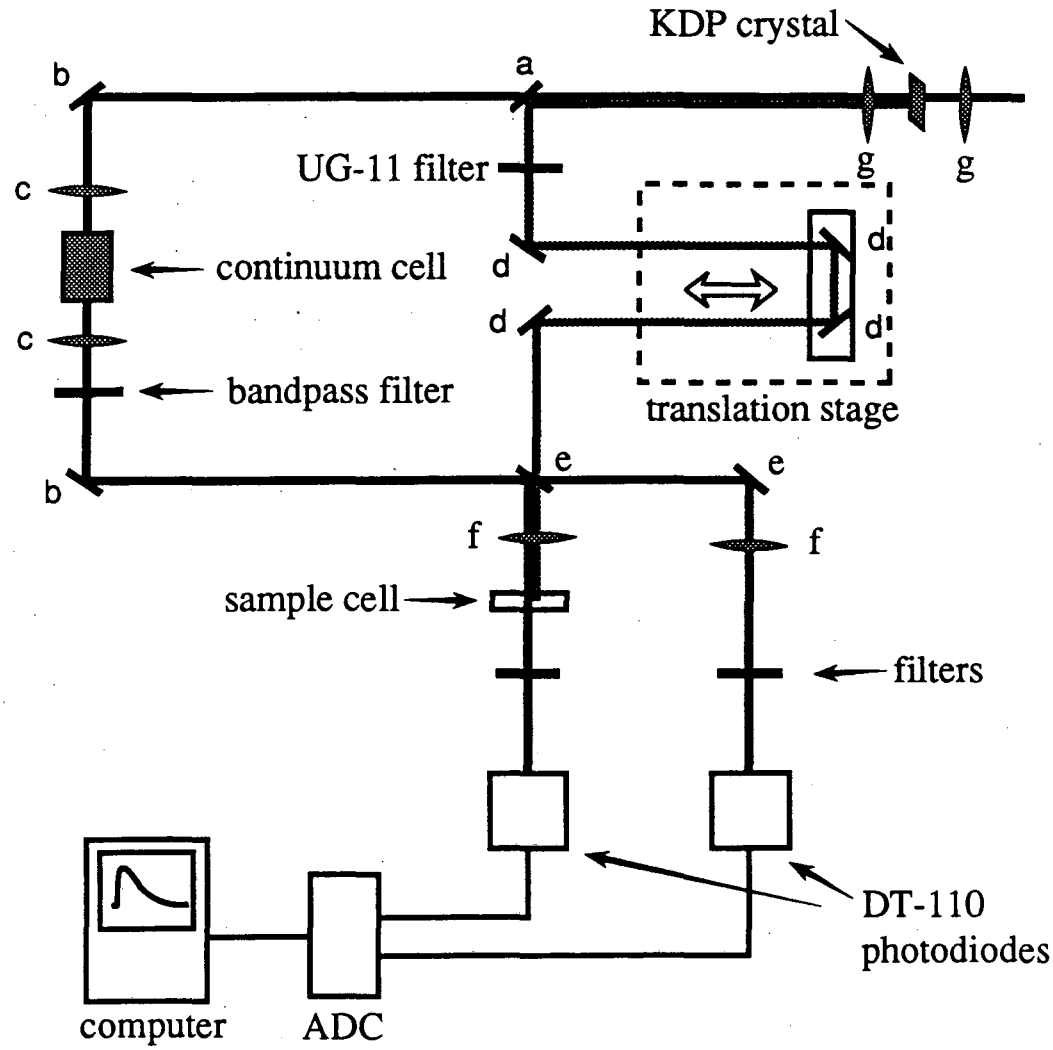

Figure 2.3 Schematic of experimental apparatus, where the labelled components are: a = dichroic mirror, b = visible high reflector, c = 50cm focal length lens, d = UV high reflector, e = quartz flat beamsplitter, f = 200mm focal length lens, g = 100mm focal length lens

the femtosecond experiments, except for those where the wavelength dependence of the data is being measured, is 620 nm. For the wavelength dependence experiments, the high pulse energies of the visible beam were used to generate a continuum of light frequencies by using 25 mm focal length lenses to focus the beam into a 2 inch long cuvette filled with benzene. The intense peak powers cause a wide variety of non-linear optical effects to occur resulting in light pulses broadened slightly from the original 100 fsec, to about 200 fsec as determined from spectral risetimes, with essentially a continuum of frequencies. For our system, the usable frequency range extends from 590 nm to 690 nm. When benzene is used as the continuum generation solvent, particularly intense lines occur at 552 nm, 584 nm, 661 nm, 680 nm and 690 nm due to stimulated Raman scattering. A three cavity bandpass filter, purchased from Ditric Optics, which passes a 10 nm window of wavelengths is then used to select out the wavelength of interest for use as a probe beam.

The time delay between the pump and probe pulses is controlled by reflecting the UV beam onto a Klinger model MT-150 translation stage, which is operated under computer control. This stage has a resolution of 0.1 μm/step, however it is used at a resolution of 1 μm because we do not have the encoder necessary for finer control with the computer.

The sample is placed in a quartz cuvette with a 1 cm pathlength, which is then sealed with a rubber septum. Oxygen

is removed from the samples by bubbling with nitrogen for at least 5 minutes prior to exposure to the UV radiation. If the sample is not deoxygenated, the UV pump beam causes photoproducts to build up on the cuvette wall at the place where the UV beam passes through the cell. The oxidation products of DPB have been reported in the literature to be epoxides, benzaldehyde, cinnamaldehyde, and endoperoxide[23,24] If photoproducts are being produced, they are easily detectable, because they scatter the probe beam, resulting in a constantly increasing slope on the background, and because the shape of the decay curve is affected. Some of the transient absorption spectra of deoxygenated samples were obtained using a translation stage to slowly move the sample cell perpendicular to the laser beams during the scan. No differences were observed between the spectra recorded with the translated sample and the spectra recorded with the stationary sample. The spectra presented in this chapter were taken with a stationary cuvette.

Noise on the laser beam is normalized out of the signal by splitting the visible beam into two parts, sending one beam through the sample and the other through a reference leg which has no sample, and then using the ratio of the two beams as the signal in a standard double-beam detection scheme. Matched quartz flats 1/2 inch thick are used to split off 9% of the visible beam for use as the sample probe beam, and 9% for the reference probe beam when the beam is p-polarized and

makes a 45° angle with the beam-splitter[25], which is the standard configuration. If s-polarized light is used, only 0.8% of the beam is reflected from each beam-splitter. The pump pulse energy at the sample is about 0.18 μJ at 310 nm and the probe pulse energy is typically about 1.7 nJ at 620 nm. The visible and UV beams are sent through the solution collinearly, and a glass flat, followed by a GG475 filter is used to remove any UV light which passes through the cell. The UV beam is focussed to 50 μm and the visible is focussed to 100 μm.

Experiments were run with the beam polarizations parallel, perpendicular, and at the magic angle of 54.7°.[26] The polarization was adjusted by using a zero-order, ≤ 2 mm thick, half-wave plate from CVI, designed to rotate wavelengths between 610 nm and 630 nm uniformly, in the probe beam.

The DPB was purchased from Aldrich as 98% pure trans, trans-1,4-diphenyl-1,3-butadiene. The DPB was used as received. The solvent used was Burdick and Jackson hexane lot# AM046.

Two DT110 photodiodes from EG&G were used as detectors. The signals are sent into a Lecroy model 4300 gated A/D convertor with 11 bit resolution, and processed in a Compaq 80386 personal computer in real time. For many of the spectra where the continuum light was used as a probe beam, ENI model 600L RF power amplifiers were used to amplify the photodiode

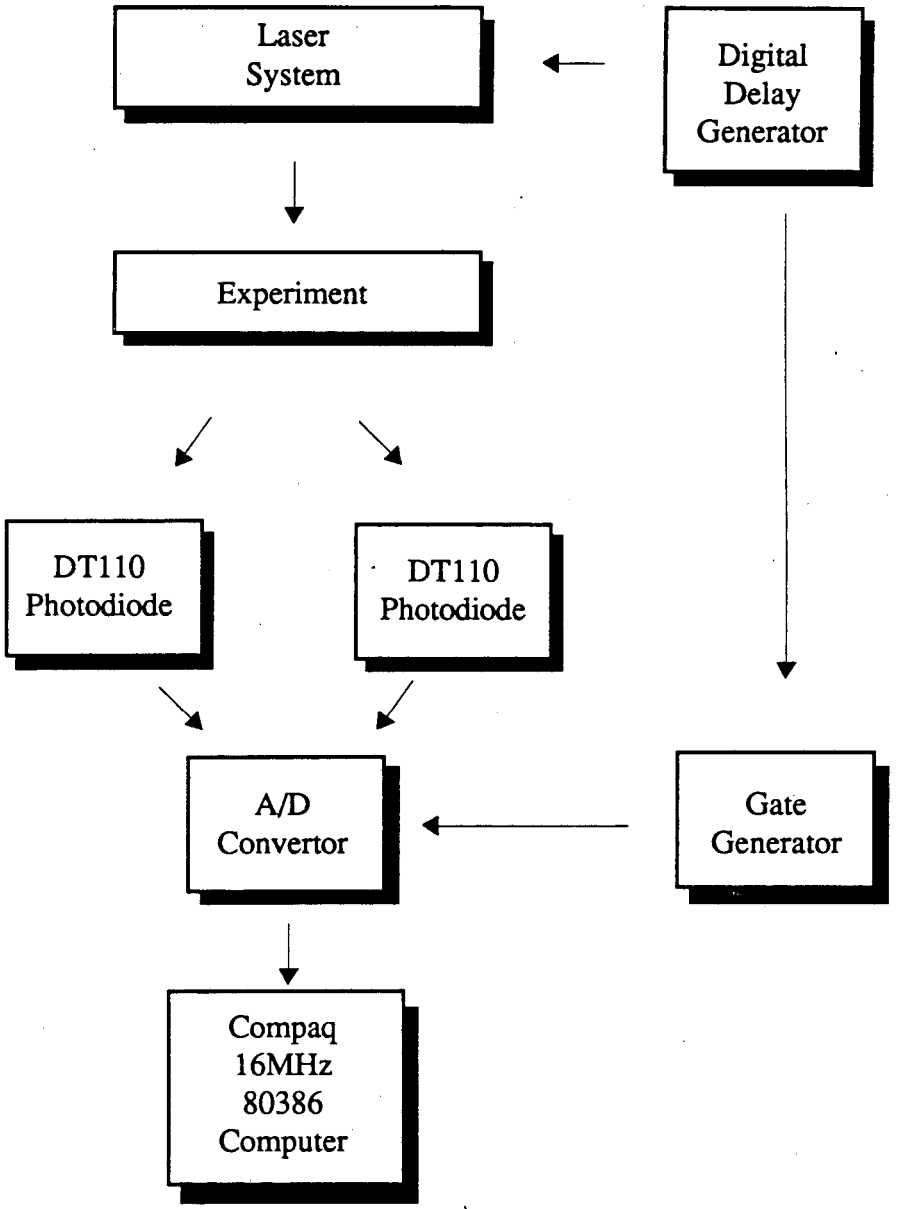

Figure 2.4 Schematic of data collection electronics associated with the femtosecond laser system.

signal to a level where the A/D convertor could detect it. A schematic of the data collection electronics is shown in figure 2.4.

2.3 Results

Transient absorption spectra were recorded as a function of relative polarization between pump and probe beams, and as a function of probe wavelength. Figure 2.5 shows a series of spectra for DPB in hexane as a function of relative pump and probe polarization. For all of these spectra, the pump wavelength was 310 nm and the probe wavelength was 620 nm. In figure 2.5a the pump and probe beams were polarized parallel relative to each other. For the spectrum in figure 2.5b the polarizations were perpendicular and for figure 2.5c at the magic angle, 54.7°, relative to each other. The function used to fit the data taken with perpendicularly polarized beams is a single exponential decay and a single exponential rise, convoluted with a gaussian pulsewidth. The fit is shown in figure 2.6. The results are summarized in table 2.1.

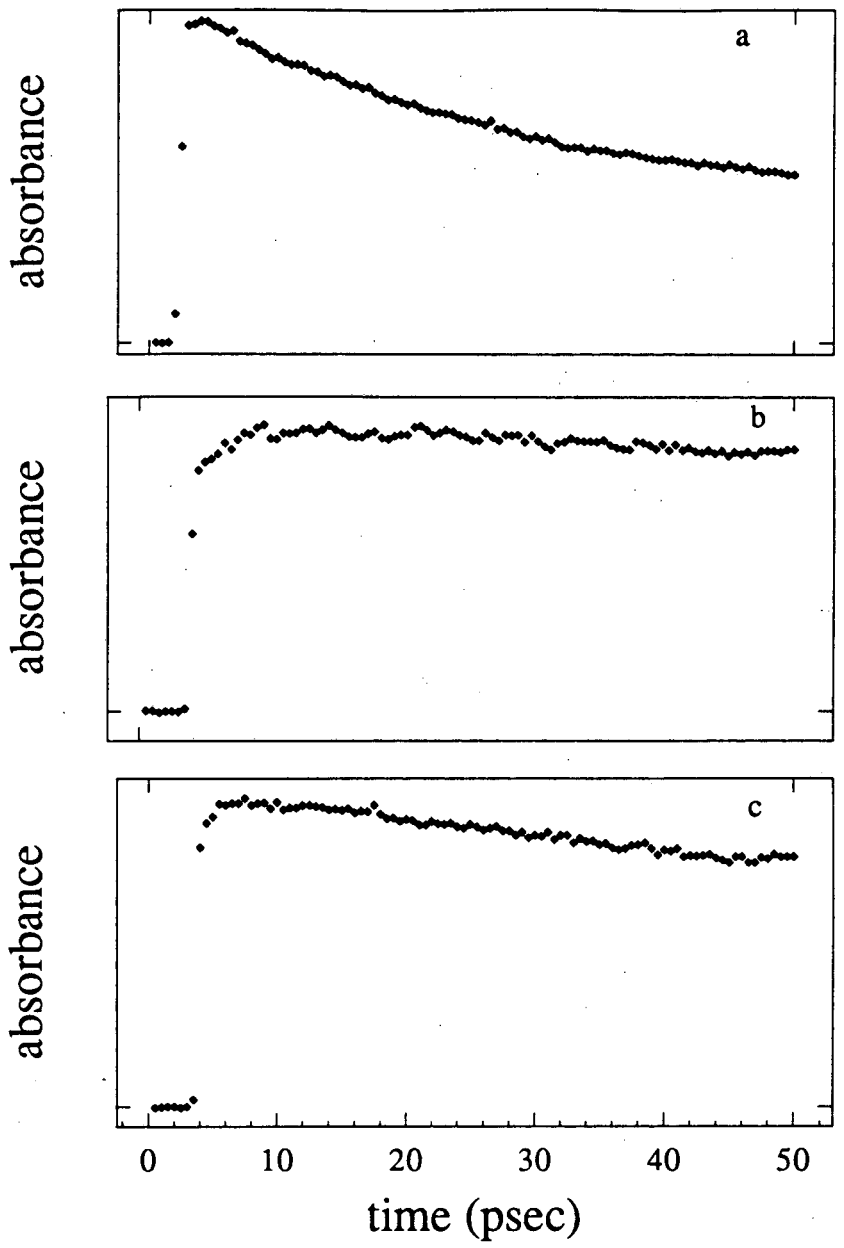

Figure 2.5 Transient absorption spectra for DPB in hexane as a function of relative polarization between pump and probe beams. In 2.5a, pump and probe polarized parallel; 2.5b, pump and probe perpendicularly polarized; 2.5c, polarizations at magic angle (54.7°)

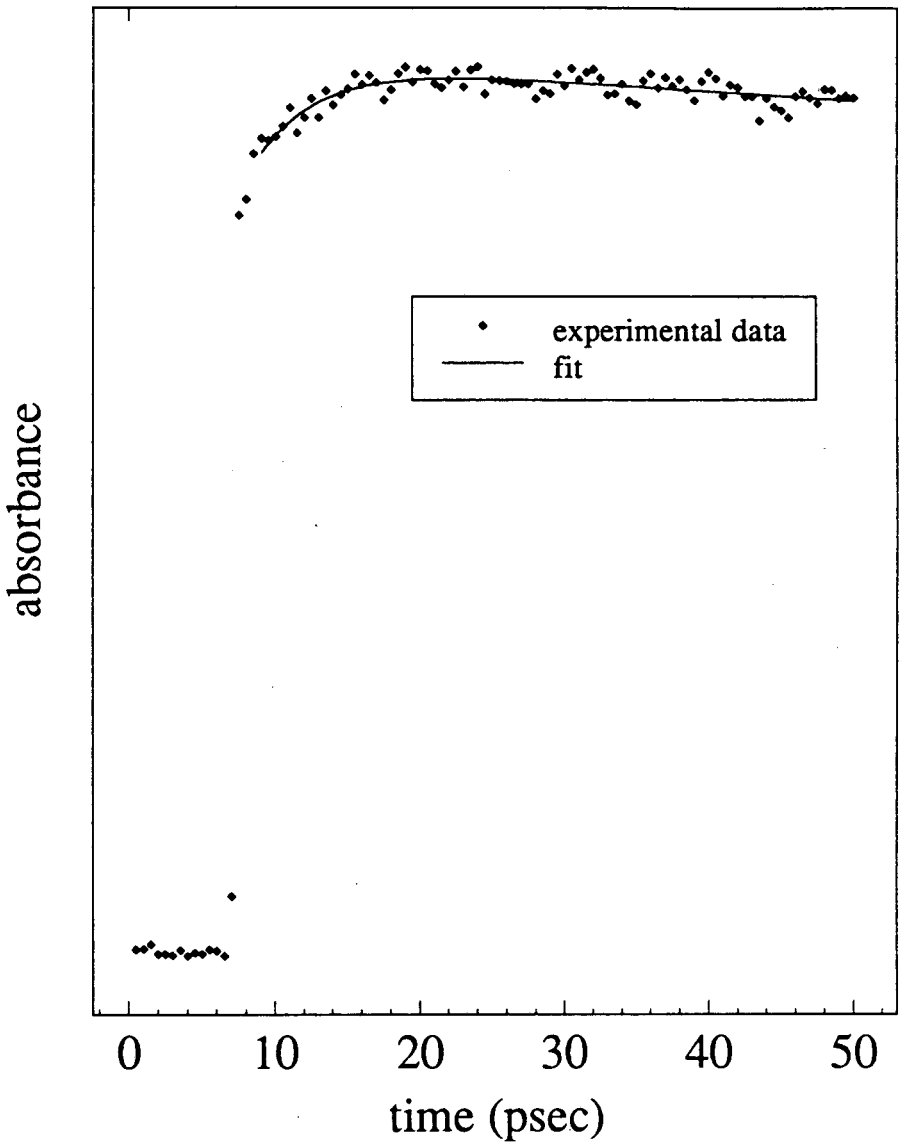

Figure 2.6 Transient absorption spectrum of DPB in hexane.

Table 2.1 DPB Polarization Dependence		
fitting parameter → relative polarization ↓	rise-time (psec)	decay-time (psec)
perpendicular	19	130
parallel	none	70
magic angle	none	180

The decay time is much longer than can be reliably fit using a 50 psec long scan, so the decay time fits should only be used as an indication of the order of magnitude of the actual value.

In order to determine whether one or two-photon processes are responsible for the signal observed using the femtosecond laser system, the power dependence of the amplitude of the transient absorption signal was determined. Spectra were obtained using the full UV beam power, and an 8% signal was observed. Cutting the UV power by a factor of two with an O. D. 0.3 calibrated silica neutral density filter cut the signal size to 4%. We can therefore conclude that the signal is due to one-photon absorption.

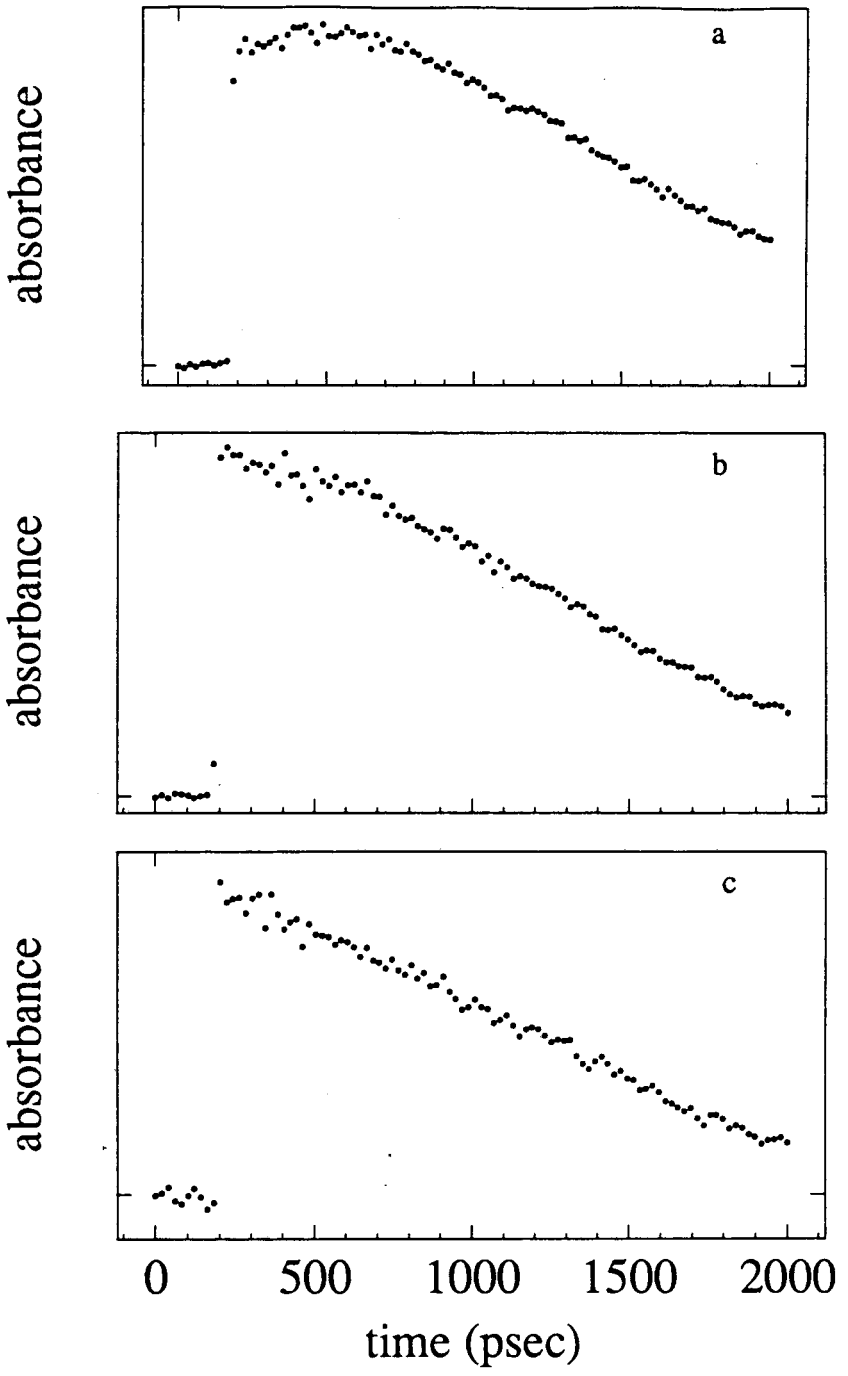

Figure 2.7 Transient absorption spectra of DPB as a function of pump pulse intensity. The pump intensity for figure 2.7b is half that for 2.7a, and the pump intensity for figure 2.7c is half that for 2.7b.

Experiments were performed using the picosecond laser system to determine the effect of very high UV excite intensities on the shape of the transient absorption decay signal. These conditions more closely approximate those under which Rulliere, et. al. obtained their data. For these experiments the excite wavelength is 295 nm and the probe wavelength is 610 nm. The spectra observed as the excite power is varied are shown in figure 2.7. The spectrum in figure 2.7a was taken using the full UV power, about 100 μJ, for figure 2.7b a calibrated neutral density filter of optical density 0.3 was placed in the UV beam, and for figure 2.7c, another N.D. 0.3 filter was added. The shape of the decay is distorted at high intensity, with a slow rise growing in, similar to that observed by Rulliere, et. al..

In order to determine if there is any wavelength dependence to the decay time, spectra were recorded for probe wavelengths of 620 nm and 680 nm. For all of these experiments the excite wavelength is 310 nm. The relative polarization of the two beams was not adjusted, so the primary orientation is with the two beams perpendicularly polarized, although the polarization of the probe beam is significantly scrambled during the continuum generation process. Spectra taken with probe wavelengths of 620 nm and 698 nm are shown in figures 2.8a, and 2.8b respectively. The data was fit using a single exponential decay. The fitting parameters for the two probe wavelengths are summarized in table 2.2. There is no

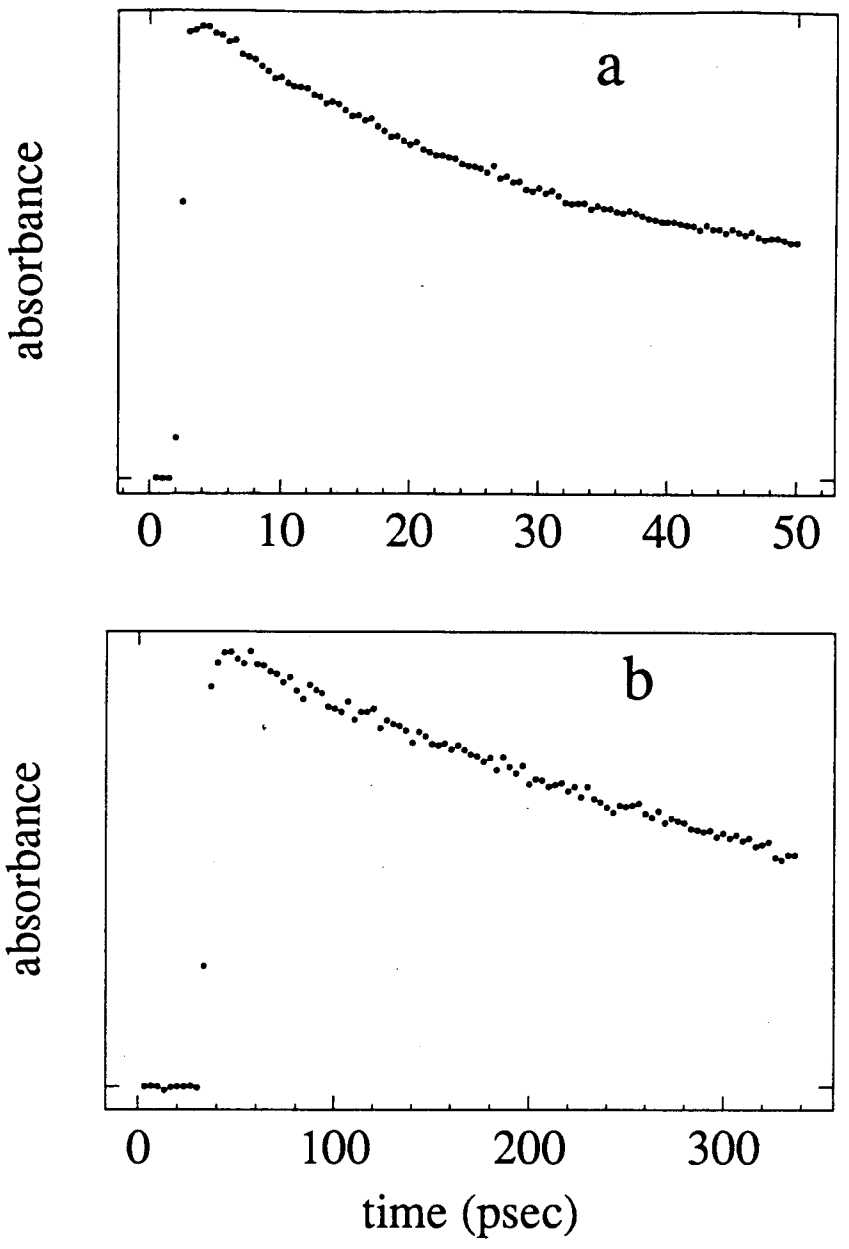

Figure 2.8 Transient absorption spectra of DPB in hexane as a function of probe wavelength. Probe wavelengths for the spectra are a) 620nm, and b) 680nm. Fitting parameters are summarized in table 2.2.

significant difference between the time constants used to fit the two spectra.

Table 2.2 DPB Wavelength Dependence	
Probe Wavelength (nm)	Decay Time (psec)
620 nm	460
680 nm	470

2.4 Discussion

In order to address the questions raised by Rulliere, et. al. in their paper[18, 62], there are several experiments to be done. The first is to reproduce the time-dependence of the transient absorption signal. The second is to look at the wavelength dependence of the transient absorption signal. A third set of necessary experiments is to look at the intensity dependence of the amplitude of the transient absorption signal.

Rulliere and coworkers measured the transient absorption spectrum of DPB in methylcyclohexane (MCH) at 20°C and found wavelength dependent dynamics. They found two maxima, a peak at 625 nm and a shoulder at 680 nm. The intensity of the band at 625 nm was found to reach its maximum intensity in about 80-100 psec. This 80 psec risetime is slightly slower than their 25 psec pulsewidth. The band at 690 nm was found to grow in more slowly, taking about 100 psec to fully appear. Both bands were found to decay in 700+/-100 psec.

The transient absorption signal we obtained using a 310 nm pump pulse and a 620 nm probe pulse looks very different from what Rulliere observed. For spectra where the beam polarizations are either parallel or at magic angle relative to each other, we observe a pulsewidth limited risetime, followed by a single exponential decay with a 460 psec decay time constant. The only evidence we see of a slow risetime occurs when the pump and probe beam polarizations are perpendicular to each other. We do not see any decays on a 700 psec timescale.

The nature of the rise of the transient absorption signal for DPB varies depending on the relative orientation of the polarizations of the pump and probe beams. The pattern we see of a pulsewidth limited risetime combined with a slower risetime when the polarizations of the excite and probe beams are perpendicular, and no slow risetime when they are either parallel or at the magic angle relative to each other is

characteristic of a molecular rotational diffusion process. When a molecule is initially excited, its transition dipole moment lies along the direction of the polarization of the exciting laser beam. If the probe beam is also polarized along that direction, then the molecule can immediately begin to absorb the probe. However, if the probe polarization is initially perpendicular to the transition dipole moment the molecule must rotate to align the polarization and the transition dipole before absorption can take place.

Waldeck, et. al. measured the rotational diffusion time of DPB in tetradecane.[27] They determined that the rotational diffusion of DPB fits well to 66 psec/cP. For hexane, the viscosity is 0.311 cP, so the rotational diffusion should be 19.4 psec. This agrees with our data very well.

We measured the transient absorption dynamics of DPB using probe wavelengths over the range of 620 nm to 680 nm. The transient absorption spectra were identical for all wavelengths over that range. No slow decay component was observed to grow in at the longer wavelengths. The absence of any wavelength dependence is an important difference between the two studies.

Rulliere, et. al. also observed changes in the absorption spectrum which did not depend linearly on the intensity of the excite beam, particularly at low temperatures. At relatively low excite intensity, the shape of the absorption spectrum was independent of the excite intensity. However, at relatively

high excite intensities, they report that as the excite intensity is increased, the amplitude of the 625 nm band increases quadratically at the expense of the 690 nm band. This indicates that they are observing two-photon processes. They claim that this does not conflict with their proposed mechanism by explaining their data in the following way: the first photon excites the DPB molecule to the $^1B_{1u}$ state, where it can relax via internal conversion to the lower excited $^1A_{1g}$ state. The second photon excites the DPB from the $^1A_{1g}$ state to a higher excited singlet state. The DPB molecule then relaxes via internal conversion from this highly excited singlet state to the $^1B_{1u}$ state. The absorption of the second photon therefore increases the population of the $^1B_{1u}$ state at the expense of the $^1A_{1g}$ state.

Our femtosecond experiments showed no evidence of two-photon processes occurring. This is probably due primarily to the fact that by exciting DPB at 310 nm, we are near the maximum of the absorption band and therefore do not need high UV intensities to obtain good signal to noise ratios. Rulliere, et. al. use either 353 nm or 265 nm light for their excitation source; both wavelengths are in the very wings of the ground state absorption band. Consequently, they must use a much more intense excite pulse to obtain good signal to noise than is required at the 310 nm excitation wavelength used in our experiments.

The possibility of multi-photon processes occurring was further investigated using the high intensity pulses from the picosecond laser system as the excitation source. The shape of the transient absorption decays obtained were distorted, with a slow rise growing in at high intensity. The decay curves look much like those obtained by Rulliere. This strongly suggests that their spectra are distorted by multi-photon absorptions. The data taken using the femtosecond laser system is not complicated by the presence of multi-photon effects.

The shape of the absorption spectrum was determined by Rulliere to be temperature dependent. At a temperature of -80°C, the absorption was dominated by the 690 nm band. At 30°C the absorption was dominated by the 625 nm band. Both of those measurements were made at a time delay of 100 psec after the excite pulse. We did not attempt to reproduce these results.

They explain their data by invoking a solvent assisted level inversion. They claim that the molecule is initially excited to the second excited singlet state, which is the $^1B_{1u}$ state. Molecules excited to this state give rise to the 625 nm transient absorption. At very low temperatures, the solvent is frozen and cannot reorganize to invert the levels, consequently the only band seen at low temperatures is the 625 nm band. At room temperature, the 625 nm band decays as the 690 nm band grows in. This is attributed to solvent-assisted

level inversion, with the 690 nm band assigned to absorption from the $^1A_{1g}$ state. In liquid solution, the DPB molecule and the solvent molecules can quickly reorient, and as they do so the two energy levels invert. They suggest that for DPB, a phenyl-ring rotation is the important motion for the level inversion. At this point, the $^1B_{1u}$ state is trapped below the $^1A_{1g}$ state. The two states are close enough in energy that the $^1A_{1g}$ state is then thermally populated to a significant extent. This explains the temperature dependence of the relative intensities of the two states. Since the two states are very close together, there is a Boltzmann distribution of energies between the two states, and the two peaks should decay with the same time constant, as observed.

Several theoretical and experimental papers have addressed the question of whether molecular isomerization is occuring and if so, what is the nature of the isomerization process. Molecular beam studies show a sharp break in a plot of quantum yield as a function of excitation energy, indicating the onset of isomerization.[8,28] A region of the absorption spectrum with no vibrational structure may also be a manifestation of an isomerization process.[28, 12] Calculations by Rulliere, et. al. indicate that the state ordering depends strongly on the angle of the phenyl ring, θ, with $\theta = 0°$ corresponding to $^1B_{1u}$ as the first excited singlet, and $\theta = 75°$ corresponding to $^1A_{1g}$ as the first excited singlet.[17] They claim that in the ground state, steric hinderence forces the

(a)

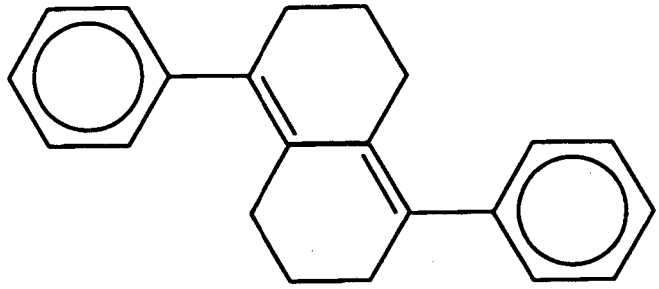

(b)

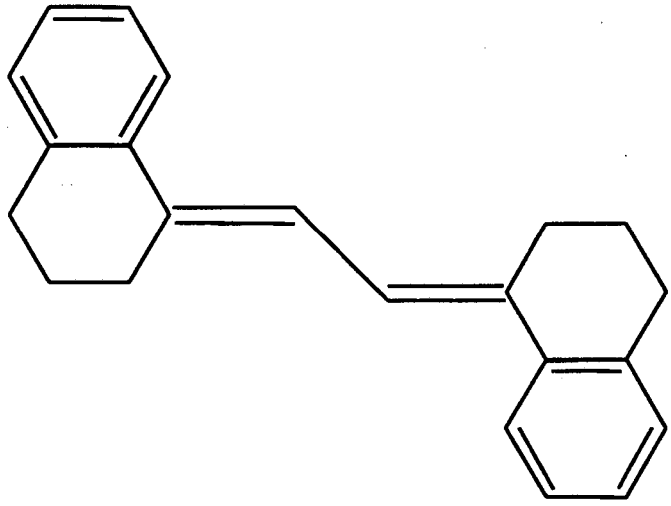

Figure 2.9 Molecular structures of the two stiff-DPB analogues. Fig. 2.9a is 1,5-diphenyl-2,3,4,6,7,8-hexahydronaphthalene. Fig. 2.9b is diphenylbutadiene with the phenyl-rings held rigid by rings of between five and seven carbon atoms.

phenyl group out of plane, and that the increased conjugation in the excited state pushes the phenyl-ring toward the polyene plane. Experiments on a stiff analogue of DPB, 1,5-diphenyl-2,3,4,6,7,8-hexahydronaphthalene shown in figure 2.9a, indicate, due to their similarity to DPB results, that relaxation of DPB is from an excited state where the polyene backbone is nearly planar.[29] In that case, the isomerization would have to be attributed to a phenyl-ring rotation. However, experiments on another "stiff-DPB" analogue, diphenylbutadiene with the phenyl-rings held rigid by rings of between five and seven carbon atoms, suggest that phenyl-ring rotation is unimportant.[30] These results indicate that the isomerization can be represented by a one-dimensional potential well, which suggests that only one motion is important for the isomerization.

Although our data is consistent with a solvent-assisted energy level inversion, the complicated explanation proposed by Rulliere, et. al. is not necessary for a consistent explanation of our data. Our data can be explained simply by excitation to the $^1B_{1u}$ state from which a transient absorption takes place. The transient absorption decays with a time constant characteristic of the fluorescence time of the DPB molecule. The isomerization rate can be extracted from the experimentally measured fluorescence time, which is a combination of the radiative and nonradiative relaxation rates, by using the following equation:

$$k_{iso} = k_f - k_r \qquad (2.1)$$

2.5 Conclusions

Our data differs greatly from that taken by Rulliere, et. al.. Our spectra at all of the wavelengths studied are fit very well by a pulsewidth-limited risetime and a single exponential decay. We do not see any slow risetimes, other than a single exponential rise due to molecular rotational diffusion, or any differences between the data taken at different wavelengths. Although our data does not rule out the possibility of a solvent-assisted level inversion, we do not need to invoke an inversion to explain the data. We see no evidence to support Rulliere's claims of solvent assisted level inversion. Our data is consistent with the $^1B_{1u}$ state being below the $^1A_{1g}$ state, in agreement with the results of the fluorescence measurements and calculated values.

2.6 References

1. B. S. Hudson, B. E. Kohler, K. Schulten, in Excited States, Vol. 6, E. C. Lim, Ed., Academic Press: New York, 1982

2. J. Saltiel and J. L. Charlton in Rearrangements in Ground and Excited States, P. Mayo, Ed.; Academic Press: New York, 1980 vol. 3

3. B. S. Hudson and B. E. Kohler, Chem. Phys. Lett., **4**, 299 (1972)

4. J. A. Bennett and R. R. Birge, J. Chem. Phys., **73**, 4234 (1980)

5. R. L. Swofford and W. M. McClain, J. Chem. Phys., **59**, 5740 (1973)

6. R. L. Swofford and W. M. McClain, Rev. Sci. Instr. **46**, 246 (1975)

7. D. J. S. Birch and R. E. Imhof, Chem. Phys. Lett., **88**, 243 (1982)

8. J. F. Shepanski, B. W. Keelan and A. H. Zewail, Chem. Phys. Lett., **103**, 9 (1983)

9. R. A. Goldbeck, A. J. Twarowshi, E. L. Russell, J. K. Rice, R. R. Birge, E. Switkes, and D. S. Kliger, J. Chem. Phys., **77**, 3319 (1982)

10. Ch. Gehrke, J. Schroeder, D. Schwarzer, J. Troe, and F. Voss, J. Chem. Phys., **92**, 4805 (1990)

11. S. P. Velsko and G. R. Fleming, J. Chem. Phys., **76**, 3553 (1982)

12. J. B. Birks and D. J. S. Birch, Chem. Phys. Lett., **31**, 608 (1975)

13. R. Wilbrandt, N. H. Jensen, and F. W. Langkilde, Chem.Phys. Lett., **111**, 123 (1984)

14. T. L. Gustafson, J. F. Palmer, and D. M. Roberts, Chem. Phys. Lett., **127**, 505 (1986)

15. J. Leclercq, and J. M. Leclercq, Chem. Phys. Lett., **57**, 54 (1978)

16. P. Tavan and K. Schulten, Chem. Phys. Lett., **56**, 200 (1978)

17. C. Rulliere, A. Declemy, Ph. Kottis, and L. Ducasse, Chem. Phys. Lett., **117**, 583 (1985)

18. C. Rulliere, A. Declemy and Ph. Kottis, Laser Chem., **5**, 185 (1985)

19. R. L. Fork, B. I. Greene, and C. V. Shank, Appl. Phys. Lett., **38**, 671 (1981)

20. W. H. Knox, M. C. Downer, R. L. Fork, and C. V. Shank, Optics Letters, **9**, 552 (1984)

21. M. Berg, Ph.D. thesis, University of California at Berkeley (1985)

22. A.L. Harris, Ph. D. thesis, University of California at Berkeley (1985)

23. J. Chen, Y. Cao, B. Zhang, and Y. Ming, Huaxue Xuebao, **43**, 601 (1980)

24. S. J. Hug, W. A. Yee, and D. S. Kliger, Chem. Phys. Lett., **168**, 385 (1990)

25. E. Hecht, Optics, (Addison-Wesley Publishing Co., 1987)

26. H. E. Lessing, A. v. Jena, and M. Reichert, Chem. Phys. Lett., **36**, 517 (1975)

27. D. H. Waldeck, W. T. Lotshaw, D. B. McDonald, and G. R. Fleming, Chem. Phys. Lett., **88**, 297 (1982)

28. A. Amirav, M. Sonnenschein, and J. Jortner, Chem. Phys., **102**, 305 (1986)

29. W. A. Yee, J. S. Horwitz, R. A. Goldbeck, C. M. Einterz, and D. S. Kliger, J. Chem. Phys., **87**, 380 (1983)

30. M. Lee, J. N. Haseltine, A. B. Smith III, and R. M. Hochstrasser, J. Am. Chem. Soc., **111**, 5044 (1989)

Chapter 3

Excited State Reaction Dynamics of Tetraphenyl-butadiene and Tetraphenyl-methylbutadiene

3.1 Introduction

The accurate prediction of the rate of a chemical reaction is one of the most important problems in the field of chemical dynamics. In the gas phase, the outcome of a reaction depends only on the reactants themselves. The reaction rates are frequently described by transition state theory with relative success. In a liquid the effects of the solvent molecules on the reaction process must be considered. The solvent molecules constantly interact with the solute, affecting its reaction rate by acting as an energy source and sink and by altering the solute potential energy surfaces. Transition state theory fails to describe chemical reactions in liquids. The most common approach to predicting reaction rates in liquids is to treat the reaction process as diffusion on a potential surface. The simplest quantitative description of this process is known as Kramers' theory.

Although Kramers' theory is commonly used to describe chemical reaction rates, it is not clear whether it is the proper description for liquid-phase reactions. Various theoretical models have been proposed for calculating reaction rates in liquids,[1,2] and have been compared with the results of many experiments, however it is still not clear how important a role the solvent-solute interactions play in determining the reaction rate and how to properly account for those interactions. An accurate description of liquid-phase reactions on a microscopic level is the goal of a large number of studies on isomerization reactions.

Isomerization reactions of the triphenyl-methane dyes and the diphenyl-polyenes are commonly used as probes for investigations of liquid-phase reaction dynamics for several reasons. They are very simple unimolecular reactions, and therefore the results are not complicated by the need for molecules to diffuse through solution or attain a certain relative geometry before reacting. These two classes of molecules complement each other since the isomerization of triphenyl-methane dyes is a barrierless process, while the diphenyl-polyenes have a barrier to isomerization. This difference permits investigation of two classes of liquid-phase reaction rate theories. The spectroscopy of the diphenyl-polyenes has been extensively studied, so the nature of the electronic potential surfaces is fairly well known, providing a solid basis for interpreting the transient

absorption spectra. Studying the isomerization process of the diphenyl-polyenes is itself interesting since it serves as a model for biologically important isomerization reactions such as the first step in the vision process.

This chapter describes an investigation of the reaction dynamics of tetraphenyl-butadiene and tetraphenyl-methylbutadiene. The ultimate goal of these experiments is to test the validity of liquid-phase reaction rate theories, and to pinpoint which aspects of the theories work and which do not. Section 3.2.1 explains Kramers' theory, the theory which is most commonly used for calculating reaction rates in liquids, and some of the modifications and extensions of that theory. Section 3.2.2 describes the molecular system we have chosen for testing these theories and an explanation of that choice. Section 3.3 describes the experimental procedure. The data are presented and discussed in section 3.4. Finally the theories we have developed to explain the data are presented and discussed.

3.2 Background

3.2.1 Kramers' theory

In 1940, H. A. Kramers developed a theory for calculating reaction rates in solution.[3] This theory, commonly referred to as Kramers' theory, has recently been treated in a review

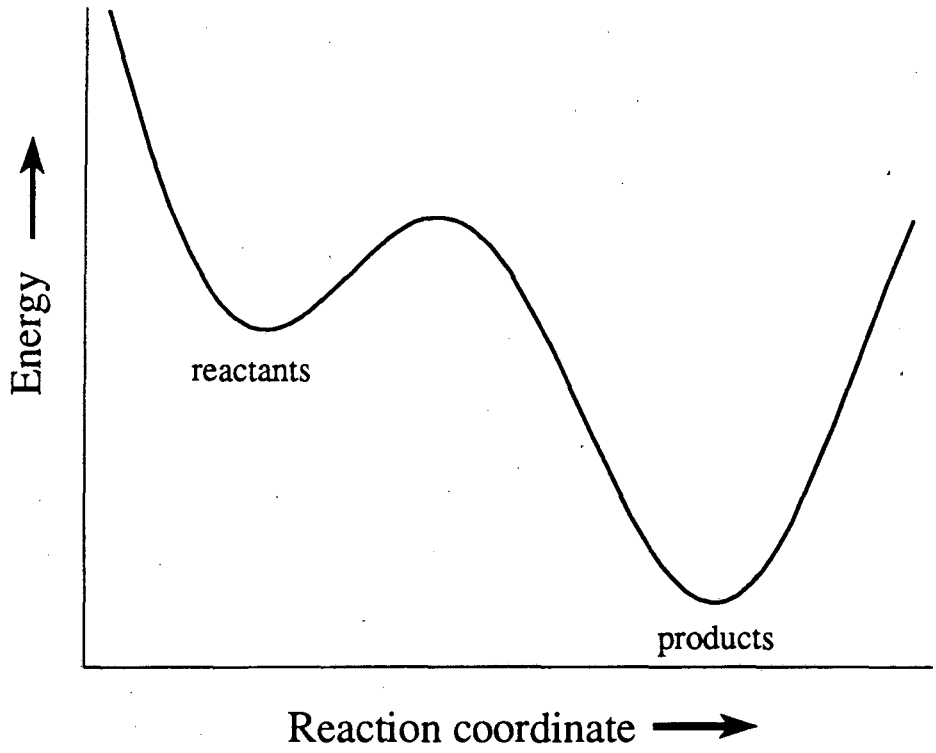

Figure 3.1 Potential energy surface for Kramers' theory

of chemical reaction rate theories.[4] Kramers' theory treats a chemical reaction as a diffusional motion along a one-dimensional potential energy surface, U(x), where x corresponds to the reaction coordinate. The reaction surface, shown in figure 3.1, is an asymmetric double well potential and the reactive motion proceeds from left to right. The theory is general, and can be applied to many different reactions, however for the sake of simplicity this discussion will describe the theory in terms of isomerization reactions.

The idea of diffusional motion on a potential surface has a very physical basis. During a reaction in a liquid, the force a molecule encounters can be viewed as consisting of three parts. The first is the force due to its own internal molecular potential. The second is a retarding frictional force on the molecule due to its interactions with the surrounding solvent molecules. The third is a random, fluctuating force due to collisions with the solvent molecules. These solvent forces prevent the molecule from following a well-defined trajectory, as it would in the gas phase where the internal molecular potential is the only force on the molecule.

In general, diffusional motion can be described mathematically by the Langevin equation,[5]

$$F=ma=-\xi u+A(t)+K(\theta)$$

the basis of which is Newton's equation. The force on the molecule is assumed to be accurately described as the sum of three terms, ξu, a retarding, frictional force due to interactions with the solvent; $A(t)$, a random, fluctuating force due to collisions with the solvent; and $K(\theta)$, the force due to the internal molecular potential. As in any physical process, energy is conserved, so the amount of energy the molecule gains from collisions with the solvent is equal to the amount of energy it loses to the solvent due to the frictional interactions. This is stated mathematically by the fluctuation-dissipation theorem:

$$\xi = \frac{m}{kT}\int_{-\infty}^{\infty} \langle A(0)\cdot A(t)\rangle dt$$

It is important to remember that since the Langevin equation is a stochastic differential equation, it can be solved only for the probability distribution of position and velocity.

There are several assumptions inherent in Kramers' theory. First, the potential barrier is piecewise parabolic. Second, the potential surface is one-dimensional, meaning that the reactive motion corresponds to a single molecular motion. It is assumed that the barrier to reaction is high enough that there is a Boltzmann distribution in the reactant well. It is

also assumed that there is no appreciable back reaction. Finally, the reaction is a Markovian process.

Formally, Kramers' theory is the solution of the Langevin equation using the Fokker-Planck equation.[5] The Fokker-Planck equation is used to calculate the time evolution of the probability density of a Brownian particle in phase space. Kramers assumed that there exists a time, τ, short enough that the velocity of the molecule at time $t + \tau$ is the same as at time t, but long enough that $A(t + \tau)$ is independent of the value of A(t). This assumption is necessary for an analytical solution of the Langevin equation using the Fokker-Planck equation. The Langevin equation can be solved analytically in two limits, low friction and high friction.

The low friction limit corresponds to the gas phase limit. In this extreme, often referred to as the inertial regime, collisions are infrequent and the reaction rate is controlled by energy diffusion. Consequently, the reaction rate increases as the viscosity, and concomitantly the collision frequency, increases. The mathematical description of the reaction rate in this limit is given by:

$$k_{iso} \propto \left(\frac{\eta}{T}\right) e^{(-E/RT)}$$

where η is the solvent viscosity.

The high friction limit corresponds to liquid phase densities, and is often referred to as the diffusive regime. In this limit, which applies to the work presented in this chapter, energy is transferred efficiently between molecules, but it is difficult for molecules to move around. In order for the isomerization to proceed, solvent molecules must be moved out of the way, so as the viscosity increases the reaction rate decreases. In this limit, the reaction rate is given by:

$$k_{iso} = \left(\frac{\omega_r \xi}{4\pi\omega_b} \right) \left\{ \left[1 + \left(\frac{2\omega_b}{\xi} \right)^2 \right]^{1/2} - 1 \right\} e^{(-E/kT)} \qquad (3.1)$$

Where ω_r is the frequency of the reactant well, ω_b is the frequency of the activation barrier, E_b is the activation energy, and ξ is the frictional constant. In this regime, the reaction rate decrease is a non-linear function of viscosity.

At very high viscosities, the frequency of the reactive motion, characterized by ω_b, is relatively small, and the transition from reactants to products is slower than the frictional response of the solvent. In the limit where $\xi > 2\omega_b$, the reaction rate is represented by the Smolochowski equation. The reactive motion in the very high viscosity limit is therefore strongly coupled to the solvent friction, and it is likely that the zero frequency friction is an adequate

description of the frictional force felt by the molecule. This means that the friction varies linearly with viscosity and is described by the Stokes-Einstein-Debye relation, which is discussed later, and the reaction rate decreases linearly as a function of viscosity. The following equation describes the isomerization rate in the Smolochowski limit:

$$k_{iso}=\left(\frac{\omega_r\omega_b}{2\pi\xi}\right)e^{(-E/kT)}$$

In between the high viscosity and low viscosity limiting cases, there is a region where the reaction rate is predicted to change smoothly from increasing with increasing viscosity to decreasing with increasing viscosity. This change is referred to as Kramers' turnover. This turnover region has been treated theoretically by several workers. Carmeli and Nitzan have developed an analytic theory which is valid at all viscosity values, and bridges the turnover region, giving the Kramers result at the high and low viscosity limits.[6] Another theory which bridges the turnover region uses a stochastic collisional model.[7] Skinner and Wolynes use interpolation to bridge between the high and low friction Kramers limits.[1]

Early attempts to observe this turnover in rate were unsuccessful. For DPB in ethane[8] down to a viscosity of 0.039 cP and for stilbene in ethane[9] down to a viscosity of 0.06 cP the isomerization rate was still increasing with decreasing

viscosity. In order for the reaction rate to begin to decrease with decreasing viscosity, a point must be reached at which energy transfer between the solvent and the solute is the rate-limiting step. These results suggest that intramolecular vibrational energy redistribution occurs very quickly, and the amount of thermal energy available is large enough that sufficient energy reaches the reaction coordinate too rapidly for the turnover in rate to be observed.[8] This idea has been quantified theoretically.[10,11]

Since that time, reports of experimental observations of Kramers' turnover region have been published. It was first observed by Jonas, et. al. using high-pressure NMR techniques to study the ring inversion of cyclohexane in solution.[12,13] They observed the turnover at the surprisingly high viscosity of 2.5 cP. These results have been questioned in the literature.[14] It is not clear that Kramers theory is applicable to this data since the small amplitude of the motion and the small mass involved in the motion mean that this reaction cannot really be described as Brownian motion.[15] However, the results have been found to fit a stochastic collisional model[16] and a generalized Langevin equation model[11] quite well. Jonas and coworkers were unable to see the Kramers turnover for 1,1,-difluorocyclohexanae, suggesting that the interaction of the dipole moment with the solvent results in long range forces which prevent the turnover.[17] Kramers' turnover has also been recently

observed by measurements of the fluorescence decay rate of stilbene in supercritical fluid ethane.[18] The turnover was observed at a viscosity of 0.03 cP. This corresponds to approximately 200 collisions before the stilbene molecule relaxes.

A large number of experiments have been performed for comparison with the predictions of Kramers' theory.[9,28, 12,13,14,15,18,19,11, 20,21,22,10, 23,24,25,26,27,28,29,30,32,33,34,35] Inherent in virtually all of the experiments is the assumption that isomerization is the primary route for non-radiative decay. Most of the work has been done using the diphenyl-polyenes, in particular stilbene and diphenyl-butadiene, as probes[19,20,21,22,23,24]. The Kramers' rate equation for reactions in high viscosity solvents (equation 3.1) can be rewritten as:

$$k = F(\xi)\, e^{(-E/kT)}$$

since the pre-exponential term is a function only of solvent viscosity, and the exponential term contains all of the temperature dependence. Two types of experiments are commonly used to test Kramers' theory. The first measures the effect of temperature on the reaction rate at constant viscosity to make an Arrhenius plot.[11, 20] The other consists of measuring the reaction rate as a function of solvent viscosity at

constant temperature. The other parameters in Kramers theory are then varied to obtain the best possible fit to the experimental data.

It is found that for stilbene and DPB, the experimentally determined reaction rate decreases more slowly with increasing viscosity than is predicted by Kramers' theory, although for very low viscosity, Kramers' theory fits well.[10, 23] In addition to the stilbene and DPB experiments, experiments using a variety of other probe molecules, including substituted stilbenes,[57,58] binaphthyl[25,26,27,28,29], anthracene derivatives[30,31], DODCI[32], and other dye molecules[33,34,35] have also been published. Kramers theory does not fit the isomerization of DODCI in alcohols[32, 33], the anthracene derivatives, or 1,1'-binaphthyl in alcohols.[29] It does, however, fit the data for binaphthyl in an alcohol series very well.[28]

In many instances, the data has been found to fit well to an equation in which the pre-exponential factor is inversely proportional to a power of the viscosity:

$$k_{iso} = (B/\eta^a)\, e^{(-E/RT)}$$

This model has been found to work well for DPB[8], stilbene[9], substituted stilbenes[57,58], and DODCI[32, 33]. The power law form

is predicted by a kinetic model for which the Langevin equation is solved.[36]

A variety of reasons have been proposed for the discrepancies between Kramers' theory and experimental data. First, it is possible that interactions with the solvent molecules affect the potential barrier. In their experiments on stilbene and DPB in gaseous and liquid ethane, Maneke et. al. observed that their data, obtained by varying the pressure of the solvent, was fit very well by a "cluster model" in which there is a solvent induced barrier shift due to solvent compression.[37,38] Measurements of the activation barrier of stilbene in n-alkanes show that the activation energy varies slightly as the viscosity of the solvent is changed, with larger barriers at higher viscosity. The origin of the differences remains unclear.[57] For experiments done in polar solvents, such as alcohols, it has been observed that the solvent does alter the barrier significantly.[35]

Another possibility is that hydrodynamics, which assumes that the solute molecule is much larger than the solvent molecules, and therefore that the solvent can be treated as a continuum, is not applicable. The hydrodynamic assumption is not an inherent part of the derivation of Kramers' theory, however it is commonly used due to its simplicity. In hydrodynamics, the friction is assumed to be proportional to the solvent viscosity, and the relationship between the two is given by the Stokes-Einstein-Debye (SED) equation:

$$\xi = (4\pi dr^2/I)\,\eta$$

where I is the moment of inertia, d is the hydrodynamic radius of the molecule, and r is the radius of gyration of the molecule. The SED relation presented above is calculated assuming slip boundary conditions.[39]

Molecular rotational reorientation times have been used to test the validity of the SED relation on a microscopic scale. Experiments for stilbene and DPB in alkanes indicate that the hydrodynamic approximation breaks down for solvents longer than the solute molecule.[24] For aniline in hydrocarbon solvents the SED equation also did not fit.[40] The SED equation does not properly describe the dynamics of the doubly charged Rhodamine 6G in alcohol[41], although is does work for the singly charged DODCI molecule in alcohols.[42] The SED relation was found to work well for p-terphenyl in alcohols[41], and for 9,10-diphenylanthracene in alkanes, but not alcohols.[43] The reorientation was twice as fast in alcohol solvents, contrary to intuition. This was explained to be due to one of two effects, one dynamic the other static. Hydrogen bonding in alcohols results in correlated motions of clusters, which means solvent fluctuations are slow. If the rotation is faster than the solvent fluctuations, the molecule feels no damping force. According to the static explanation, hydrogen bonding creates cavities in which the solute sits, and where

it feels a smaller friction. The large molecule BTBP was found to fit well to SED behavior.[44] No consensus has yet been reached on the validity of the SED for describing the microscopic friction felt by intermediate-sized molecules.

One technique for obtaining a more realistic value for the friction is to measure the microscopic friction directly. This value can then be used in Kramers' equation in place of the hydrodynamic friction. One approach is to use a Hubbard relation which relates the friction coefficient to the overall rotational diffusion time of the molecule.[45]

$$\tau_{rot} = \frac{I\xi_{or}}{6kT}$$

The assumption is made that the friction felt by the isomerizing portion of the molecule is proportional to the friction felt by the rotating molecule.

$$\xi_{iso} = p\,\xi_{or}$$

The isomerization of 1,1'-binaphthyl is fit well by the Kramers-Hubbard theory[29]. Data for stilbene[24] and "stiff-DPB"[15,24] can be fit well, but the barrier frequencies are unrealistically small. Kramers-Hubbard theory fits data for DODCI in alcohol solvents very poorly.[32, 33]

The force an isomerizing molecule feels as it crosses the activation barrier depends on the frequency of that barrier,

ω_b. A high-frequency barrier means a large force on the isomerizing molecule, which in turn means that the molecule moves rapidly through the barrier region. Conversely, a low frequency barrier results in slow movement across the barrier. If the solute molecule moves slowly through the barrier region, the solvent molecules have enough time to rearrange completely and the solute feels both high and low frequency components of the solvent rearrangement. However, if the solute moves rapidly across the barrier, low-frequency solvent motions occur on a timescale long by comparison and they do not affect the isomerization. Rephrasing, an isomerizing molecule crossing a high frequency barrier is primarily affected by the high frequency friction components.

This is important for answering the question of whether the isomerization is a Markovian process. One of the assumptions of Kramers' theory is that the timescale for the reactive motion is much slower than the solvent collision frequency, which means that any solvent correlations can be considered unimportant. This is not necessarily a good assumption. Collisions in a liquid occur on a 100 fsec timescale, so for processes occurring on that timescale, correlation effects must be considered. For a high-frequency barrier, correlations in solvent motion are an important factor, since the motion across the barrier is rapid enough that solvent correlations are not yet averaged away. Kramers' theory, which assumes zero-frequency, hydrodynamic friction

and a Markovian system, is not equipped to deal with the problems associated with a high frequency activation barrier.

Grote and Hynes have developed a theory which incorporates frequency-dependent friction effects.[46] Their theory is based on a generalized Langevin equation (GLE).

$$F=A(t)-\int_0^t d\tau\,\xi(\tau)\,v(t-\tau)+K(\theta)$$

where

$\zeta(t)$ = time dependent friction

A(t) = Gaussian random force

The GLE is formally solved by Laplace transformation as an initial value problem, and the rate is given by the self-consistent equations

$$\kappa=\kappa^{TST}(\lambda_r/\omega_b)$$

where

$$\kappa^{TST}=(\omega_R/2\pi)\,e^{-\beta E_0}$$

and

$$\lambda_r = \frac{\omega_b^2}{\lambda_r + \hat{\xi}(\lambda_r)/\mu}$$

where

$$\xi(p) = \int_0^\infty dt e^{-pt} \xi(t)$$

The Grote-Hynes theory has been tested experimentally by measurements on stilbene and found to fit the data better than Kramers' theory.[19] However, in order to fit the data, a barrier frequency of 8 cm^{-1} is needed, which would mean the barrier is virtually flat, a very unphysical assumption.

A basic assumption of Kramers' theory is that the reaction coordinate is one-dimensional. This assumption provides another possible cause for the discrepancies between Kramers' theory and the experimental results, since it seems very likely that in a real molecular system non-reactive motions play an important role in determining the reaction rate. This problem has been addressed theoretically by a number of workers.

One approach has been to look at how the solvent couples reactive and non-reactive modes.[47,48,49] For example, the solvent can couple vibrational and translational modes in a molecule if the frictional force on one atom is greater than

on another. These theories use a generalized Langevin equation in which the friction term is a combination of the direct friction on the reaction mode and the influence of non-reactive modes by the "coupling friction." They find that the reaction proceeds in the direction of least friction, and that as the frictional coupling increases, the increased coupling between modes can increase the reaction rate.[48,49] The coupling effectively changes the reaction coordinate as the friction changes. Another study found that allowing the reactive mode to couple to non-reactive modes was like adding additional friction and noise to the system.[50]

Recently, Agmon and Kosloff solved the time-dependent diffusion equation for the isomerization of stilbene on a two-dimensional potential energy surface.[51] They assume that the reactive motion is the rotation around the carbon-carbon bond, and the non-reactive motion coupled to it is the rotation of a phenyl-ring. They find that the motion on the surface is highly dependent on the viscosity of the solvent. At low viscosities, motion along the reaction coordinate is preferred, while at high viscosities the small amplitude motion along the phenyl twist coordinate is preferred. This means there are two paths the isomerizing molecule can follow, and the net effect of changing the viscosity is to change the reaction coordinate. Motion along the phenyl-ring twist direction facilitates isomerization around the C-C bond. At low viscosity, the existence of a two-dimensional potential

surface has a relatively small impact on the isomerization rate, but at higher viscosity, the phenyl-ring rotation plays a more important role. Their results predict the fractional viscosity dependence which has been observed experimentally.

Experimental evidence also exists for the need to consider a multi-dimensional potential energy surface for the isomerization of stilbene and DBP. Experiments by Kottis, et. al.[18, 62], which were addressed in the previous chapter, suggest that both phenyl-ring and carbon-carbon bond rotation are occurring simultaneously. Molecular beam studies of the vibronic spectrum of stilbene reveal that a significant population exists in vibrational modes related to phenyl motions.[52] The equilibrium geometry of stilbene is planar, however several low frequency modes, including the olefinic carbon (C_o)-phenyl and C_o-C_o-phenyl bending motions and the C_e-phenyl torsional motion, are significantly populated. Transient Raman studies of stilbene in solution have also shown a significant population in the phenyl coordinate.[53,54,55,56] These studies lend credence to the idea that rotation around the olefinic carbon-phenyl bond may occur.

Experiments in which the isomerizing species is constrained to be one-dimensional fit well to Kramers' theory, supporting the role of multi-dimensionality in the stilbene experiments. Lee and coworkers[15] performed experiments using structural analogs of DPB in which the phenyl-rings are

prevented from rotating by the presence of 2-4 carbon atom long chains forming rings between the ortho-carbon on the phenyl-ring and the nearest butadiene carbon. A diagram of the molecule is shown in figure 2.9. The system is thus constrained to a one-dimensional reaction coordinate. They found that by using a friction value obtained with a Hubbard relation, Kramers' theory fit their data very well. Similar results were found for "stiff-stilbene."[19] The isomerization of 1,1'-binaphthyl is clearly one-dimensional and the data in alcohol solvents fits Kramers' theory very well.[28]

Other experiments indicating the necessity of a two-dimensional potential energy surface were performed by Park and Waldeck.[57,58] They measured the isomerization rate as a function of viscosity for a series of substituted stilbenes and fit their data to a power law form. They found that as the size of the phenyl group substituent increases, both the isomerization rate and the viscosity dependence of the isomerization decrease, which they explained qualitatively using arguments very similar to those of Agmon and Kosloff.[51] Because of its small amplitude, the phenyl ring rotation is assumed to be viscosity independent. The carbon-carbon bond rotation rate, assuming no phenyl-ring rotation, has an inverse viscosity dependence. Those two factors combine to form a two-dimensional rate in the following way. At low solvent viscosities, the stilbene molecule rotates fairly easily around the C-C bond, so the isomerization does not

depend on whether the phenyl ring is parallel or perpendicular to the direction of motion. Consequently, the isomerization rate at low solvent viscosities is virtually unaffected by the size of the substituent on the phenyl-ring. At high viscosities, however, it is much easier for the C-C bond rotation to take place if the phenyl ring has rotated such that it presents the minimum surface area to the solvent. Consequently, substituting the larger groups onto the phenyl-ring of stilbene decreases the viscosity dependence.

Although the diphenyl-polyenes have proven to be a good model system for testing liquid-phase reaction rate theories, the studies which have been performed leave unanswered many of the questions concerning the details of the effect of the solvent on the reaction. Using a different molecular system to test the ideas which have been developed by the diphenyl-polyene studies should provide new insights into the mechanisms and rates of liquid-phase chemical reactions.

3.2.2 Selection of a class of test molecules

The molecules we have chosen for study are trans-1,1',4,4'-tetraphenyl-1,3-butadiene (TPB) and trans-1,1',4,4'-tetraphenyl-2-methyl-1,3-butadiene (TPMB), shown in figure 3.2. These molecules are interesting for several reasons. First, they fall into the same class of molecules as the

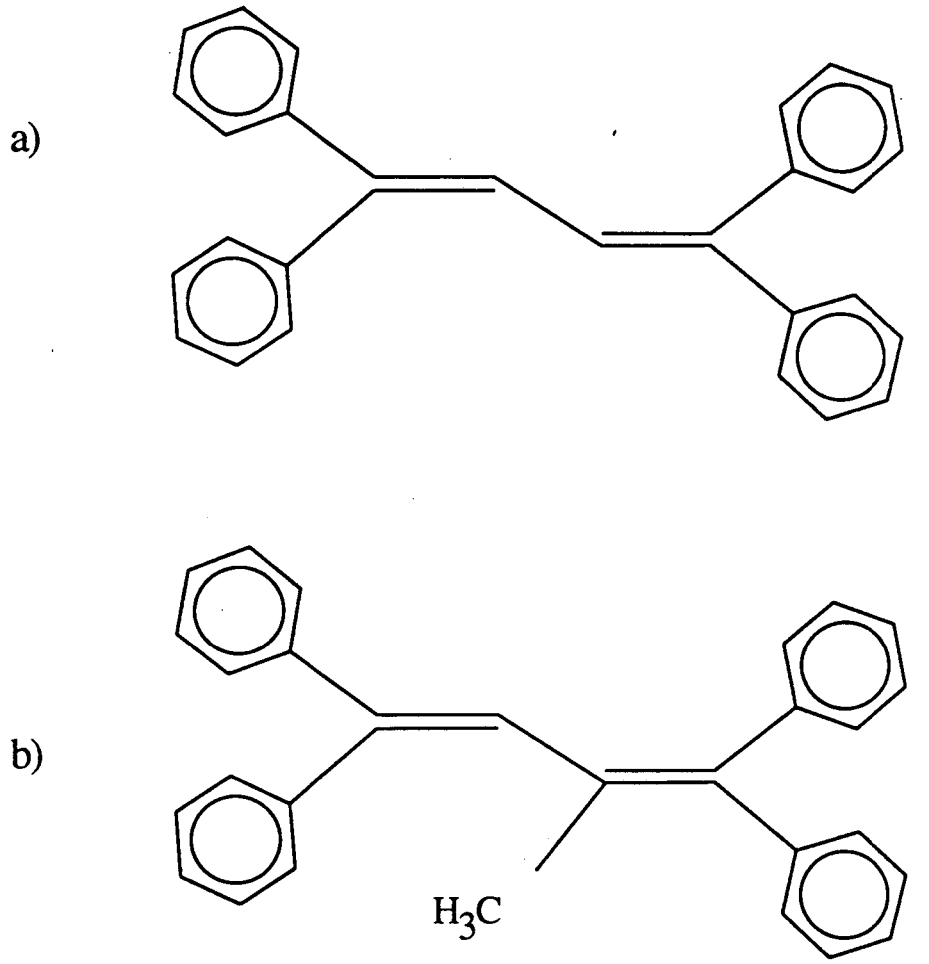

Figure 3.2 Molecular structure of a) 1,1',4,4'-tetraphenyl-1,3-butadiene, and b) 1,1',4,4'-tetraphenyl-2-methyl-1,3-butadiene

diphenyl-polyenes, which have been used extensively as probes for testing the applicability of Kramers' theory to liquid phase reactions. The large body of data which has been published for the diphenyl-polyenes provides a good basis for comparison. The structure of TPB is very similar to that of the diphenyl-polyenes, and it should act very similarly upon excitation. There is, however an important difference between the structure of the diphenyl-polyenes and that of TPMB. The diphenyl-polyenes are planar molecules, which upon excitation undergo an isomerization process causing them to twist to a more out-of-plane configuration. TPMB, however, begins in an out-of-plane configuration due to steric hinderance between the methyl and phenyl groups. Upon excitation, TPMB moves to a more planar configuration. This difference may alter the reaction coordinate significantly, providing a new type of test molecule for liquid-phase reactions. For example, since the phenyl group is initially not in the plane of the molecule it may be easier for the phenyl-ring rotation and carbon-carbon isomerization to occur simultaneously. If that is the case, a two-dimensional potential surface would be necessary to accurately describe the reactive motion. The only difference between TPB and TPMB is the methyl group, so comparison of the spectra should highlight the differences caused by the methyl group.

Very little data is available in the literature about the photophysical properties of either TPB or TPMB. We have

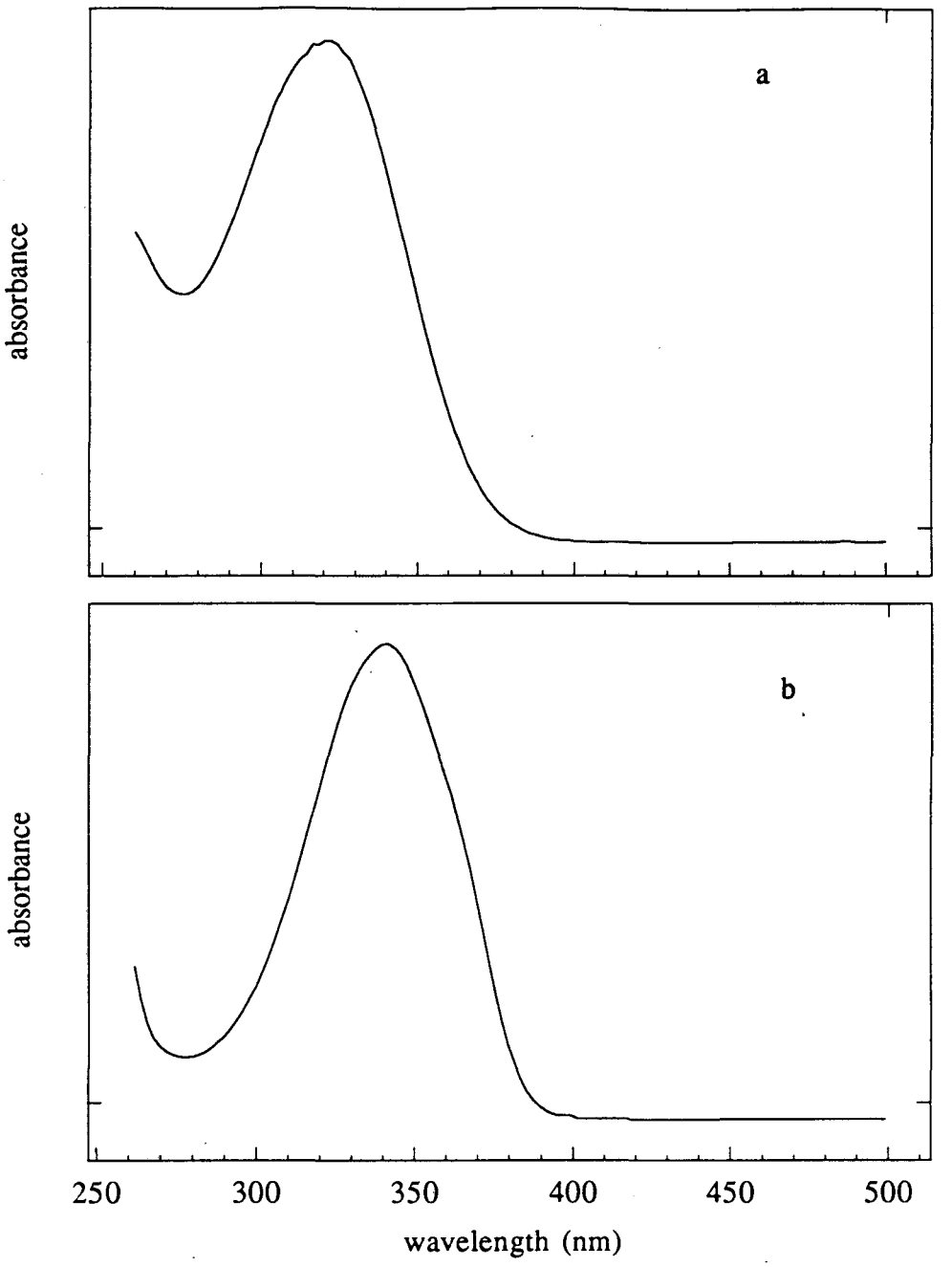

Figure 3.3 Ground state absorption spectrum of a) TPMB in decane and b) TPB in hexane

measured the ground state absorption spectra, shown in figure 3.3, and found them to be in good agreement with the published spectra.[59] The absorption spectra of the two molecules are similar, although the TPB spectrum is slightly red-shifted compared to that of TPMB. This adds support to the idea that the two additional phenyl-rings in TPMB lie out-of-plane, since if the entire TPMB molecule were planar, it would be completely conjugated, and the absorption spectrum would be identical to TPB.

Steady-state fluorescence studies have been performed for both molecules. El-Bayoumi and coworkers have measured the fluorescence spectrum as a function of solvent temperature, and thus viscosity. They recorded the fluorescence spectra of TPMB and TPB over the temperature range of 77K to 300K using methyl-cyclohexane (MCH) as the solvent.[60,61] At 77K, MCH is a rigid glass, while at 300K it is a liquid.

For TPMB they observed a very large blue-shift, 3700 cm^{-1}, of the fluorescence spectrum in the glass as compared to the liquid. They also measured the fluorescence quantum-yield of TPMB as a function of viscosity and found that the quantum yield decreased dramatically as a function of viscosity.[60,61] At room temperature in a methylcyclohexane-isopentane solvent mixture the quantum yield was determined to be 0.003, while at 77K where the solvent is a rigid glass, the quantum yield is nearly unity. These results indicate relaxation via a viscosity dependent intramolecular twisting process.

Some information about the activation barrier to isomerization in TPMB can be inferred from the steady state fluorescence measurements. It was observed in hydrocarbon solvent mixtures that over a viscosity range of 0.5 cP to 45 cP the frequency of the fluorescence remains constant, while the fluorescence intensity increases by a factor of 7.2. This is interpreted to indicate a relatively small activation barrier, on the order of a couple hundred wavenumbers.[60]

The two primary observations in the fluorescence studies of TPB are that in a rigid glass at 77 K there is vibrational structure, and in a room temperature fluid, the vibrational structure vanishes and the fluorescence spectrum is blue shifted.[59] These results are explained in a manner very similar to the TPMB data. In the glass, the TPB cannot isomerize, and the fluorescence is from the initial geometry. In a liquid, the TPB isomerizes and fluoresces from the equilibrium torsional angle.

These earlier studies indicate that TPMB relaxes via an intramolecular isomerization, and that this relaxation process can be indirectly observed by fluorescence spectroscopy. The effect of viscosity on the relaxation process in TPMB is very large compared to that on the diphenyl-polyenes or on TPB. The question is, why is TPMB so different? One possibility is that the methyl-substituted butadiene backbone makes phenyl-ring rotation more facile in TPMB. The results which are presented below explore the dynamical processes resulting from

photoexcitation, and probe the potential energy surfaces of TPB and TPMB.

3.3 Experimental procedure

Two laser systems, the amplified CPM system and the amplified picosecond system, were used for the experiments in this chapter. Both systems are described more fully in chapter 2. The experimental set-up and data collection set-up are also identical to those used in the diphenyl-butadiene experiments described in chapter 2.

Experiments were performed to determine if the relative polarization of the pump and probe beams has any effect on the data taken with the CPM laser system. To do this, the relative polarization between the two beams was adjusted with a half-wave plate. No difference was observed between the spectra taken with the polarizations parallel and those taken with the polarizations perpendicular to each other, so all CPM spectra reported here were taken with the relative polarization between the two beams perpendicular to avoid using the half-wave plate which broadens the femtosecond light pulse. Adjusting the relative polarization on the picosecond system is more complicated due to the nature of the experimental set-up, so the polarizations were left in their original configuration, approximately perpendicular.

All of the solvents used for these experiments, except the hexane, were purchased from Aldrich as 99% purity or greater and were used as received without further purification. The hexane was purchased as spectral grade from Burdick and Jackson or from Omnisolve, and was also used as received. The suitability of the solvent for use in these experiments was checked by running background spectra on the pure solvent. Using the CPM laser system, a very small background signal was observed in the decane and dodecane solvents, indicating that these solvents have some UV absorbing impurities. However, due to the high concentrations of solute used, and the high absorption cross-section of the solutes, any effects due to solvent impurities should be negligible in our data. However, using the picosecond laser system very large signals were easily obtained from all of the solvents. To eliminate artifacts due to this solvent signal, the intensity of the UV excite beam was reduced using neutral density filters until no signal was observed from a cell containing only the pure solvent. Typically the filters used have an optical density of 1.7 for a 100 μJ/pulse UV beam. The sample was then substituted for the blank cell, and the amount of neutral density filter was left at the value determined by the blank.

The TPMB sample was synthesized by Prof. M. A. El-Bayoumi and Prof. M. Nashed. A summary of the synthesis procedure is

given in Appendix II. The TPB was purchased from Aldrich as scintillation grade, 99+% pure and was used as received.

The TPMB concentration for all of the solutions was set to 1.5 mM by using 2.8 mg/5 mL solvent. Decomposition of the sample occurs, causing noticeable changes in the transient absorption spectrum, if the sample is in solution for more than a few days. Consequently, all solutions were made the same day they were used. Saturated solutions of TPB were used.

To avoid sample decomposition and photo-product build-up, all TPMB samples were flowed constantly at a rate of about 4.5 ml/min during data collection using a Cole-Parmer peristaltic pump system with size 14 viton tubing. All samples were also deoxygenated prior to use by sealing the sample reservoir with a rubber septum and bubbling dry nitrogen through the solution for at least five minutes. Dry nitrogen was continuously flowed over the solution in the sample reservoir during data collection. A custom designed flow cell from Hellma Cells with a 1 mm optical pathlength in both directions was used to minimize the sample volume required. A total of 5 ml of solution was used for each scan. A 1 cm pathlength static quartz cell was used in the TPB experiments, since group velocity dispersion effects, which will be discussed in detail later in this chapter, are negligible on the picosecond time scale and photo-product build-up could be eliminated by dexoygenation. Any photo-product build-up would be readily

observable from the decrease in amplitude of the sample signal relative to the reference signal, and no problems were observed for any of the data presented here.

In order to vary the viscosity of the solvent in a known and reproducible manner, a series of long-chain alkanes from hexane to hexadecane was used as the solvent. This technique has been well established in the literature.[8,11, 20,62] Table 3.1 presents the viscosities of the alkane solvents at room temperature[63]. This technique has the drawback that in addition to the viscosity, other properties, such as the polarity and the polarizability of the solvent, change as the identity of the solvent is changed. For an alkane series, the polarity does not change significantly, although the polarizability of the solvents change slightly and may have a minor effect on the potential surfaces.

Table 3.1

ALKANE VISCOSITY AT 295 K

solvent	viscosity
hexane	0.311
heptane	0.400
octane	0.529
nonane	0.712
decane	0.883
undecane	1.17
dodecane	1.47
tridecane	1.84
tetradecane	2.24
pentadecane	2.76
hexadecane	3.27

3.4 Results

3.4.1 Effect of group velocity dispersion on the TPMB results

Initially, the TPMB transient absorption spectra were fit to a biexponential decay function convoluted with the laser pulsewidth and the decay times and the ratio of the amplitudes of the fast and slow decays demonstrated general trends as a function of solvent viscosity, but the reproducibility of the data was very poor. The decay times would vary by about a factor of 7 among scans taken on different days or using

different solutions on the same day. Before any meaningful experiments could be performed using TPMB as the solute, the reproducibility of the transient absorption spectra had to be improved.

Purity checks of the TPMB by thin layer chromatography, NMR spectroscopy, and gas chromatography/mass spectroscopy indicated that the sample was pure. The details of the analyses are given in Appendix II. Since impurities were not the cause of the irreproducibility, the problem had to be in either the lasers or the experimental set-up.

A common problem in short pulse laser experiments is multi-photon excitation of the sample due to the high peak powers. To check for this, the excite pulse intensity was varied by using neutral density filters up to an optical density of 0.5, and the only change observed was the expected linear dependence of the signal amplitude on excite intensity. The irreproducibility was therefore not attributable to multi-photon excitation of the TPMB.

The amplified CPM laser system runs at an 8 kHz repetition rate, which is high enough that molecules could conceivably not have time to relax completely between laser pulses leading to reactions between excited species. The repetition rate of the amplified laser system was varied between the standard 8 kHz repetition rate and 200 Hz by changing the cavity dumper repetition rate, with no change in either the signal shape or intensity.

The possibility that the 150 fsec laser was being broadened by passing through the sample was eliminated by autocorrelating the laser pulse after the sample. The pulse-widths before and after the sample were identical. Care was taken to ensure that no UV light was reaching the photodiode face and causing artifacts.

Varying the TPMB concentration caused the TPMB transient absorption spectrum to change, both in relative amplitude between fast and slow decay components and in the values of the decay times. Figures 3.4 and 3.5 show the effect of concentration on the fast and slow decay times respectively. The decay times become faster and the ratio of the amplitude of the slow decay to the amplitude of the fast decay becomes smaller as the TPMB concentration is increased. For a 1 mm pathlength sample cell, the plots level out at concentrations above 1 mM. The same effect was observed for the transient absorption decay of coronene in xylene. However, the diphenyl-butadiene spectrum is independent of concentration. These observations indicate that it is unlikely that any form of molecular interaction between solute molecules, such as Forster energy transfer or excimer formation is responsible. The molecular structure of TPMB is very different from that of coronene, and very similar to the structure of DPB. Any molecular mechanism argues for TPMB and DPB to behave similarly, which is not what was observed.

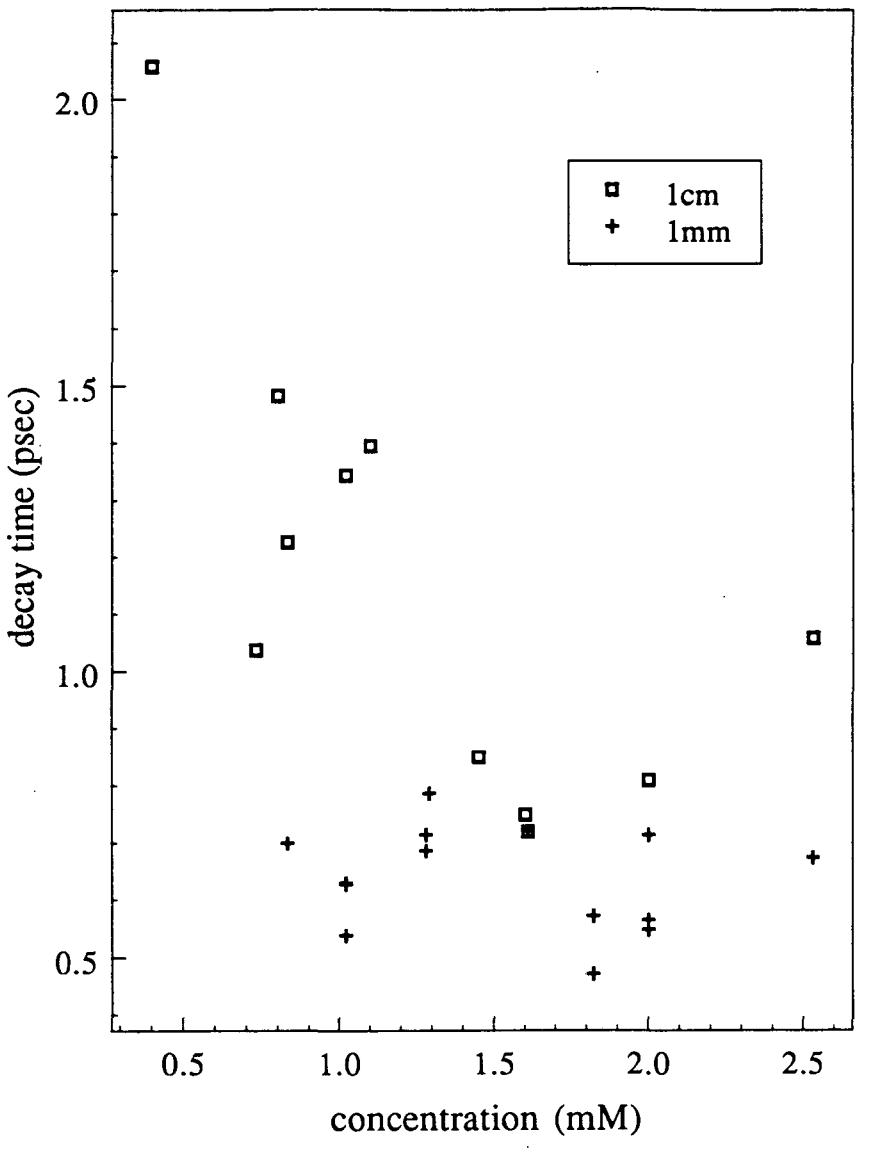

Figure 3.4 Effect of concentration on TPMB transient absorption decay constants for the fast decay component

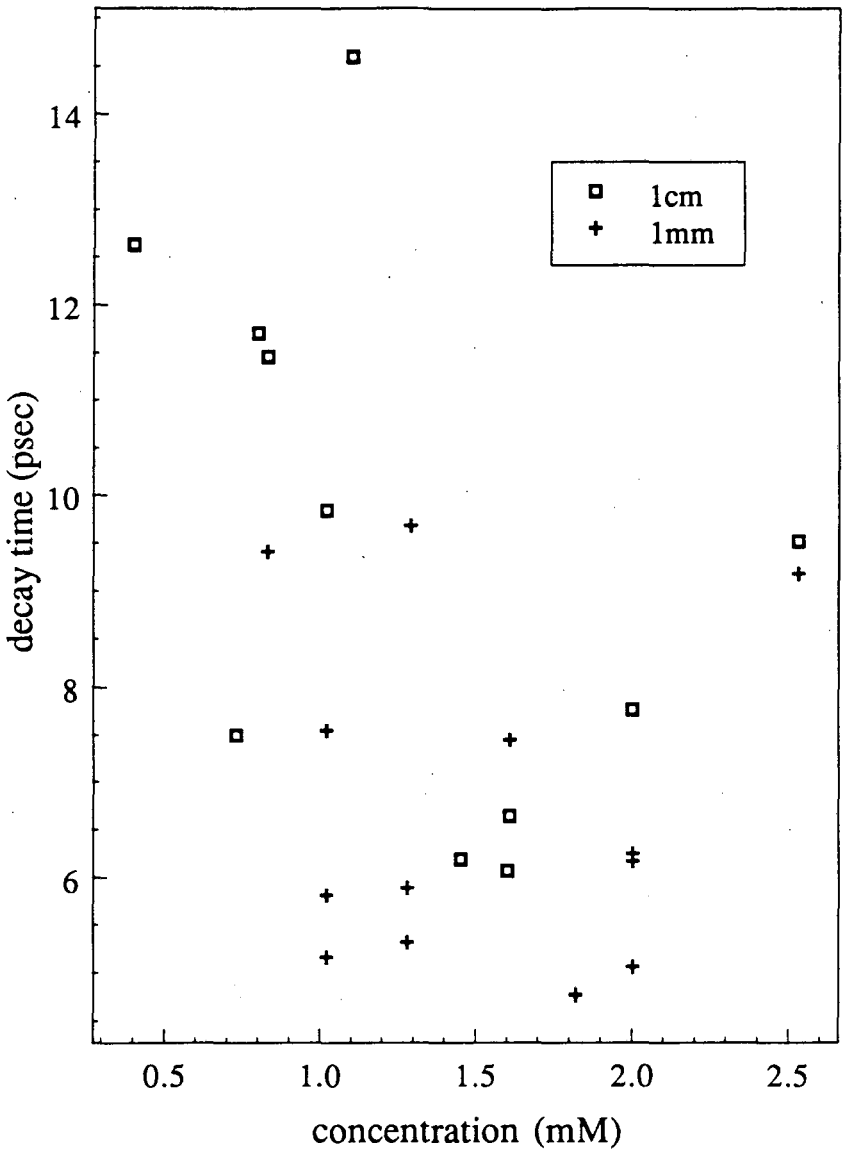

Figure 3.5 Effect of concentration on TPMB transient absorption decay times for the slow decay component

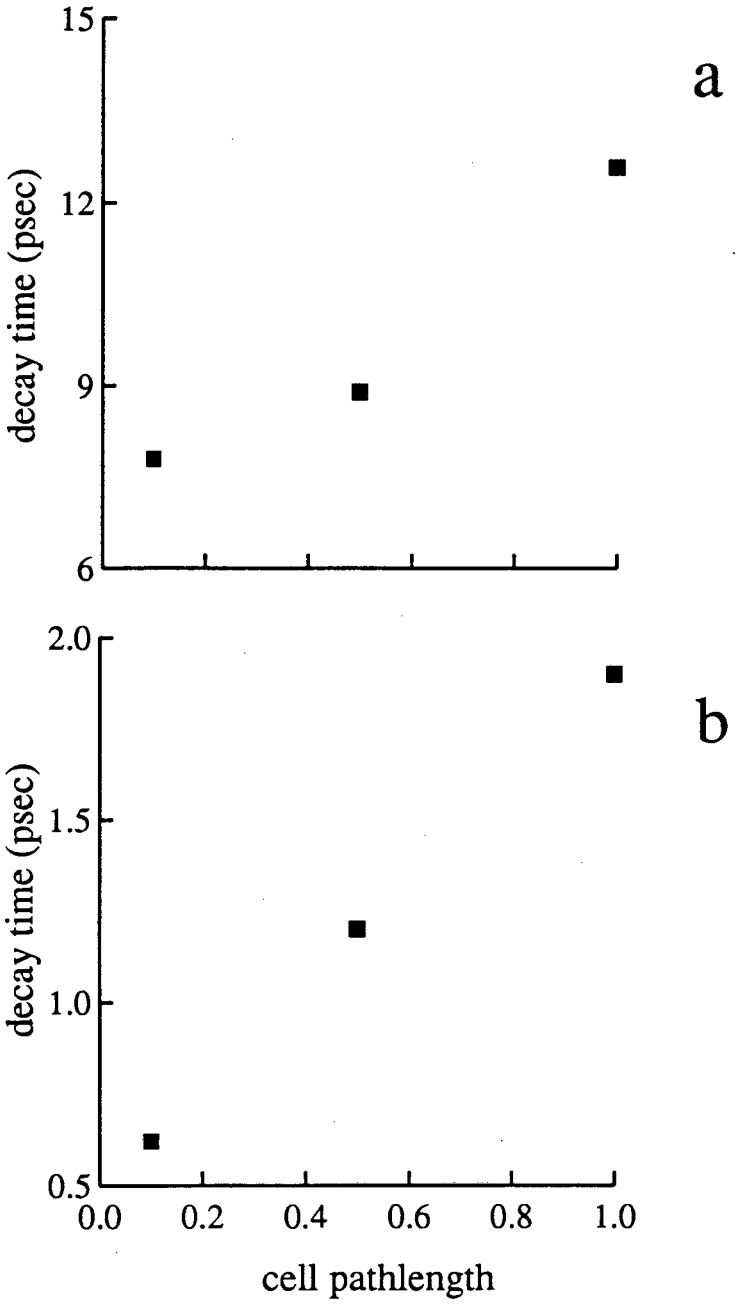

Figure 3.6 Decay time as a function of pathlength for the a) slow and b) fast decay components for the transient absorption decay of TPMB in decane

Changing another experimental variable, the sample cell pathlength, also changes the decay times and relative decay component amplitudes. The effect of pathlength on the decay time is illustrated in figure 3.6. As the cell pathlength is decreased at constant TPMB concentration, the decay times also decrease.

The changes induced by decreasing the cell pathlength are identical to those induced by increasing the TPMB concentration. This can be readily explained by noting that as the TPMB concentration is increased, the distance the laser beam penetrates into the sample before being completely absorbed decreases. Changing the sample concentration in effect changes the pathlength, which appears to be the relevant variable. Data taken at concentrations above 1 mM and pathlengths shorter than 1 mm should be, and in fact are reproducible.

The effect of the sample pathlength on the transient absorption decays can be explained by the fact that different frequencies of light travel at different speeds through a dispersive material due to group velocity dispersion (GVD). The pump beam used in these experiments has a wavelength of 310 nm, and the probe beam has a wavelength of 620 nm. If GVD is responsible for the observed pathlength dependence it would have the following effect. At the entrance face of the sample cell, the pump and probe pulses overlap at a time t_0. As the two pulses move through the cell, the probe pulse (red)

travels faster than the pump pulse (blue). Passing through the cell has therefore effectively caused t_0 to shift to an earlier time. The output signal is a convolution of the signals from each point in the cell, each of which has a different time origin.

The magnitude of the group velocity dispersion for 620 nm and 310 nm light pulses in quartz (which is similar to alkanes) can be calculated very easily. A numerical fit using two UV and one IR wavelength for the index of refraction of quartz gives the following parameters[64]:

$$n^2-1=\sum \frac{b_i \nu_i^2}{\nu_i^2-\nu^2}$$

where

$b_1 = 0.6961663$

$\nu_1 = 2.137141 \times 10^{10}$ (cm^{-1})

$b_2 = 0.4079426$

$\nu_2 = 7.400796 \times 10^9$

$b_3 = 0.8974994$

$\nu_3 = 1.0210958 \times 10^6$

The expansion is valid between 10,000 cm^{-1} and 50,000 cm^{-1}. The group velocity dispersion is given by:[65]

$$v_g=\frac{c}{n(\omega)+\omega\left(\frac{dn}{d\omega}\right)}$$

and substituting in

$$n=\left[1+\sum \frac{b_i \nu_i^2}{\nu_i^2-\nu^2}\right]^{1/2}$$

$$\frac{dn}{d\nu}=\frac{1}{2}\left[1+\sum \frac{b_i \nu_i^2}{\nu_i^2-\nu^2}\right]^{-1/2}\left[\sum \frac{2\nu b_i \nu_i^2}{(\nu_i^2-\nu^2)^2}\right]$$

gives

$$v_g=c\left\{\left[1+\sum \frac{b_i \nu_i^2}{(\nu_i^2-\nu^2)}\right]^{1/2}+\frac{\omega}{2}\left[1+\sum \frac{b_i \nu_i^2}{\nu_i^2-\nu^2}\right]^{-1/2}\left[\sum \frac{2\nu b_i \nu_i^2}{(\nu_i^2-\nu^2)^2}\right]\right\}^{-1}$$

This calculation gives a 6% difference in velocities between 310 nm and 620 nm, which works out to a difference of 200 fsec/mm. So in a 1 cm cell, there is a 2 psec difference between the time origins for the front of the cell and the back. This difference is roughly the same size as the decay times for TPMB in alkanes, and would be expected to have a large effect on the shape of the spectrum.

A simple simulation of this effect reproduces the qualitative features of the TPMB data very well. The data is

represented in the simulation by an instantaneous risetime and a double exponential decay time, convoluted with a gaussian to account for the width of the laser pulse. This function is then convoluted with a single exponential decay, which accounts for the shifting time origin for absorptions occurring at different points in the cell. The assumption that the absorption signal decays exponentially with distance into the cell corresponds to a Beer's law assumption. This is not valid at the high absorbances in the TPMB samples, but suffices as a first approximation.

The simulations were run for a series of single exponential decay times, and the results for four simulations are shown in figure 3.7. For all four simulations, the characteristics of the gaussian and the biexponential were held constant at values selected to mimic the relative sizes of the components of the data. The gaussian is set to a FWHM of 2, and the biexponential fast decay is set to time = 6, amplitude = 1, slow decay is set to time = 80, amplitude = 0.5. For all of the simulations shown in figure 3.7, the x-axis is scaled the same, and the y-axis is set to 1.0 full scale. As the decay time of the exponential is made slower, the data is affected in several ways. First, the decay times are slowed. Second, the relative amplitudes of the two decays change, with the slow decay becoming more prominent. A risetime grows in, with the risetime increasing as the exponential decay is made slower.

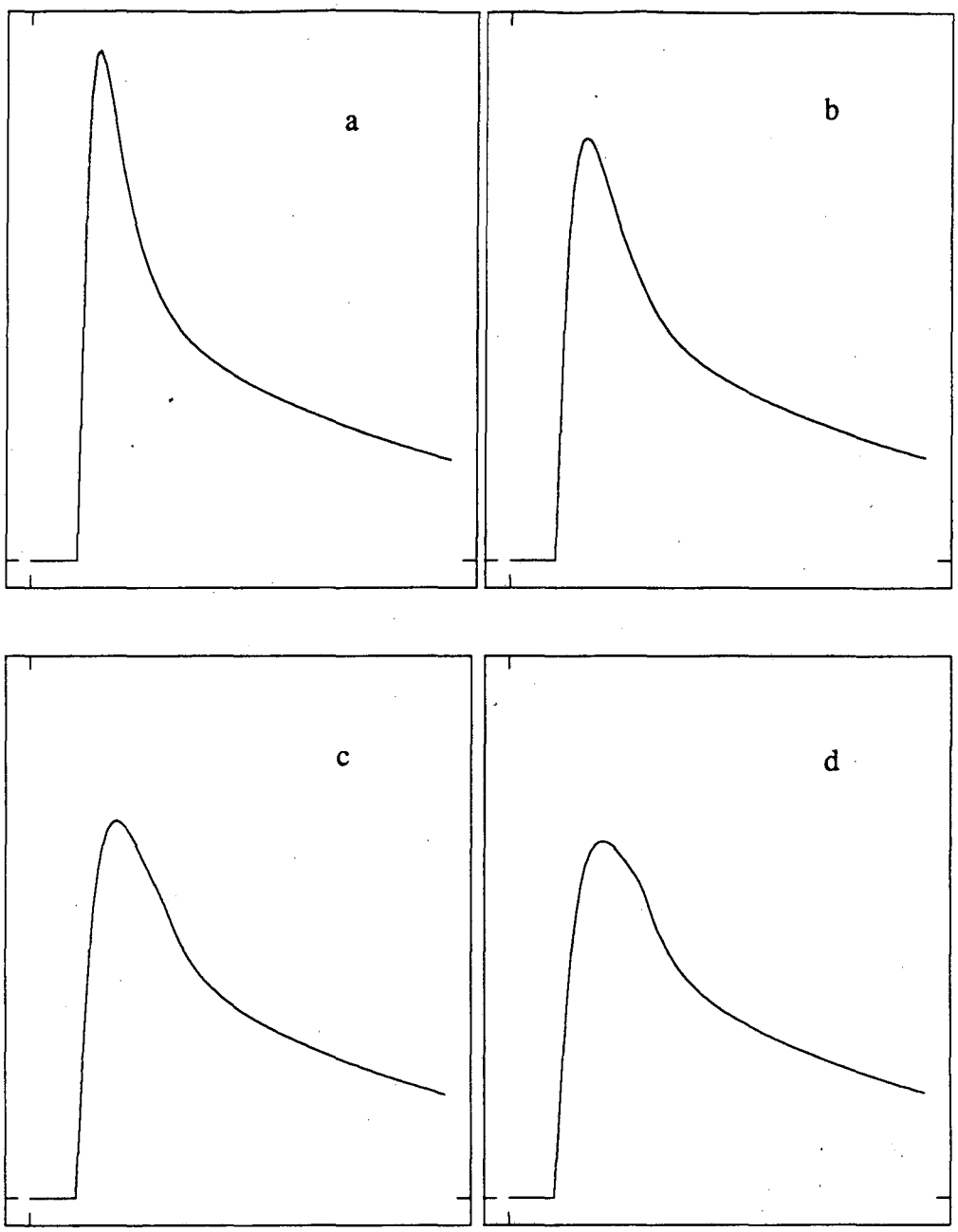

Figure 3.7 Convolution simulation results for exponential decay times of a) 2, b) 4, c) 6, and d) 8. The other parameters are gaussian FWHM = 2, biexponential fast decay time = 6, amplitude = 1, slow decay time = 80, amplitude = 0.5

These results are exactly what is observed experimentally. As the concentration is lowered or the pathlength of the cell is increased, the exponential time-constant representing the distance over which the decay points are convoluted increases. So lower concentrations should correlate with longer decay times and a higher slow decay relative amplitude. These simulation results reproduce the important qualitative aspects of the TPMB concentration and pathlength data remarkably well. The simulations also reproduce the surprisingly large amount by which a small change in pathlength can change the shape of the transient absorption decay. The simulation results strongly support the assignment of the pathlength effect to GVD.

Artifacts due to GVD effects are easily prevented. The reproducibility of the data is dramatically improved by using a 1 mm pathlength cell and TPMB concentrations above 1 mM. A 1mm pathlength is short enough that the amount of GVD that occurs is very small. The fact that under these conditions the data is constant for a wide concentration range as shown in figures 3.4 and 3.5 supports the idea that the decay curves measured are free from any GVD distortion.

3.4.2 TPMB photoproducts

Before irradiation with UV light, a solution of TPMB in alkanes is colorless, as can be seen from the absorption

spectrum of TPMB shown in figure 3.3. After being exposed to 310 nm light from the amplified CPM laser system, the solution sometimes turns yellow enough that it can be easily observed by eye. The color persists for approximately 15 minutes after irradiation stops. To ensure that this photoreaction does not interfere with the dynamics of interest in the transient absorption experiments, a series of diagnostic tests was run.

The first goal was to identify the nature of the photoproduct by measuring its electronic absorption spectrum. First, a cuvette containing a 1 mM TPMB solution in decane was irradiated with the 312 nm line from a mercury arc lamp for about 15 minutes with the cuvette open to atmosphere. The absorption spectrum of the sample, shown in figure 3.8a, was recorded about 15 minutes after the arc lamp was turned off. The absorption band centered at 310 nm has completely disappeared, indicating that the TPMB has been dissociated. An identical measurement, except that now oxygen has been removed from the TPMB solution by sealing the cuvette with a rubber septum and bubbling nitrogen through the sample for about five minutes, produced the spectrum shown in figure 3.8b. The spectrum of the deoxygenated solution is identical to that of the unphotolyzed species. Neither sample showed any yellowing after exposure to the arc lamp.

A deoxygenated 1mM TPMB solution was exposed to the 295 nm UV light from the picosecond laser system. After about 15 minutes of UV irradiation, there was still no yellowing,

indicating that the photolysis wavelength may be an important parameter. No yellow photoproduct was observed in any of the experiments using the picosecond laser system.

Whether or not the solution turns yellow appears to depend on the intensity of the CPM laser. The solution only turns yellow if the average UV power is above 3 mW. This fact, combined with the inability of the arc lamp at 312 nm and the picosecond laser at 295 nm to cause the solution to turn yellow suggests that the yellow color may be due to a multi-photon absorption process.

The absorption spectrum of a yellowed TPMB solution was measured and is shown in figure 3.9. The spectrum is identical to the spectrum for the unphotolyzed sample. This suggests that only a small fraction of the TPMB molecules are affected by the process causing the yellow color. The one-photon transient absorption spectrum should not be significantly affected by yellowing of the solution.

For all of the TPMB transient absorption data reported below, a 1 mm flow cell was used to avoid problems with GVD and photoproducts. In TPB, a 1 cm static cell was used since neither GVD, due to the length of the 1 psec laser pulse, nor photoproducts presented a problem.

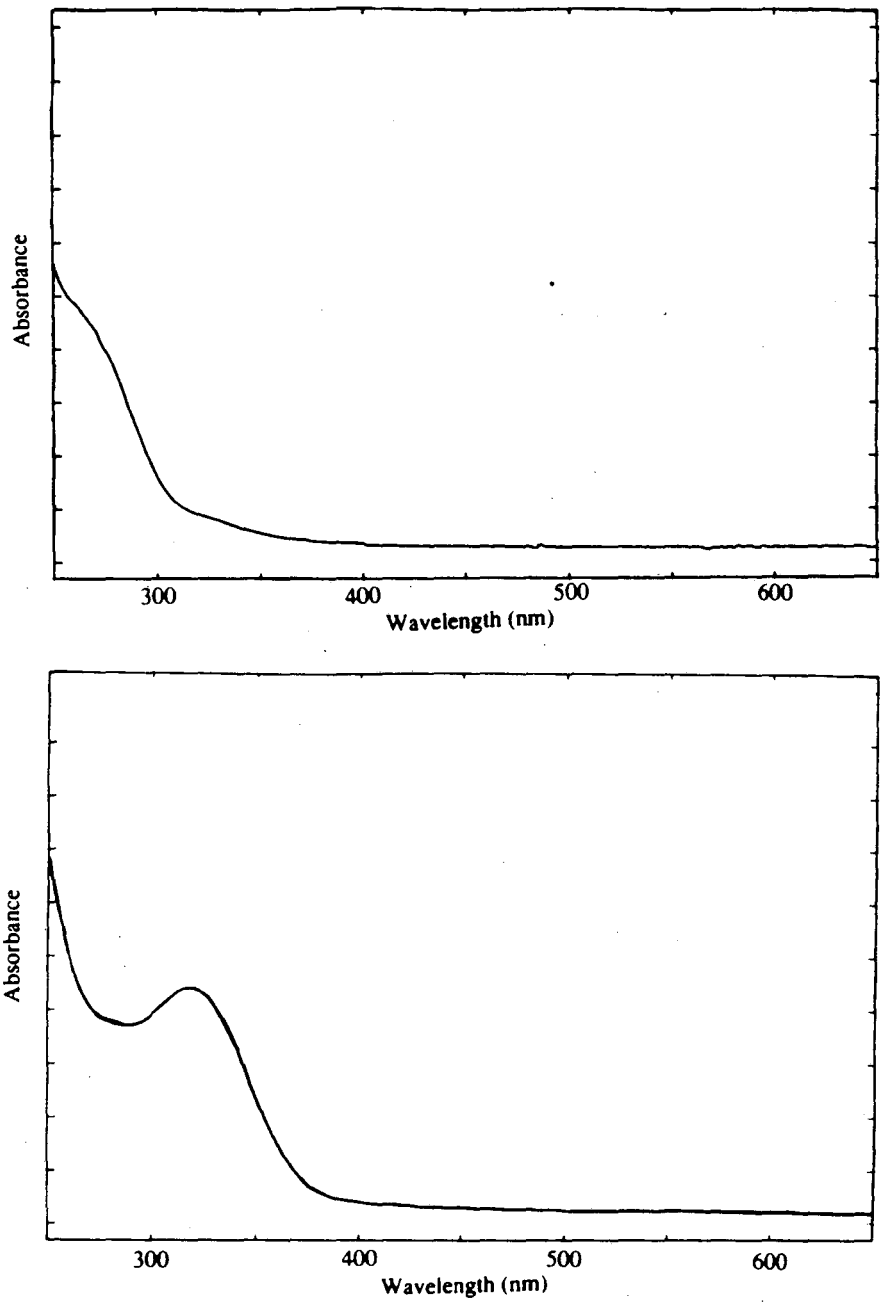

Figure 3.8 Steady state absorption spectra of 1 mM TPMB in decane after photolysis with the 312 nm line of a mercury arc lamp. For 3.8a the solution was exposed to atmosphere. For 3.8b, the solution was deoxygenated.

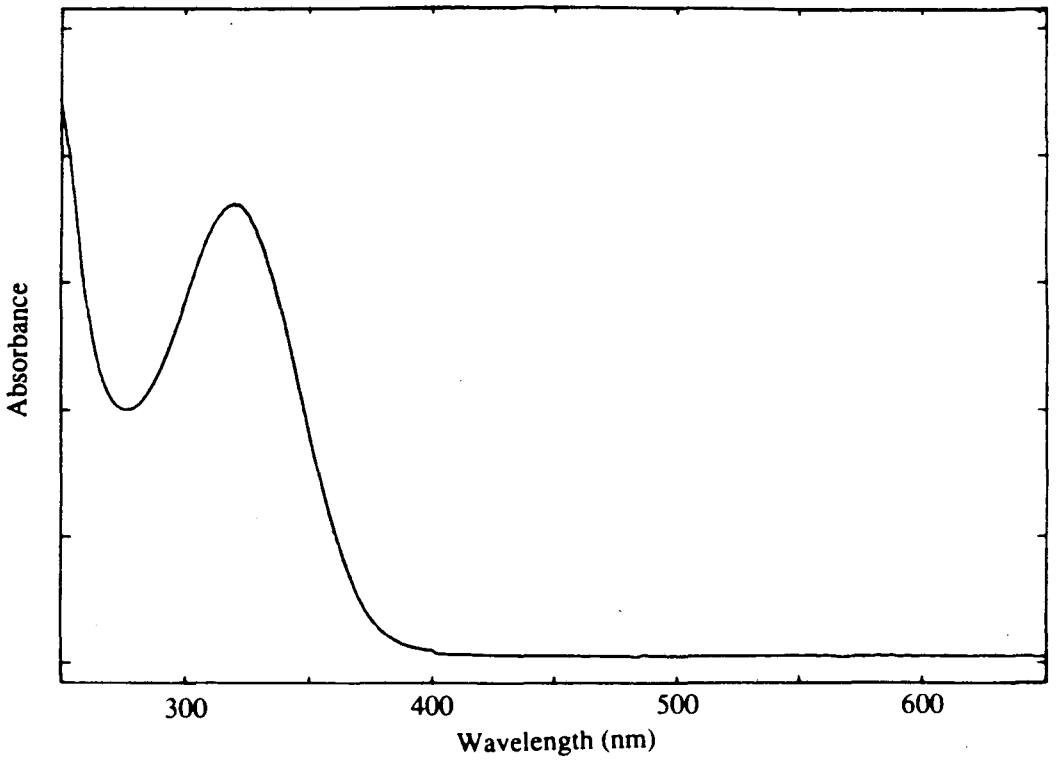

Figure 3.9 Steady state absorption spectrum of a TPMB solution in decane which has turned yellow.

3.4.3 TPB Data

The transient absorption spectra of TPB in hexane, shown in figures 3.10 and 3.11, were obtained using the picosecond laser system. The probe wavelengths used were 500 nm, 560 nm, 620 nm, and 900 nm. The curve at 500 nm corresponds to an increase in transmission, the curves at 620 nm and 900 nm correspond to transient absorptions, and the curve at 560 nm is a combination of absorption and emission. Looking at the fluorescence spectrum, shown in figure 3.12, large amounts of stimulated emission would be expected at 500 nm, resulting in an apparent increase in transmission. A small amount of stimulated emission should occur at 560 nm, with none at the redder wavelengths.

The TPB data is fit very well by combinations of exponential rise and decay times. The stimulated emission spectrum at 500 nm has a 3.5 psec and a 25 psec risetime and a 1.7 nsec decay. At 560 nm, the transient absorption has a pulsewidth limited rise time and a 25 psec decay. The much smaller amplitude stimulated emission signal at 560 nm has a 25 psec rise time and an approximately 1.5-3.5 nsec decay time. The emission signal is very small, so an accurate decay time is very difficult to obtain. The transient absorption spectra have pulsewidth limited risetimes and decay times of 1.9 nsec at 620 nm, and 2.0 nsec at 900 nm. Table 3.2 summarizes the fitting parameters.

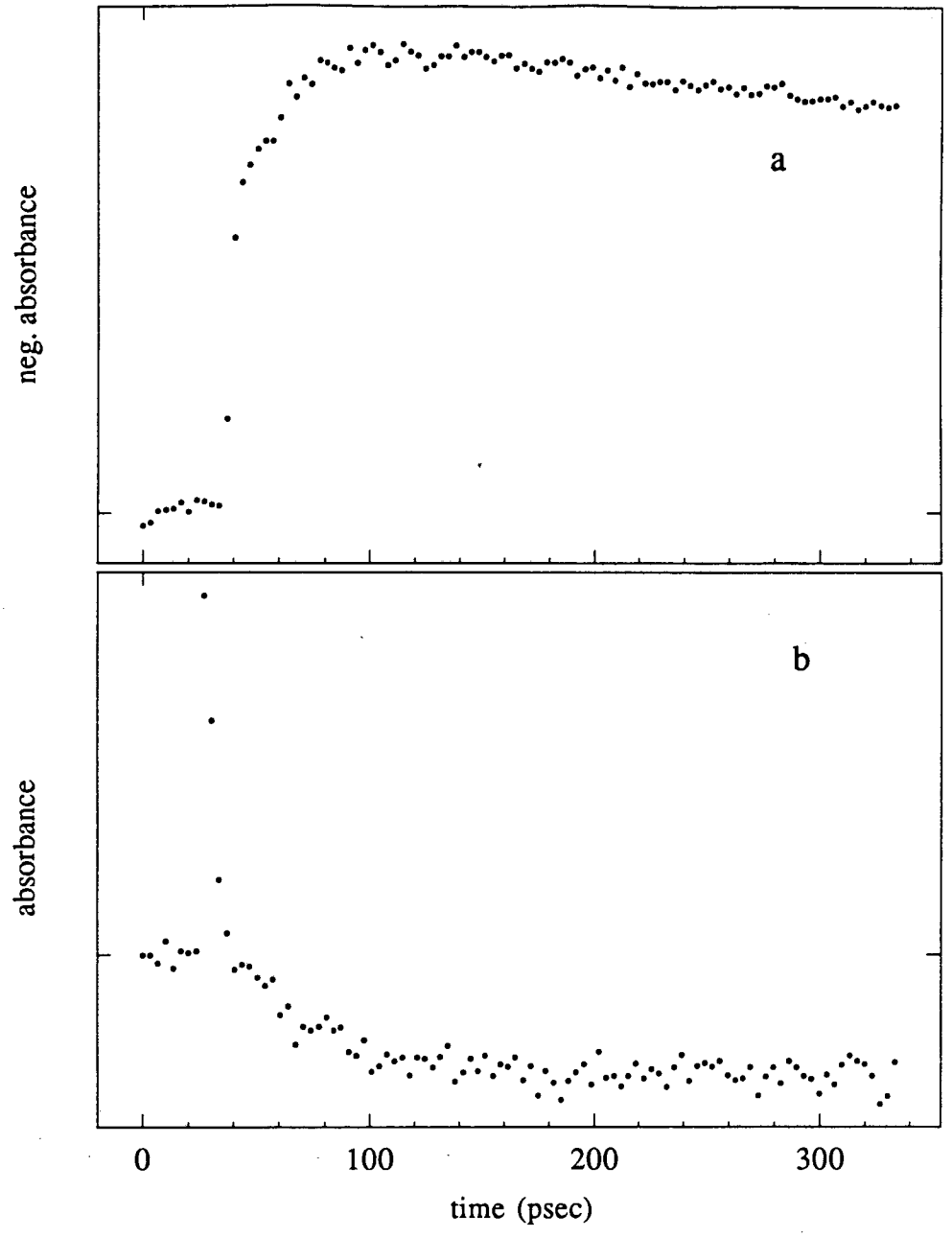

Figure 3.10 Transient absorption spectra of TPB in hexane at probe wavelengths of a) 500 nm and b) 560 nm

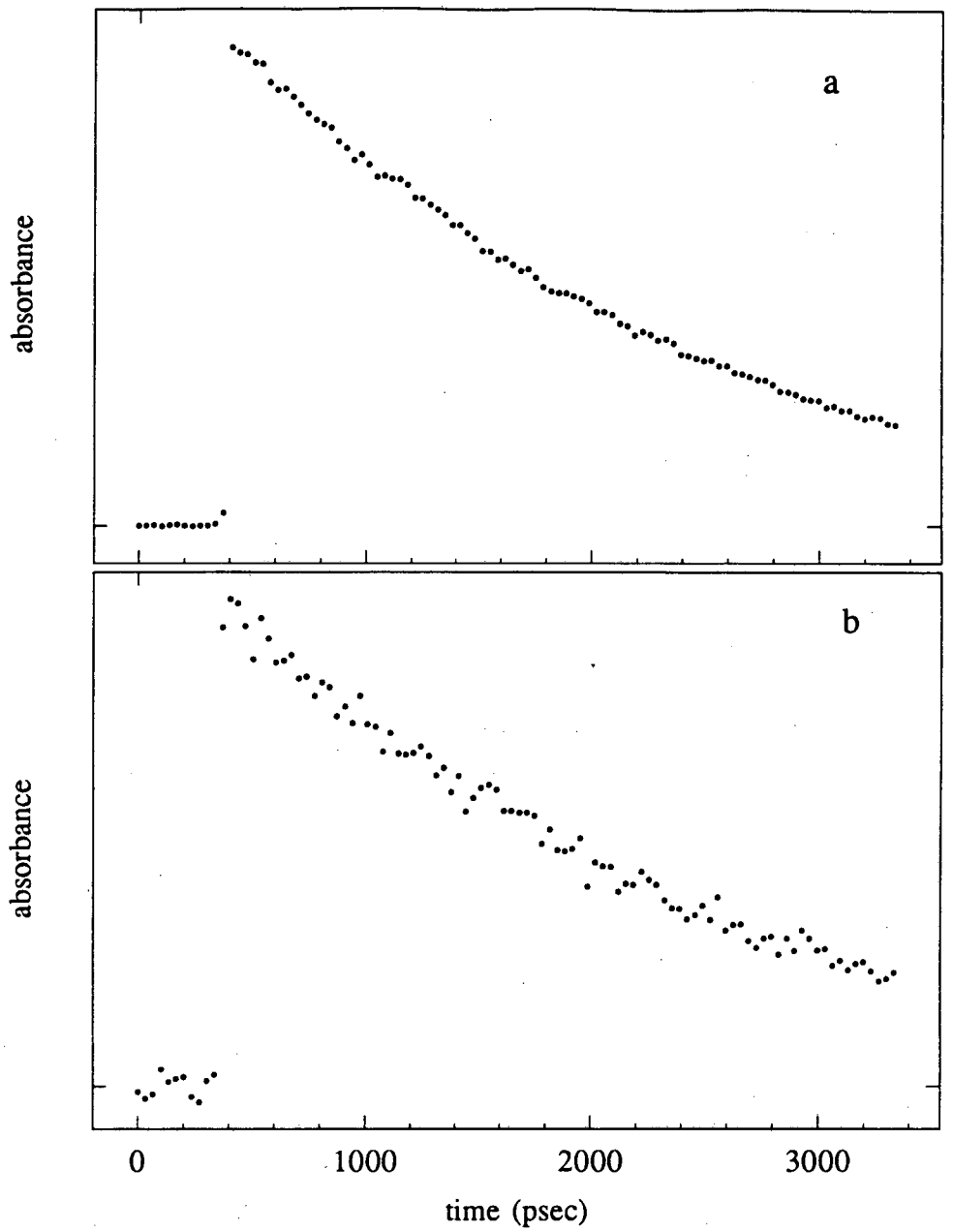

Figure 3.11 Transient absorption spectra of TPB in hexane at probe wavelengths at a) 620 nm and b) 900 nm

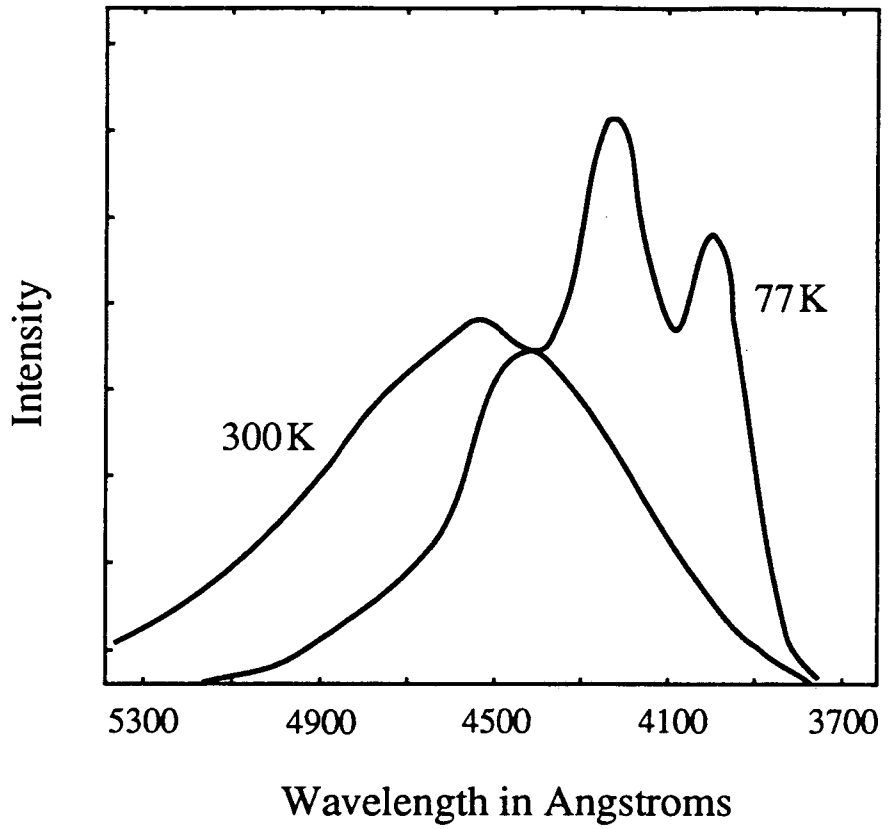

M.A. El-Bayoumi et. at., *J. Chem. Phys.* **48**(6) 1968, p.2536

Figure 3.12 Fluorescence spectrum of TPB in a methylcyclohexane/isopentane mixture

Table 3.2
TPB Transient Absorption Fitting Parameters

probe wavelength	absorption/ emission	rise time (psec)	decay time (nsec)
500 nm	emission	3.5	1.7
	emission	25	
560 nm	absorption	pulsewidth limited	0.025
	emission	25	1.5-3.5
620 nm	absorption	pulsewidth limited	1.9
900 nm	absorption	pulsewidth limited	2.0

3.4.4 TPMB Data

The first series of experiments run on TPMB used the CPM laser system as the excitation source. Transient absorption spectra were recorded for TPMB in hexane and tetradecane solvents using a 310nm pump pulse and probe pulses of 620nm and 680nm. No difference was observed for either solution between the spectra with probe wavelengths of 620nm and 680nm. This result is not surprising considering that the frequency difference between 620 nm and 680 nm is relatively small.

The next series of experiments, again using the CPM laser system, investigated the effect of changing the solvent viscosity on the spectra. The transient absorption curve

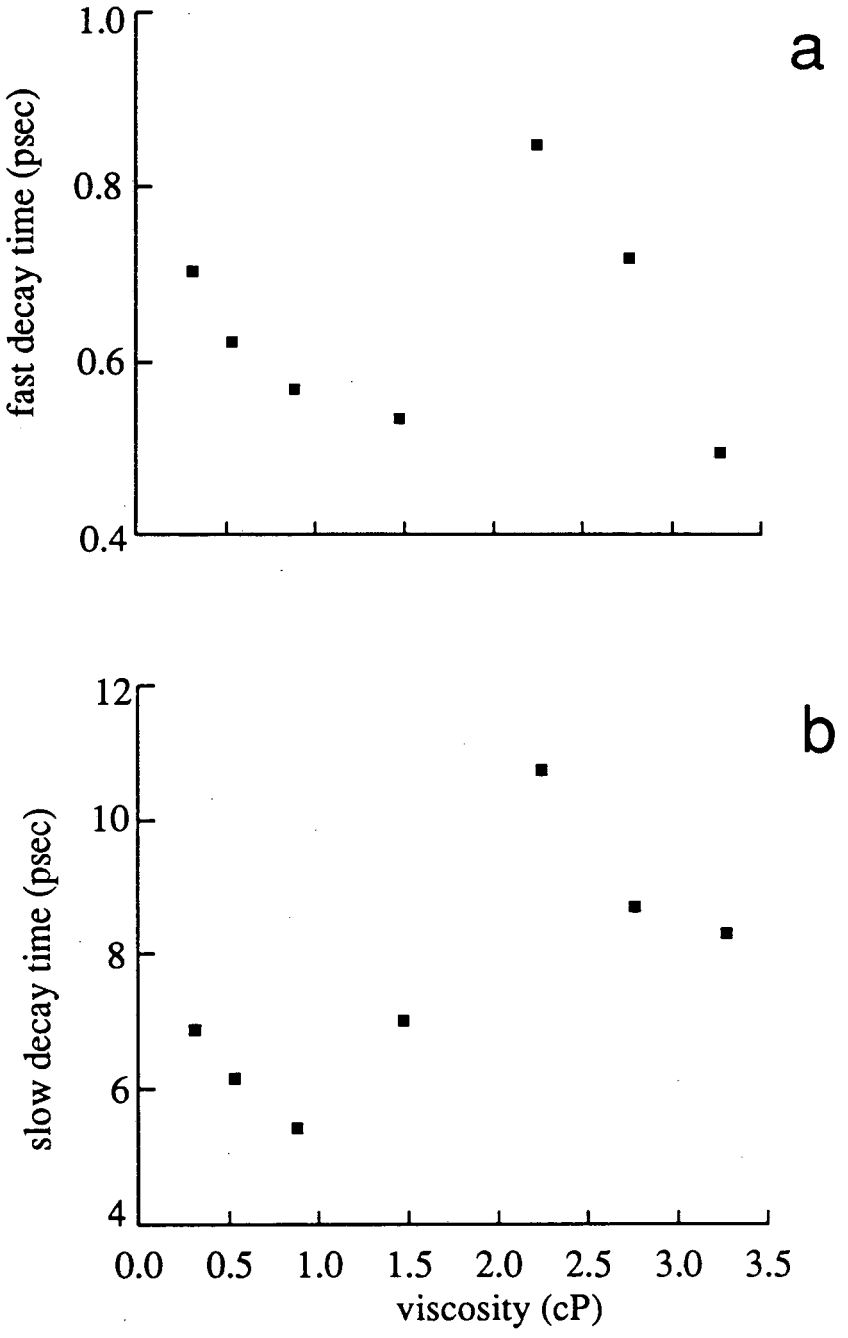

Figure 3.13 Transient absorption decay times for TPMB in alkane solvents as a function of viscosity. Figure 3.13a shows the fast decay component, figure 3.13b shows the slow decay component.

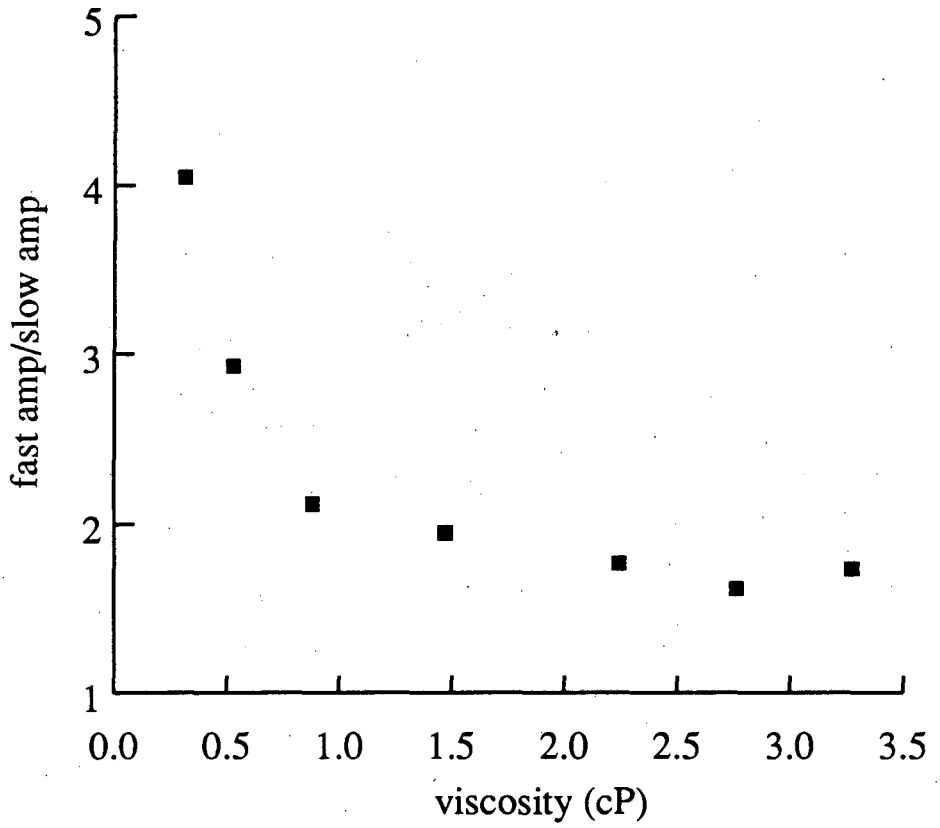

Figure 3.14 Ratio of fast decay amplitude to slow decay amplitude for TPMB in alkane solvents as a function of viscosity

changed shape as the viscosity of the solvent was changed. The data was fit to a double exponential decay convoluted with a gaussian pulsewidth. Although this function did not fit the data perfectly, no other functional form was found that fit better, so due to its simplicity, the biexponential was used for fitting. The decay times, shown in figure 3.13, are independent of viscosity. However, as the viscosity of the solvent increases, the amplitude of the slow decay component increases relative to the fast decay component. The trend is pronounced enough to be noticed just by looking at the data. A plot of the amplitude ratio as a function of viscosity is shown in figure 3.14.

The transient absorption spectra of TPMB were measured in hexane and hexadecane at a variety of probe wavelengths using the picosecond laser system. For all of the picosecond system data, the pump wavelength is 295 nm. The probe wavelengths used in both solvents are 500 nm, 620 nm, and 900 nm. The spectra are presented in figures 3.15 and 3.16. The data were fit with functions which are combinations of exponentials. The hexane solution data are essentially the same as the hexadecane data, except that the processes in general occur more rapidly. The fitting parameters are summarized in table 3.3.

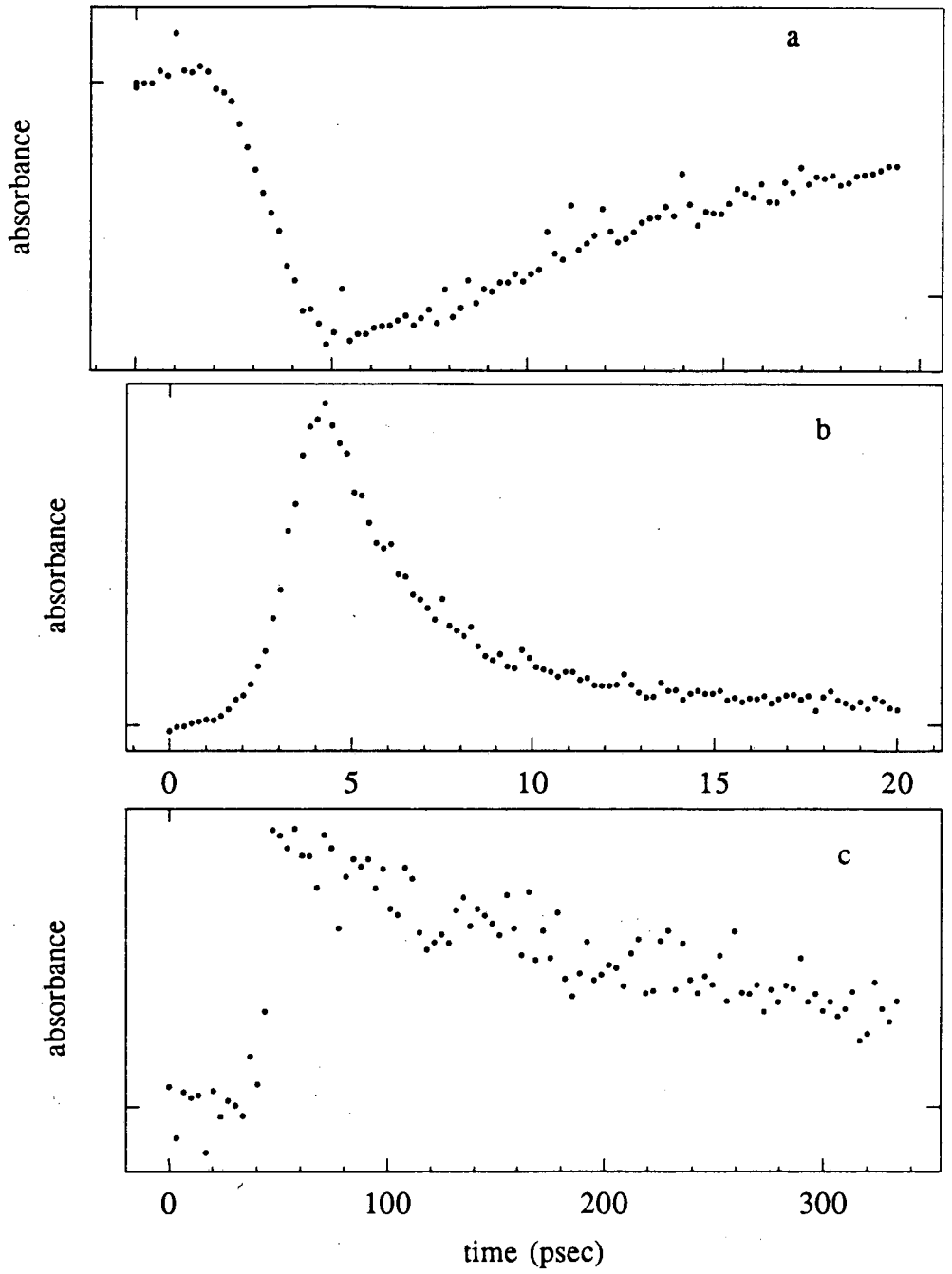

Figure 3.15 Transient absorption spectra of TPMB in hexane at probe wavelengths of a) 500 nm, b) 620 nm, and c) 900 nm

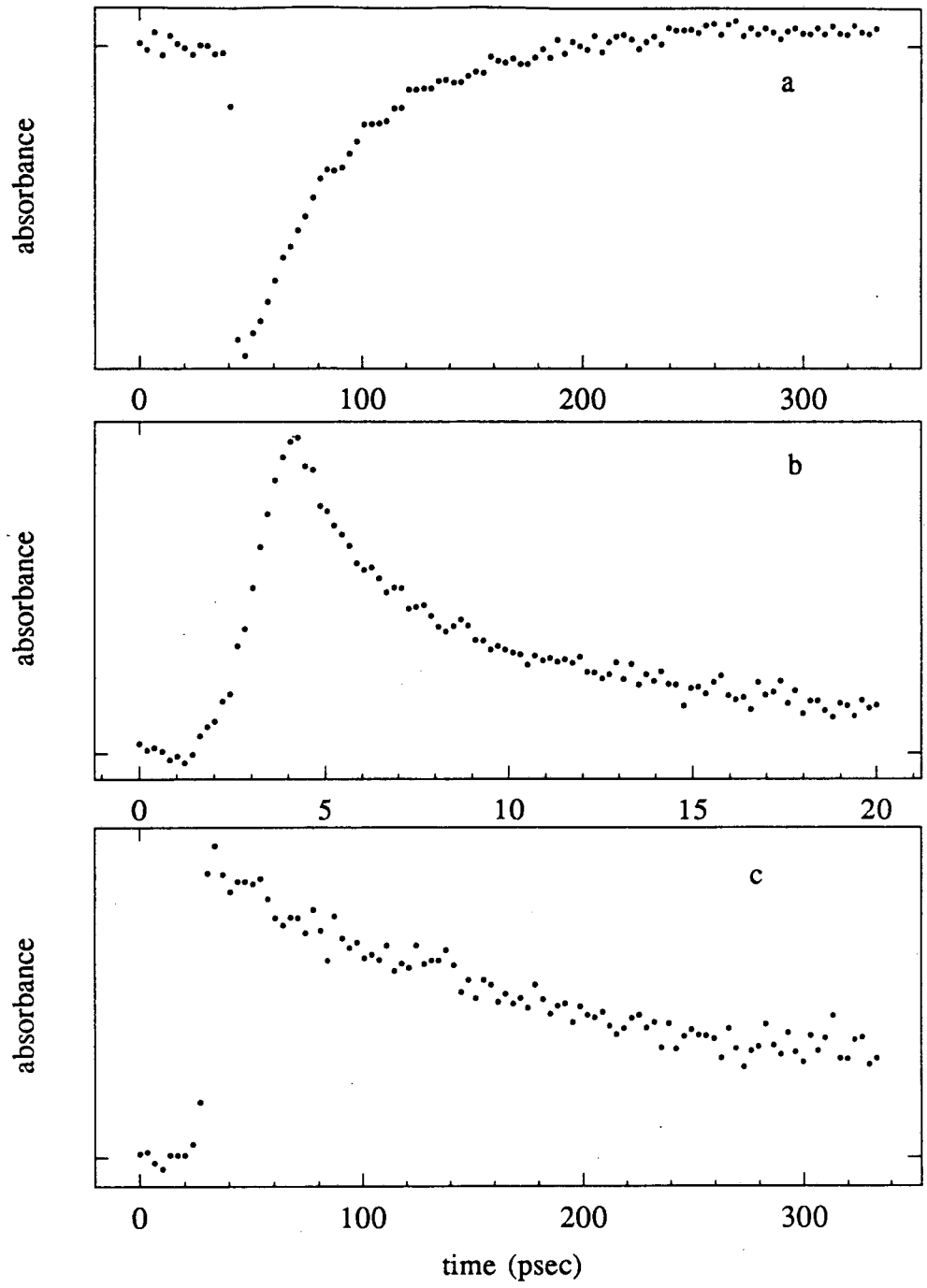

Figure 3.16 Transient absorption spectra of TPMB in hexadecane at probe wavelengths of a) 500 nm, b) 620 nm, and c) 900 nm

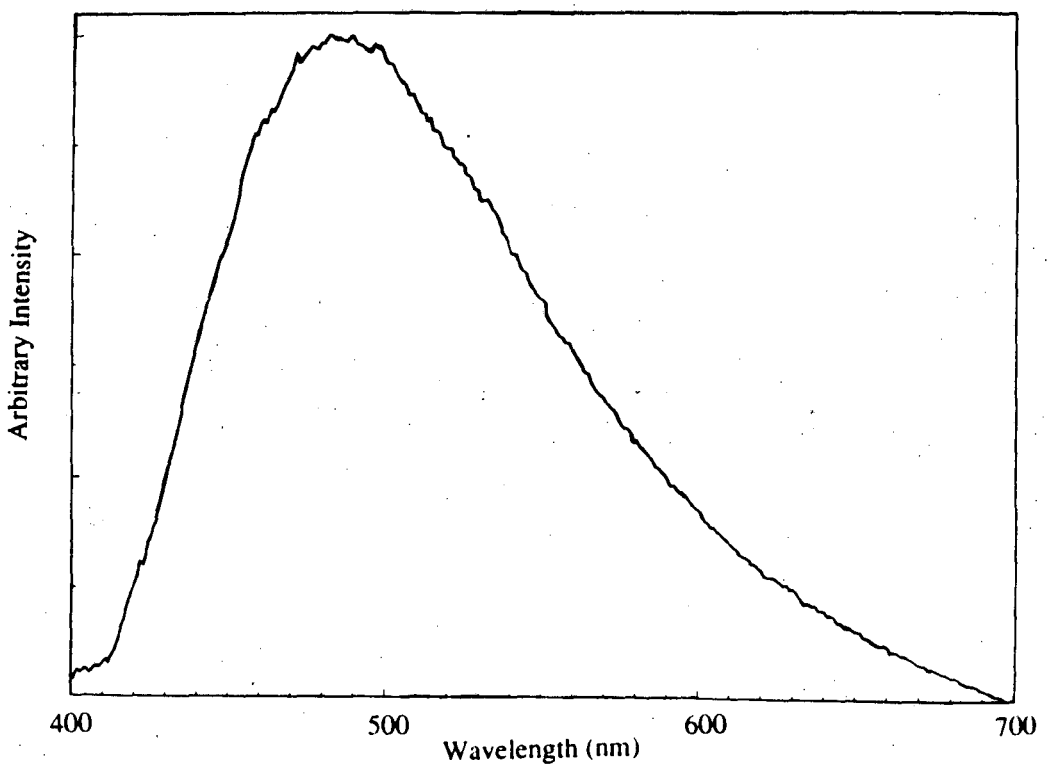

Figure 3.17 TPMB fluorescence spectrum in methylcyclohexane

Table 3.3

TPMB Transient Absorption Fitting Parameters

solvent	probe wavelength	rise (psec)	decay (psec)	decay (psec)
hexane	500 nm (emission)	pulsewidth limited		23
hexadecane	500 nm (emission)	pulsewidth limited		51
hexane	620 nm (absorption)	pulsewidth limited	0.6	11
hexadecane	620 nm (absorption)	pulsewidth limited	0.6	12
hexane	900 nm (absorption)	pulsewidth limited		172
hexadecane	900 nm (absorption)	pulsewidth limited		271

At a probe wavelength of 500 nm, there is a stimulated emission peak which has a pulsewidth limited risetime and decays in 23 psec. This is consistent with the fluorescence spectrum of TPMB, shown in figure 3.17, which peaks at 500 nm. At 620 nm there is a transient absorption signal, which is fit using a double exponential decay. No significant viscosity effect is observed at 620 nm; in both solvents the fast decay is observed to be 600 fsec, while the slow decay is 11 psec in hexane and 12 psec in hexadecane. At 620 nm there is no stimulated emission peak in the transient absorption data, however, the molecule does fluoresce at 620 nm, and it is possible that a small amount of stimulated emission is occurring, complicating the shape of the 620 nm data. A transient absorption is observed at 900 nm for TPMB in both hexane and hexadecane, and both decays fit well to a pulsewidth limited risetime and a single exponential decay. In hexadecane, the decay curve fits to a decay time of 271 psec, while in hexane the data fits to a decay time of 172 psec.

3.5 Discussion

3.5.1 TPB

The transient absorption results for TPB can be explained using a one-dimensional potential energy surface very similar

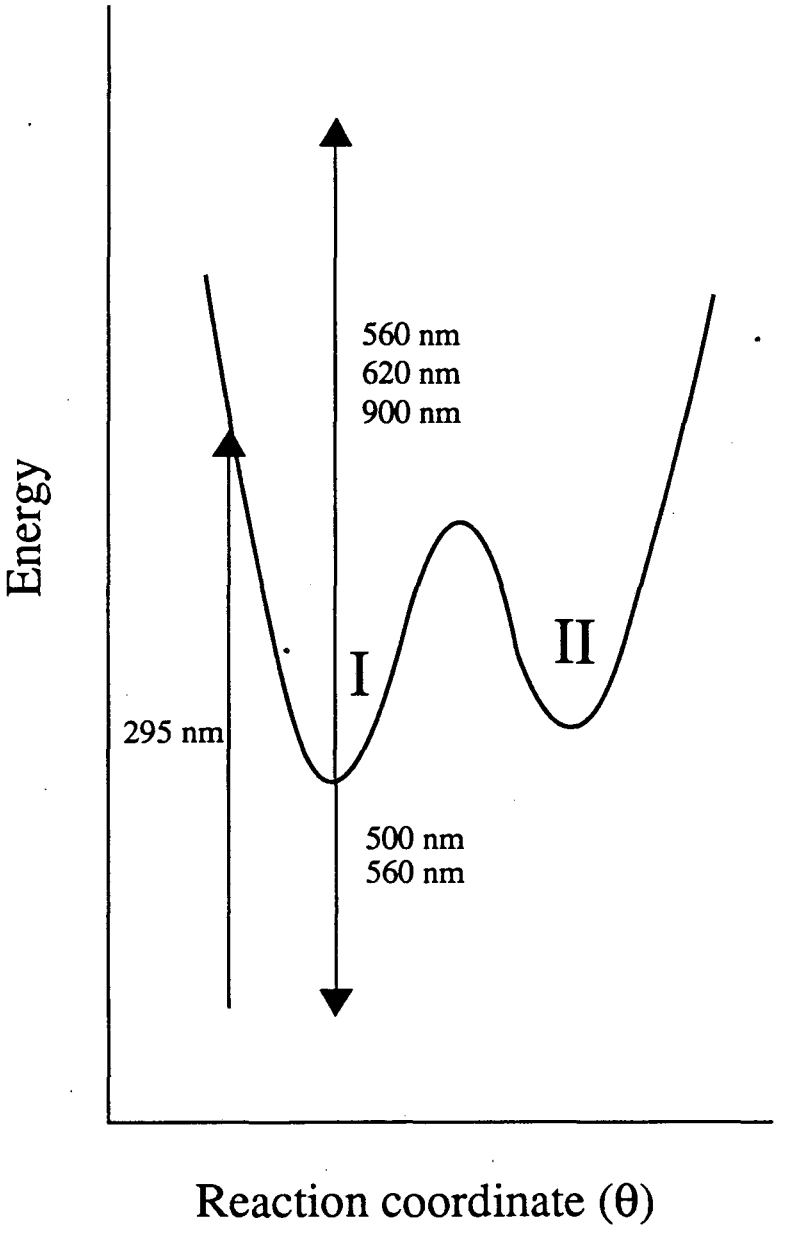

Figure 3.18 Potential energy surface for the excited state dynamics of TPB.

to those used to explain the dynamics of the diphenyl-polyene molecules which have been studied. The potential surface, with the potential wells labelled for use in the discussion below, is shown in figure 3.18. The TPB molecules are promoted to the excited state, where they undergo vibrational and conformational relaxation. The activation energy for isomerization is assumed to be high enough that the molecules cannot cross from well I to well II. The molecules are effectively trapped in well I and the population relaxes by making a radiative transition to the ground state.

This model is built up from the data in the following way. Stimulated emission is observed at 500 nm, with a double rise time of 3.5 psec and 25 psec, and a decay of 1.7 nsec. The 3.5 psec risetime most likely corresponds to the time required to relax to the bottom of the well where TPB fluoresces. From steady state fluorescence measurements in glasses and liquids, it is known that some torsional relaxation must occur before TPB can fluoresce at 500 nm, so the 3.5 psec risetime may correspond to a small amplitude torsional relaxation.[59] The rotational reorientation of DPB takes approximately 25 psec, as observed in the experiments described in the previous chapter, and results in a small rise component on the observed signal. The 25 psec rise observed on the TPB signal looks identical to that on the DPB signal, and is therefore attributed to rotational reorientation of the TPB molecule as a whole. The fact that this slow rise

component does not appear on the data at 620 nm and 900 nm is not inconsistent with the molecular reorientation explanation. The transition dipole responsible for transient absorption may lie close to the magic angle or perpendicular relative to the excite beam, in which case the reorientation of the molecule would never appear in the data.

For the diphenyl-polyenes, the observed fluorescence decay times are a combination of radiative and non-radiative relaxation times, and the non-radiative time is assumed to be due to isomerization around the carbon-carbon backbone. In these molecules, the observed fluorescence lifetime is on the order of tens to hundreds of picoseconds. The fluorescence lifetime of TPB in heptane solution has been determined to be 1.8 nsec[66]. The radiative lifetime of DPB in heptane solution has been determined to be 1.8 nsec.[67] Given these values, the 1.7 nsec decay time of the 500 nm stimulated emission signal is most likely the radiative lifetime of the molecule. This necessitates the assumption that the activation barrier to isomerization is too large to cross. The single exponential decay times of 1.9 nsec and 2.0 nsec observed for probe wavelengths of 620 nm and 900 nm, respectively, agree well with the 500 nm stimulated emission decay time, suggesting that these absorptions also occur from well I, and the decay time is the same as the radiative lifetime.

The signal at 560 nm is slightly more complicated, with both absorption and emission components. The transient absorption signal has a 25 psec decay time, which is much faster than the decay times at redder wavelengths. From the fluorescence spectrum we would expect some stimulated emission at 560 nm, but with a smaller amplitude than that at 500 nm. The stimulated emission at 500 nm has a 25 psec risetime, which agree well with the 560 nm absorption decay time. The 25 psec decay time on the transient absorption is therefore attributed to the onset of stimulated emission. After 25 psec, the absorption and emission signals approximately cancel out, although there is a very small stimulated emission signal which decays on approximately the same timescale as the other signals.

The TPB data is very different from the results reported in the literature for tetraphenyl-ethylene (TPE) in hexane. For TPE, which is structurally similar to TPB, transient absorption measurements showed a two-component decay, with times of 5 psec and 30 nsec at a probe wavelength of 640 nm.[68] The fast decay was assigned to carbon-carbon torsional motion and the slow decay to a long-lived partially twisted excited state species. These results assume that the activation barrier in TPE is very small, which differs greatly from our explanation of TPB.

The model for the TPB dynamics is very similar to that for the diphenyl-polyenes. The differences lie in the height

of the barrier to isomerization on the excited state potential surface. In the diphenyl-polyenes, the activation barrier is small enough that the molecules can cross it, making the observed fluorescence time much shorter than the radiative lifetime. For TPB the activation barrier is high enough that relaxed molecules cannot cross it, and the fluorescence time observed is presumably the radiative lifetime.

The extremely high barrier makes the reaction dynamics of TPB different from other structurally similar molecules. Although this makes TPB unsuitable as a probe for liquid-phase reaction rate theories by itself, comparison of the dynamics of TPB with the dynamics of TPMB should allow the identification of any changes caused by the addition of the methyl-group to the butadiene backbone.

3.5.2 TPMB

The transient absorption spectra for TPMB are fit well by combinations of exponential rise and decay functions. At 500 nm, the signal corresponds to stimulated emission with a pulsewidth limited rise, followed by a viscosity dependent decay time of 23 psec in hexane and 51 psec in hexadecane. At 900 nm, the signal is a transient absorption with a pulsewidth limited rise, followed by a viscosity dependent decay time of 172 psec in hexane and 271 psec in hexadecane. At 620 nm, the decay times are viscosity independent, with a pulsewidth

limited rise (measured on the CPM laser system as less than 100 fsec), and two decay times of 600 fsec and about 11 psec. In addition, the relative amplitude ratio of the two decay components is viscosity dependent, with the slow component becoming more important at higher viscosities.

These results put severe constraints on the model which is developed to explain them. The 500 nm emission and the 900 nm absorption must take place from different positions on the potential surface since the decay times are different. The faster, 500 nm decay cannot correspond to a species isomerizing to form the species which absorbs at 900 nm, since that would require a 25 psec risetime on the 900 nm curve. The fact that the processes responsible for both of these decays are viscosity dependent indicates that they correspond to a molecular motion. This is in contrast to the processes responsible for the 620 nm decays, which are viscosity independent.

The 620 nm results can be explained within the framework provided by the other transient absorption data and the steady state fluorescence studies. The fluorescence studies indicate that a conformational relaxation must occur for the TPMB molecule to fluoresce at 500 nm.[59] This relaxation could correspond to the 600 fsec decay in the 620 nm data. Phenyl ring rotations can occur on this timescale if the relaxation is a barrierless process.[69,70,71] Since a phenyl-ring rotation is such a small amplitude motion, it would be

relatively unaffected by viscosity. If there is a 600 fsec risetime on the 500 nm and 900 nm data it would not be resolved with the 1 psec laser pulse. The slower 620 nm component could correpond to vibrational relaxation down the well from which the fluorescence is occurring. Changing the solvent viscosity can change the effective potential surface slightly, which could result in the branching ratio between the two wells changing, as observed in the 620 nm data.

A consistent picture of the dynamics emerges from these observations. The 295 nm laser pulse excites the molecules to the upper potential surface. The molecules then decay in 600 fsec to a saddle point on the surface, at which point the population splits into two parts. A transient absorption is observed at 620 nm, decaying in 11 psec as the population relaxes down one of the wells. The population in one well absorbs light at 900nm, decaying in 172 psec in hexane, and 271 psec in hexadecane. The population in the other well undergoes stimulated emission at 500 nm, with the signal decaying in 23 psec in hexane and 51 psec in hexadecane. An 11 psec risetime need not appear on the 900 nm or the 500 nm data if it is assumed that 620 nm light is never absorbed in the 900 nm well and that the 500 nm stimulated emission cross section is approximately constant in the entire well. The 620 nm absorption cross section changes as the population relaxes down the 500 nm well. For both 900 nm and 500 nm, the decay times are much too fast to be the pure radiative lifetime,

which is 1.8 nsec for TPB, and are significantly faster than the times observed for molecules undergoing just carbon-carbon rotation. This suggests that these molecules are relaxing by isomerizing around the carbon-phenyl bond, either alone or in combination with the carbon-carbon bond.

Figure 3.19 shows the two-dimensional potential surface developed by Agmon and Kosloff for the relaxation of stilbene,[51] which can serve as a qualitative guide for the motion of TPMB on a two-dimensional surface. The quantitative details of such a surface, however, would be different for TPMB. For example, in TPMB the barrier to phenyl-ring rotation could be much smaller due to methyl interaction. The plot of the potential surface illustrates several important points in the discussion of the dynamics of TPMB. First, there are several positions to which the molecule can be excited which decay to a saddle point leading to the population being divided on the surface. It is also apparent how much smaller the activation barriers are along the phenyl-ring coordinate than along the carbon-carbon coordinate. The rapid decay times on the 500 nm and 900 nm signals are indicative of a facile isomerization process, in this case, phenyl-ring rotation.

If the decays at 500 nm and 900 nm are due to molecular isomerizations, then the magnitude of the effect of viscosity on the relaxation times should be roughly predicted by Kramers' theory. The values of the barrier frequencies for

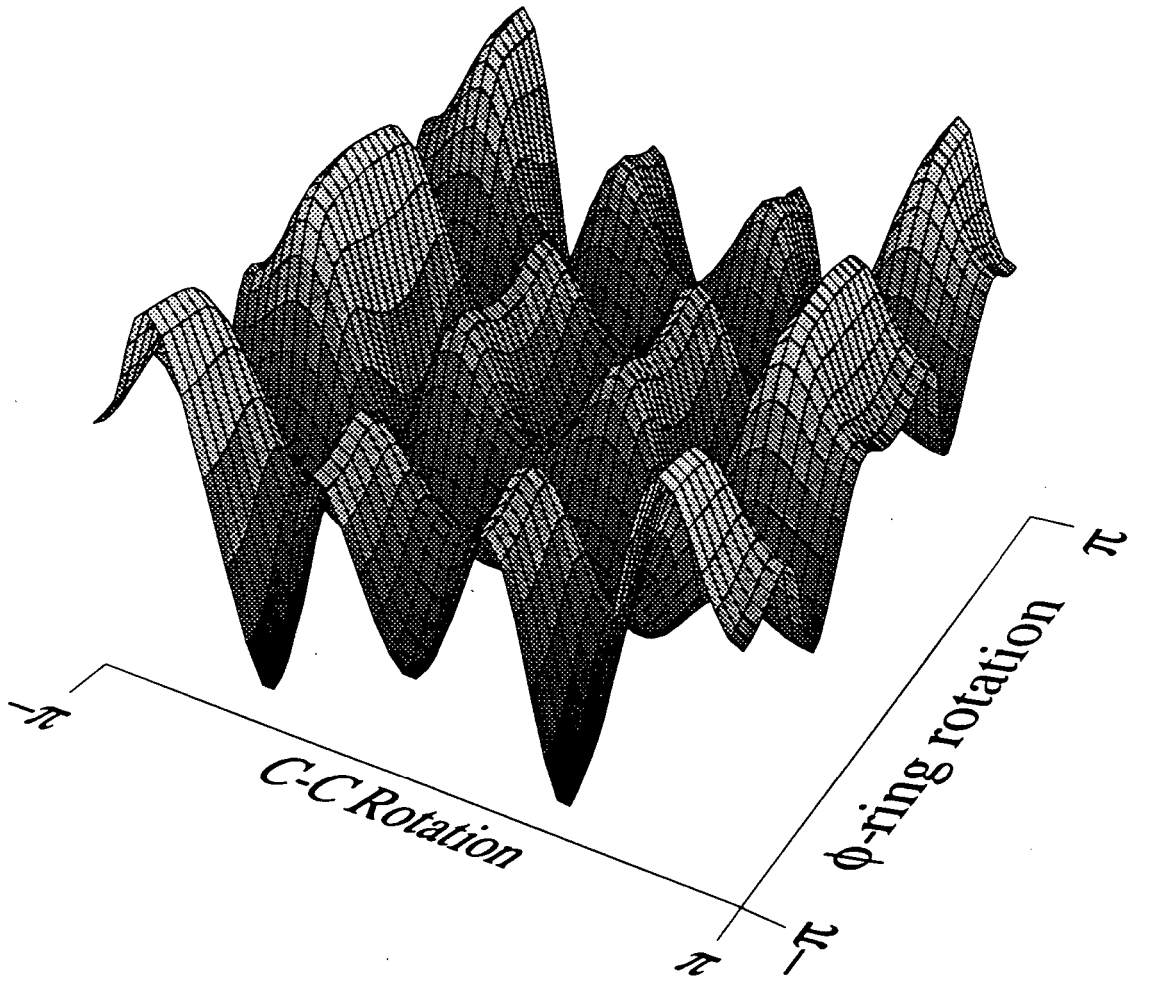

Figure 3.19 Two-dimensional potential energy surface developed for the isomerization of stilbene.

TPMB are unknown, but they have been determined for stilbene, and the effect of viscosity on the relaxation processes in TPMB should be roughly comparable to its effect on the isomerization of stilbene. For the following calculation, it is assumed that the activation energy and the well and barrier frequencies are viscosity independent, and that the SED relation holds. For stilbene, the following values have been determined:[19]

$$d = 3.7 \text{ Å}$$

$$r = 2.5 \text{ Å}$$

$$I = 9.9 \times 10^{-45} \text{ kg}^2$$

$$\omega_b = 5.7 \times 10^{13} \text{ s}^{-1}$$

Using these numbers in Kramers equation, along with the viscosities of hexane and hexadecane, gives a ratio of approximately 2 for the isomerization rate of stilbene in hexane and hexadecane. For the process occurring at 500 nm, the ratio of the rates is 2.2, while at 900 nm the ratio is 1.6. The calculation is very sensitive to the value of the barrier frequency, so within the error inherent in using the stilbene values, the viscosity effect is the same as that predicted by Kramers' theory.

The TPMB data differs from the TPB data primarily in the timescales on which the relaxation processes occur. In TPMB all of the relaxations are much faster than in TPB. The only structural difference between the two molecules is the presence of the methyl-group in TPMB, suggesting that the

change in absorption decay times is due to the addition of the methyl-group. The methyl-group shifts the phenyl-ring out of the plane of the molecule, possibly allowing the phenyl-ring to rotate more easily. This is consistent with the use of a two-dimensional potential surface to explain the dynamics of TPMB.

3.6 Conclusions

The dynamical processes in TPB can be explained well using models similar to those used extensively for TPE and the diphenyl-polyenes. The excited state potential energy surface is a double well potential with a very high activation energy for isomerization. The molecules undergo vertical excitation to the reactant well, and cross back to the ground state radiatively from the initially excited well.

The TPMB spectra are interpretable by invoking a two-dimensional potential energy surface. The molecules are initially excited and relax down the potential energy surface. They reach a saddle point, from which they can further relax into one of two wells. The decay times from both wells are affected by an isomerization process which has a small activation barrier. The initial rapid decay into the two wells is observed, in addition to the decay times from both wells.

The only difference between TPB and TPMB is the methyl-group, suggesting that its presence causes the dynamical differences. Comparing the TPB and the TPMB data lends credence to the idea that for at least some molecules a two-dimensional potential energy surface is necessary for an accurate description of the excited state dynamics. Further investigations of TPMB may prove valuable in determining the nature of deviations from Kramers' theory caused by potential energy surface multi-dimensionality, and subsequently developing correct theoretical descriptions of molecular dynamics under such conditions.

3.7 References

1. J. L. Skinner and P. G. Wolynes, J. Chem. Phys., **69**, 2143 (1978)

2. J. L. Skinner and P. G. Wolynes, J. Chem. Phys., **72**, 4913 (1980)

3. H. A. Kramers, Physica, **7**, 284 (1940)

4. P. Hanggi, P. Talkner, and Michal Borkovec, Rev. Mod. Phys. **62**, 251 (1990)

5. D. A. McQuarrie, Statistical Mechanics, (Harper & Row, 1976) pg. 452.

6. B. Carmeli and A. Nitzan, Phys. Rev. Lett., **51**, 233 (1983)

7. D. K. Garrity and J. L. Skinner, Chem. Phys. Lett., **95**, 46 (1983)

8. S. H. Courtney and G. R. Fleming, Chem. Phys. Lett., **103**, 443 (1984)

9. S. H. Courtney and G. R. Fleming, J. Chem. Phys., **83**, 215 (1985)

10. A. Nitzan, J. Chem. Phys., **82**, 1614 (1985)

11. H. L. Fang, R. J. Thrash, and G. E. Leroi, Chem. Phys. Lett., **57**, 59 (1978)

12. D. L. Hasha, T. Eguchi, and J. Jonas, J. Am. Chem. Soc., **104**, 2290 (1982)

13. D. L. Hasha, T. Eguchi, and J. Jonas, J. Chem. Phys., **75**, 1571 (1981)

14. B. D. Ross and N. S. True, J. Am. Chem. Soc., **105**, 4871 (1983)

15. M. Lee, J. N. Haseltine, A. B. Smith III, and R. M. Hochstrasser, J. Am. Chem. Soc. **111**, 5044 (1989)

16. D. K. Garrity and J. L. Skinner, Chem. Phys. Lett., **95**, 46 (1983)

17. J. Ashcroft, M. Besnard, V. Aquada, and J. Jonas, Chem. Phys. Lett., **110**, 420 (1984)

18. M. Lee, G. R. Holtom, and R. M. Hochstrasser, Chem. Phys. Lett., **118**, 359 (1985)

19. G. Rothenberger, D. K. Negus, and R. M. Hochstrasser, J. Chem. Phys. **79**, 5360 (1983)

20. S. P. Velsko and G. R. Fleming, J. Chem. Phys. **76**, 3553 (1982)

21. S. H. Courtney, S. K. Kim, S. Canonica, and G. R. Fleming, J. Chem. Soc. , Faraday Trans. 2, **82**, 2065 (1986)

22. B. Bagchi and D. W. Oxtoby, J. Chem. Phys., **78**, 2735 (1983)

23. G. Maneke, J. Schroeder, J. Troe, and F. Voss, Ber. Bunsen-Ges. Phys. Chem., **89**, 896 (1985)

24. M. Lee, A. J. Bain, P. J. McCarthy, C. H. Han, J. M. Haseltine, A. B. Smith III, and R. M. Hochstrasser, J. Chem. Phys. **85**, 4341 (1986)

25. R. M. Hochstrasser, Can J. Chem., **39**, 459 (1961)

26. H. T. Jonkman and D. A. Wiersma, J. Chem. Phys., **81**, 1575 (1984)

27. C. V. Shank, E. P. Ippen, O. Teschke, and K. B. Eisenthal, J. Chem. Phys., **69**, 5547 (1977)

28. D. P. Millar and K. B. Eisenthal, J. Chem. Phys., **83**, 5076 (1985)

29. R. M. Bowman, K. B. Eisenthal, and D. P. Millar, J. Chem. Phys., **89**, 762 (1988)

30. S. R. Flom, V. Nagarajan, and P. F. Barbara, J. Phys. Chem., **90**, 2085, 2092 (1986)

31. A. M. Brearly, S. R. Flom, V. Nagarajan, and P. F. Barbara, J. Phys. Chem., **90**, 2092 (1986)

32. S. P. Velsko, D. H. Waldeck, and G. R. Fleming, J. Chem. Phys., **78**, 249 (1983)

33. S. P. Velsko and G. R. Fleming, Chem. Phys., **65**, 59 (1982)

34. S. K. Kim and G. R. Fleming, J. Phys. Chem., **92**, 2168 (1988)

35. E. Akesson, V. Sundstrom, and T. Gilbro, Chem. Phys. **106**, 269 (1986)

36. B. Wilhelmi, Chem. Phys., **66**, 351 (1982)

37. S. Maneke, J. Schroeder, J. Troe, and F. Voss, Ber. Bunsen-Ges Phys. Chem., **89**, 896 (1985)

38. Ch. Gehrke, J. Schroeder, D. Schwarzer, J. Troe, and F. Voss, J. Chem. Phys., **92**, 4805 (1990)

39. D. H. Waldeck, W. T. Lotshaw, D. B. McDonald, and G. R. Fleming, Chem. Phys. Lett., **88**, 297 (1982)

40. A. B. Myers, M. A. Pereira, P. L. Holt, and R. M. Hochstrasser, J. Chem. Phys., **86**, 5146 (1987)

41. L. A. Phillips, S. P. Webb, and J. H. Clark, J. Chem. Phys., **83**, 5810 (1985)

42. D. H. Waldeck and G. R. Fleming, J. Phys. Chem., **85**, 2614 (1981)

43. D. Ben-Amotz and T. W. Scott, J. Chem. Phys., **87**, 3739 (1987)

44. D. Ben-Amotz and J. M. Drake, J. Chem. Phys., **89**, 1019 (1988)

45. P. S. Hubbard, Phys. Rev., **131**, 1155 (1963)

46. R. F. Grote and J. T. Hynes, J. Chem. Phys., **73**, 2715 (1980)

47. R. F. Grote and J. T. Hynes, J. Chem. Phys., **74**, 4465 (1981)

48. G. van der Zwan and J. T. Hynes, J. Chem. Phys., **77**, 1295 (1982)

49. G. van der Zwan and J. T. Hynes, Chem. Phys., **90**, 21 (1984)

50. B. Carmeli and A. Nitzan, Chem. Phys Lett., **106**, 329 (1984)

51. N. Agmon and R. Kosloff, J. Phys. Chem., **91**, 1988 (1987)

52. L. H. Spangler, R. van Zee, and T. S. Zwier, J. Phys. Chem., **91**, 2782 (1987)

53. H. Hamaguchi, C. Kato, and M. Tasumi, Chem. Phys. Lett., **100**, 3 (1983)

54. H. Hamaguchi, T. Urano, and M. Tasumi, Chem. Phys. Lett., **106**, 153 (1984)

55. T. L. Gustafson, D. M. Roberts, and D. A. Chernoff, J. Chem. Phys., **79**, 1559 (1983)

56. T. L. Gustafson, D. M. Roberts, and D. A. Chernoff, J. Chem. Phys., **81**, 3438 (1984)

57. N. S. Park and D. H. Waldeck, J. Chem. Phys., **91**, 943 (1989)

58. N. S. Park and D. H. Waldeck, J. Phys. Chem., **94**, 662 (1990)

59. M. A. El-Bayoumi and F. M. Abdel Halim, J. Chem. Phys., **48**, 2536 (1968)

60. J. Kordas and M. A. El-Bayoumi, J. Am. Chem. Soc., **96**, 3043 (1974)

61. J. Kordas, P. Avouris, and M. A. El-Bayoumi, J. Phys. Chem., **79**, 2420 (1975)

62. C. Rulliere, A. Declemy, and Ph. Kottis, Laser Chem., **5**, 185 (1985)

63. D. S. Viswanath and G. Natarajan, Data Book on the Viscosity of Liquids, (Hemisphere Pub. Corp., 1989)

64. Private communication from Andy Schreeve

65. J. D. Jackson, Classical Electrodynamics, (John Wiley & Sons, 1975)

66. A. N. Nikiting, G. S. Ter-sarkisyan, B. M. Mikhailov, and L. E. Minchenkova, Opt. Sepctrosc. (USSR), **14**, 347 (1963)

67. M. Sumitani, N. Nakashima, K. Yoshihara, and S. Nakagura, Chem. Phys. Lett., **51**, 183 (1977)

68. B. I. Greene, Chem. Phys. Lett., **79**, 51 (1981)

69. D. Ben-Amotz and C. B. Harris, J. Chem. Phys., **86**, 4856 (1987)

70. D. Ben-Amotz and C. B. Harris, J. Chem. Phys., **86**, 5433 (1987)

71. D. Ben-Amotz, R. Jeanloz, and C. B. Harris, J. Chem. Phys., **86**, 6119 (1987)

Appendix I

Copper Vapor Laser
Timing Feedback Circuit

The time delay between when the coper vapor laser is triggered and when a laser pulse is produced changes as the CVL warms up during the course of a day. The "black box" is a feedback circuit, designed at AT&T Bell Labs and described to us by Fred Beisser, which monitors that time delay and adjusts the trigger signal to keep the delay constant. The circuit design was modified slightly by the chemistry department electronics shop (Tom), and they have an accurate circuit diagram on file.

The box requires two input signals, one from the CVL laser output, and one from the trigger signal to the CVL. For the laser output signal, part of each CVL laser pulse is sent into a photodiode, which is adjusted to produce a minimum signal amplitude of -120mV. This signal is amplified to a +4.5V pulse by passing it through a fast/slow logic interface NIM module (use +4V output on NIM module). This laser signal is then sent into the photodiode input connector on the black

box. The digital delay generator signal which is normally used to trigger the CVL (+4V baseline with 600nsec pulses dropping to 0V at 8kHz) is sent into the trigger input connector on the black box instead. The trigger output signal from the black box is used to trigger the CVL.

Using the black box requires that a fairly complicated series of steps be followed. First, the CVL must be warmed up on internal trigger. After the CVL is lasing, and you are ready to do experiments, the trigger signal must be synchronized. To do this, place a BNC "T" in the trigger output signal, sending one part of the signal to the CVL trigger input and the other part to the 50 Ohm input on the storage oscilloscope. Trigger the oscilloscope off of the T0 output of the digital delay generator. You should see the CVL triggering signal scrolling about 500 nsec about every one-half second.

The next steps require two people. One person holds down the reset button on the black box, which stabilizes the trigger signal time. After the trigger signal has stabilized, the other person switches the CVL to external trigger. Do not switch the CVL to external trigger if the trigger signal is still scrolling across the oscilloscope screen. Continue to hold the reset button until the CVL has warmed up again and is producing a large enough photodiode signal. Now release the reset button and quickly use the output adjust button to make the trigger pulse stable in time. (Output adjust acts as a

coarse adjustment, the input adjust is a fine adjustment.) At this point, the CVL should be firing normally.

In order to free up the oscilloscope for other uses, the BNC cable can be terminated into 50 Ohms. The CVL will temporarily stop triggering while the BNC is unterminated. The BNC cable must remain terminated at all times.

When the black box is in use, the shutter on the CVL cannot be closed. In order for the circuit to work, it needs input from the CVL photodiode. If the shutter is closed, the CVL no longer receives a trigger signal, and it will stop lasing. The CVL beam can be blocked by using a beam block outside of the safety shielding box.

Appendix II

Preparation and Purification of Trans-1,1,4,4-tetraphenyl-2-methylbutadiene (TPMB)[1]

II.1 Procedure

The starting material, 1-methyl-2,2-diphenylcyclopropanecarboxylic acid (I), m. p. 182-183°, was provided by Professor H. Walborsky.[2] Structures of the intermediates are shown in figure II.1. The methyl ester (II) was prepared by the addition of diazomethane in ether to the acid in dichloromethane at 0°. The ester was crystallized from methanol, m. p. 92-92.2°, and was chromatographed over a silica gel column using a 4:1 mixture of hexane-ethylacetate as the solvent. The purity of the ester was confirmed by thin layer chromatography (TLC) and NMR.

The preparation of 1-methyl-2,2-diphenylcyclopropyldiplenylcarbinol (III) was performed by slowly adding 30 ml of a 2.0 M solution of butyllithium in hexane to 14 ml of bromobenzene in 60 ml dry ether at -78° C.[3,4] The resulting solution of phenyllithium (about 0.06 mole) was warmed to 0° C. To this solution, 5.56 g of the methyl ester (II) was added slowly, and the solution was stirred at room temperature for one hour. An aqueous solution

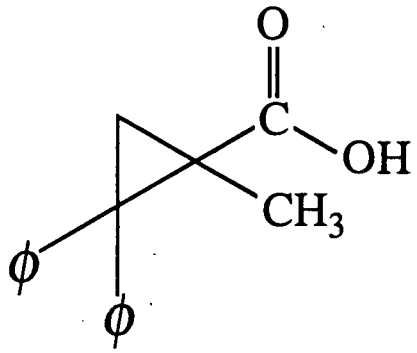

I

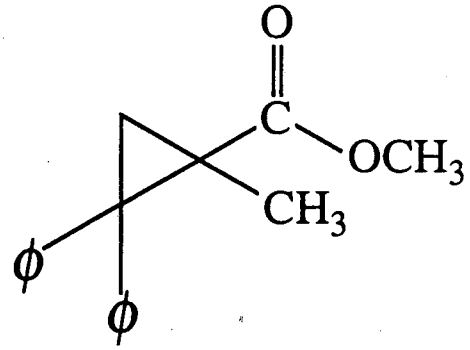

II

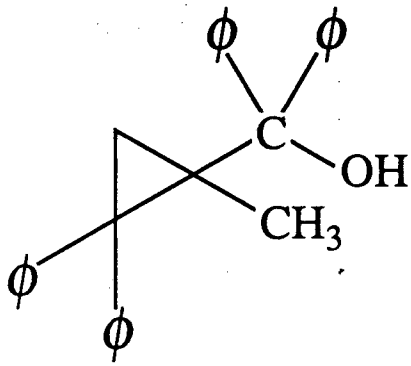

III

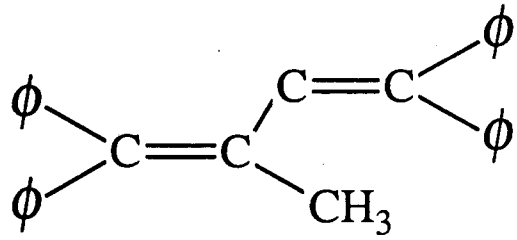

IV

Figure II.1 Structures of the important intermediates in the synthesis of TPMB.

of ammonium chloride (10 g in 100 ml of H_2O) was added cautiously. The aqueous phase was extracted with ether, the ether extract was dried over anhydrous sodium sulfate, and the solvent was stripped under vacuum. TLC showed only one spot.

Finally, TPMB was obtained by refluxing a solution of the carbinol in dry toluene with a small amount of iodine for fourteen hours using a Dean-Stark apparatus. The toluene solution was extracted using aqueous sodium thiosulfate solution, dried and the solvent was stripped under vacuum. A dark brown oil was obtained and was crystallized from 95% ethanol. TLC showed only one spot. TPMB was recrystallized from ethanol and its purity was confirmed using: UV absorption, fluorescence, NMR, mass spectroscopy and vapor phase chromatography. The UV absorption spectrum is shown in figure 3.3. The fluorescence spectrum is shown in figure 3.17. The NMR spectrum is shown in figure II.2. The mass spectroscopy data is presented in table II.1.

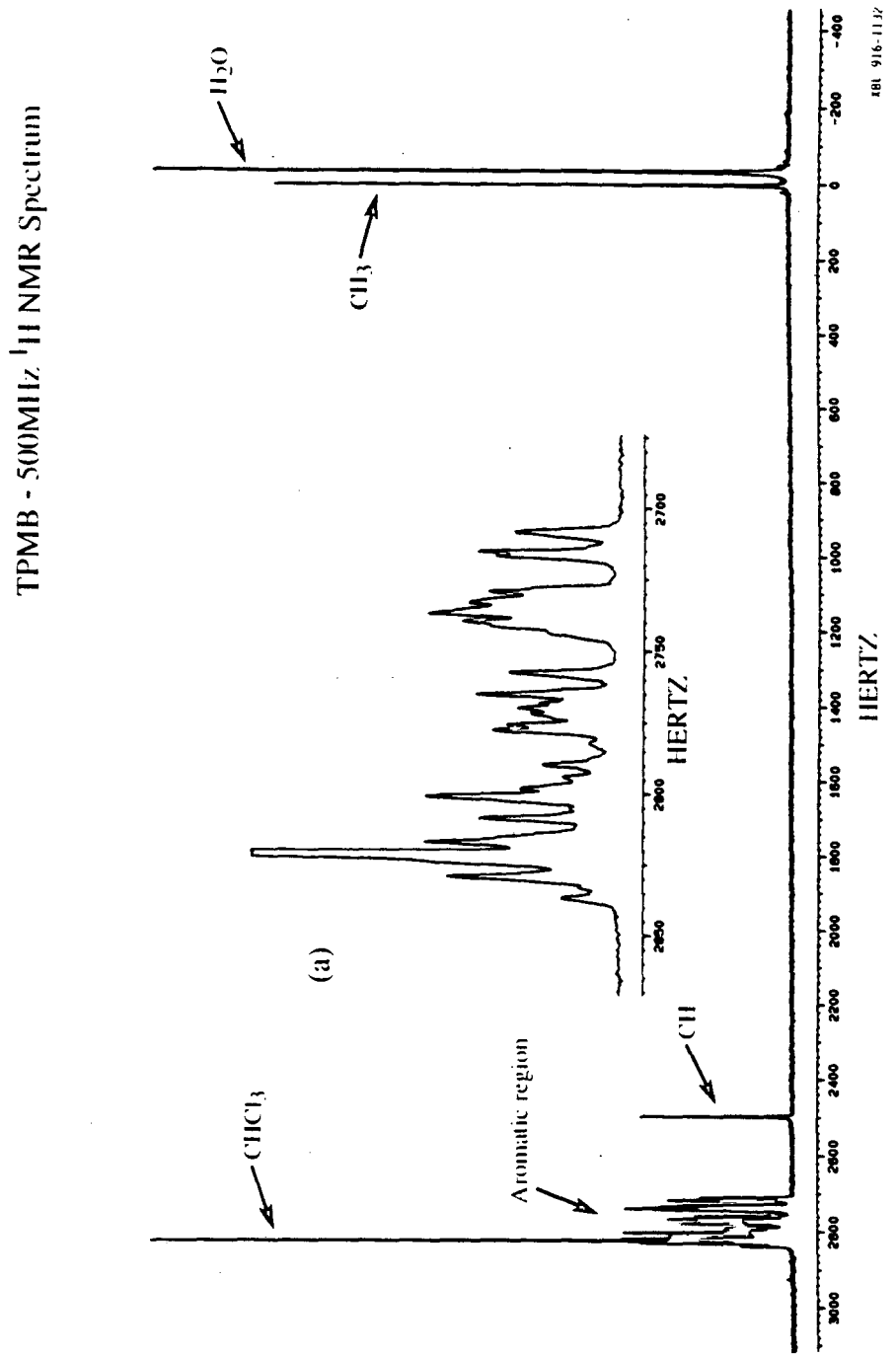

Figure II.2 NMR spectrum of TPMB in deuterated chloroform.

Table II.1
TPMB Mass Spectral Data

m/z	abund	m/z	abund	m/z	abund
50.95	232	132.10	77	181.10	58
51.95	49	133.00	89	187.00	34
63.05	79	138.10	166	188.10	36
65.00	99	139.10	235	189.10	324
75.00	39	141.10	36	190.15	183
76.10	56	143.70	30	191.15	237
77.10	377	144.60	66	192.15	71
78.10	249	146.00	40	193.15	28
79.10	42	147.10	143	200.05	75
88.10	24	150.10	77	201.05	115
89.10	98	151.10	140	202.15	664
91.10	366	152.10	551	203.15	572
92.10	37	153.10	8	204.15	235
101.10	45	156.60	59	205.15	736
102.10	75	162.10	46	206.15	132
103.10	165	163.00	169	213.05	70
105.10	133	164.10	171	214.15	29
108.00	60	165.10	1231	215.05	453
113.10	62	166.10	425	216.05	206
115.00	300	167.10	6438	217.05	286
116.00	43	168.10	949	218.05	57
117.10	39	169.10	93	226.05	70
119.50	36	175.10	48	228.15	40
125.00	34	176.10	155	229.05	32
126.00	157	177.10	96	237.05	34
127.00	133	178.10	386	239.05	167
128.00	138	179.10	206	240.05	63
129.10	43	180.10	34	241.15	55

Table II.1 (cont.)
TPMB Mass Spectral Data

m/z	abund	m/z	abund	m/z	abund
250.05	79	293.15	216	354.20	53
251.15	41	294.15	372	355.20	102
252.05	351	295.15	520	356.20	137
253.15	222	296.15	125	357.20	1182
254.15	147	300.05	43	358.20	340
255.15	124	301.15	25	359.20	49
256.15	29	302.05	64	372.20	5142
263.15	210	313.05	80	373.20	1640
264.05	121	314.05	37	374.20	233
265.05	609	315.05	135		
266.15	300	316.10	57		
267.05	944	324.20	24		
268.15	248	326.10	121		
269.15	34	327.10	99		
274.15	65	328.20	123		
275.15	39	329.10	102		
276.15	468	330.20	44		
277.05	519	331.10	98		
278.15	664	339.20	146		
279.15	1658	340.10	72		
280.15	779	341.20	228		
281.15	668	342.20	182		
282.15	157	343.20	172		
287.05	55	344.20	61		
289.15	207	350.10	47		
290.15	72	351.10	40		
291.15	158	352.20	59		
292.15	63	353.20	68		

II.2 References

1. Private communication from M. A. El-Bayoumi.

2. H. M. Walborsky and F. M. Hornyak, J. Am. Chem. Soc., **77**, 6026 (1955)

3. H. M. Walborsky, and J. F. Pendleton, J. Am. Chem. Soc., **82**, 1405 (1960)

4. H. M. Walborsky, and F. M. Hornyak, J. Am. Chem. Soc., **77**, 6396 (1955)

LAWRENCE BERKELEY LABORATORY
UNIVERSITY OF CALIFORNIA
INFORMATION RESOURCES DEPARTMENT
BERKELEY, CALIFORNIA 94720